ACKNOWLEDGEMENT

First and for most I want to thank Professor Niyazi Serdar Sariciftci, who enable this dissertation, for his supervision during the last years.

I would also thank Dr. Helmut Neugebauer for his supervision, all the discussions and his comments, that are always dead-on.

Special thanks go to Beatriz Meana Esteban for all the fruitful discussion and her friendship and to Martin Egginger, who shared the office with me now for many years, for all the help, the long discussions and his critical opinion on everything. I have to thank Edina Mujcinovic a lot for her work and help in the laboratory.

I want to give thanks to the people of LIOS that keep everything running: Petra Neumaier and Birgit Paulik, who do a great job in the secretary's office, Gerda Kalab, who keeps the laboratories running and Manfred Lipp for a all his technical assistance.

Fredrik Sunfors and Ana Österholm are acknowledged for sputtering of Platiunum.
Robert Köppe, Philipp Stadler, Gebi Matt, Pavel Troshin and Serap Günes: many thanks for all the good collaboration in the last years!

I am also very thankful to my coworkers in the CO_2 project: Ercan Avci, Klaus Brandstätter, Martin Kruijen, Kertin Oppelt, Engelbert Portenkirchner and Peter Trefflinger (who left already). I want to thank all the other members of LIOS for the good collaboration (some of them left already): Mamatimin Abbas, Elif Arici-Bogner, Daniel Egbe, Jacek Gasiorowski, Wolfang Huber, Sandor Lattante, Alberto Montaigne Ramil, Almantas Pivirikas, Stefan Schaur, Birendra, Serpil Tekoglu, Singh, Patchanita Thamyongkit, Matthew White and especially to everyone, who is not in the list, but should be there!

The Solar Fuel Technology GmbH & CoKG, especially Dipl.-Ing. ETH, MBA Gregor Waldstein, is acknowledged for financial funding.

Last but not least I want to thank my family for all the support, especially to Ralf for his love and patience!

ZUSAMMENFASSUNG

Energieversorgungssysteme basierend auf Wind- und Sonnenenergie werden in der heutigen Zeit immer mehr implementiert. Wind- und Solarkraftwerke produzieren Strom, welcher direkt in das Stromnetz eingespeist wird. Da hierbei die Stromproduktion jedoch Fluktuationen aufweist, ist eine Energiespeicherung von Nöten. Durch ihre hohe Energiedichte stellen Kohlenwasserstoffe eine interessante Variante der Energiespeicherung dar. Für eine sinnhafte Nutzung solcher Brennstoffe sollte sie mit Hilfe erneuerbarer Energien CO_2 neutral hergestellt werden. Wird CO_2 aus der Luft als „C1“ Baustein verwendet, kann dies gewährleistet werden.

Unterschiedliche Prozesse um atmosphärisches CO_2 in einen Brennstoff umzuwandeln an Hand von Beispielen aus der Literatur vorgestellt im ersten Kapitel vorgestellt. Das zweite Kapitel beschreibt einen existieren Prototypen der Solar Fuel GmbH, welcher CO_2 aus der Luft in Methan umwandelt. Gespeist wird jene Anlage mit Wasser, Luft und Strom, welcher beispielsweise durch ein Windrad generiert wird. Die Produkte sind CO_2 abgreicherte Luft und Methan. Die Hauptenergieverbraucher sind hierbei der Elektrodialysestack und der Wasserelktrolyseur. Die Elektrodialyse produziert ein Säure, welche CO_2 aus der Absorptionslösung freisetzt, und der Elektrolyseur stellt Wasserstoff, welcher zur Reduktion von CO_2 zu Methan benötigt wird, her. Beide Prozesse basieren auf der elektrochemischen Wasserspaltung.

Im dritten Kapitel wird eine systematische Studie an einem Zweikammerelektrolyseverfahren, welches alternativ zur Elektrodialyse eingesetzt werden kann, vorgestellt Verschiedenster Versuchsparameter, wie Temperatur, Elektrolytkonzentration, etc., wurden variiert. Dabei zeigt sich, dass ein solches Elektrolyseverfahren eine attraktive Alternative zur Elektrodialyse darstellt.

In Kapitel vier werden in situ spektroelektrochemische Untersuchungen an einem Katalysator für die elektrochemische Wasseroxidation beschrieben, mit besonderem Augenmerk auf Stabilität in verschiedenen Elektrolytlösungen. Dabei zeigt sich, dass in sauren Elektrolytlösungen der Katalysator aufgelöst wird. Durch die Verwendung eines Dreikammerelektrolyseverfahrens mit bipolaren Membrane, kann jedoch gleichzeitig eine Säure produziert und der Katalysator verwendet werden.

Die Reduktion von CO_2 mittel Wasserstoff zu einem Brennstoff stellt nicht die einzige Möglichkeit dar: Weiter CO_2 Reduktionsverfahren werden in Kapitel fünf diskutiert.

ABSTRACT

Nowadays the amount of wind- or solar power stations is rising. Wind turbines and solar cells convert the wind or solar energy to electricity with fluctuations. Hence storage of energy is needed. Carbon based fuels are very appealing for this as they show high energy densities. However, the produced fuel should be CO_2 neutral. By using atmospheric CO_2 as carbon source for fuel production this can be achieved.

Different possible pathways from the existing literature for converting atmospheric CO_2 into a fuel are discussed in the first section of this thesis. The technical feasibility of such process is shown in the second section on the example of a prototype from Solar Fuel GmbH. It converts atmospheric CO_2 into methane. The inputs are water, air and electricity generated for example by a wind turbine. As outputs methane and CO_2 depleted air. As the main energy consuming parts are the electrodialysis stack and the water electrolyzer can be found. Both of them work on the principle of electrochemical water splitting. With the electrodialysis process an acid, which is used to release CO_2 from the absorption liquid, is generated and the water electrolyzer produces hydrogen gas, that is needed for methane synthesis.

Another electrochemical setup for acid generation is an electrolysis cell, which is discussed in detail the third chapter. The cell can either be built in a two- or three chamber geometry. Various experimental parameters, like temperature, electrolyte concentration etc., were investigated by using a two chamber geometry and their influence on the performance is discussed. The results suggest that such electrolysis process is an interesting alternative to the electrodialysis in terms of efficiency.

In the fourth chapter in situ spectroelectrolchemical investigations on a catalyst for water oxidation are presented, focusing on the stability of the catalyst in different electrolyte solutions. In acidic solutions a complete dissolution of the catalyst is observed. A possible solution for implantation the catalyst in electrolysis cells, where an acid is generated, is to use a three chamber geometry with bipolar membranes.

Finally an overview over other reduction stratagies, excluding hydrogenation, is given.

Table of Contents

Chapter 1

Motivation and Introduction

The usage of fossil fuels to serve the energy demand of mankind is known to cause problems like production of greenhouse gases and is in addition limited in terms of long term availability. Hydrogen produced from non fossil sources would be a possible energy carrier of the future but problems like storage and distribution still have to be overcome. On the other hand, fuels like methane (natural gas) or methanol are well known and distribution as well as storage can be realized easier. Beside the known sources, mainly fossil, they could be synthesized from CO_2 taken out of the air .Therefore, transforming CO_2 from air into methane or methanol using wind- or solar energy could lead to a CO_2 neutral energy supply as combustion of these fuels leads to the same amount of CO_2 that was previously used for synthesis.

1.1 Introduction

The current energy feedstock of human society is mostly based on fossil fuels that are related to several problems. The reserves are decreasing and their final depletion seems to be just a matter of time.[1] In addition, combustion of fossil fuels leads to the emission of CO_2, which, beside water and methane, is considered as a main greenhouse gas.[2] The consequence of the greenhouse effect (increased temperatures) and the depletion of fossil fuels on oncoming generations has recently led to controversial discussions but there is definitively a need for environmentally benign energy systems.[3] For sure it can be said that that the atmospheric CO_2 concentrations are increasing since several decades. The Intergovernmental Panel on Climate

Change (IPCC) reports that current concentrations of CO_2 are far exceeding preindustrial values found in polar ice cores. The concentration has risen from a pre-industrialization value of around 280 ppm to 379 ppm in 2005. The primary sources of increased atmospheric CO_2 levels are emissions from fossil fuels and the effects of land use change on plant and soil carbon.[4] Several approaches have been done to replace fossil fuels by sustainable techniques like solar and wind energy, hydroelectric power, energy from biomass, etc. Up to now none of these were able to fully replace fossil fuels. Usually electricity is used as energy carrier for renewable energy conversion. Using solar cells, for example, leads to a diurnal variation of energy in locally isolated or remote locations. Therefore there is a need for cost effective storage of solar electricity. This could be obtained by using batteries but at present these are not inexpensive enough for the cost per Watt targets.[5] An effective storage method for electricity is to produce fuels. The energy density for example for gasoline is 46.4 MJ/kg[6] (12.9 kWh/kg) which is significantly higher compared to batteries used for electro cars (Li ion battery has an energy density of 150 Wh/kg).[7] The lead acid battery has an energy density of 35Wh/kg.[7] By fuelling a typical tank in a gasoline car (~ 40 l) thus 380 kWh are transferred within around 2 min (~ 11.4 MW transfer power). This corresponds to a current of around 1 MA under the assumption of a 12 V battery. The amount of gasoline has a weight of 29.5 kg. For storing the same energy in a Li ion battery a weight of 2533 kg is needed which is a factor of 85 higher compared to gasoline. In addition the charging of a Li ion battery takes around 2.5 h .[7] In all these considerations other parameters like different motor efficiencies are not taken into account.

Fuels like methane or methanol can be synthesized from CO_2 and H_2. Depending on the catalyst used, various types of fuels can be obtained, e.g., methane, methanol, formic acid and others.[8,9] As the actual value of atmospheric CO_2 is around 384 ppm (October 2009)[10], air seems to be a reasonable source of CO_2. Using renewable energies like solar or wind energy to extract CO_2 from air and to transform it into a fuel, would create a climate neutral energy carrier from recycled CO_2, as the combustion of this fuel would release the same amount of CO_2 as has been used for its synthesis.[11] Possible processes for CO_2 recycling were previously described in the literature and include the following processes: capture of CO_2 from air, release of pure CO_2 and finally fuel synthesis.[11,12,13,14]

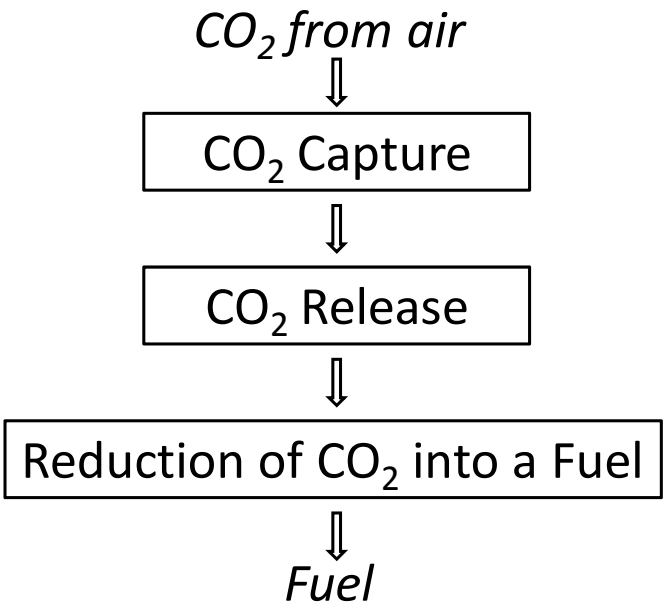

Figure 1.1 Schematic drawing of the CO_2 recycling process

The process for transforming CO_2 from air into a fuel can be divided into the following steps and is schematically shown in Figure 1.1 :

- CO_2 capture from air: The concentration of CO_2 in air is around 380 ppm nowadays. For fuel synthesis pure CO_2 is needed. For this reason, CO_2 is first to be captured from air.
- CO_2 release: After the capturing of CO_2 by suitable methods it has to be released for reduction into a fuel.
- Reduction of CO_2 into a fuel: For fuel synthesis CO_2 has to be reduced. This can be done either directly (electrochemically or photochemically) or in an indirect way using for example hydrogen gas. The reduction processes usually needs catalysts. Carbon neutral hydrogen can be obtained from water electrolyzers. For the reduction using hydrogen gas depending on the catalyst used, different fuels such as methane, dimethylether, methanol and higher hydrocarbons can be synthesized from hydrogen and carbon dioxide.

In the following part of this chapter an overview over a possible pathways for CO_2 recycling is given.

1.2 CO_2 recycling process

1.2.1 CO_2 capture from air

In the reduction process CO_2 with a high purity is needed. Therefore dilution of CO_2 with air impurities has to be avoided as they can for example poison the synthesis catalyst. For capturing CO_2 from air the main problem is the low concentration.[15] 380 ppm of CO_2 correspond to 0.038 Vol% and thus for capturing 1 kg of CO_2 around 1 334 m^3 of air are needed. Using a perfect mechanism for achieving the absorption of CO_2, only the free energy of mixing have to be overcome. The energy of mixing is given by

$$\Delta G = RT \ln \frac{P}{P_0}. \qquad \text{(eq. 1.1)}$$

In the equation P_0 is 1 bar, P is 3.8 x 10^{-4} bar, T is the temperature and R the ideal gas constant.[16,17,18] At 300 K, ΔG is ~ -20 kJ/mol, where the negative value means that mixing is always spontaneous. For CO_2 absorption (a "demixing" process), 20 kJ/mol is the minimum energy requirement, however the practical value might be much higher. A further requirement for CO_2 capturing from air is that the partial pressure over the saturated absorption (or adsorption) medium is lower than the partial pressure of air (3.8 x 10^{-4} bar). In practice, 2 systems fulfill this requirement: adsorption on solid sorbents (molecular sieves) and absorption in metal hydroxide solutions.[15]

1.2.1.1 Adsorption on solid molecular sorbents (molecular sieves)

Different industrial processes use molecular sieves for gas separation and purification. The adsorbent has to be regenerated after using. This can be either done by pressure swing or temperature swing absorption. Pressure swing absorption is one potential technique[19] where gases are separated due to their molecular characteristics and an affinity to an adsorbent under pressure conditions and desorbed afterwards under lower pressure.[20] The sorbents used usually show higher affinity for water and as the water partial pressure in air is around 6 mbar the sorbent will require ~ 20 times more energy to release the water. [13,15] In addition, dust or other impurities can block the active adsorption centers of the molecular sieves.[15] Adsorbers for larger air volumes are expensive compared to the absorption process using metal hydroxide solutions.[13] Therefore molecular sieves can be considered as not suitable for the large scale CO_2 capture from air at the moment.

1.2.1.2 Absorption using metal hydroxide solutions

Metal hydroxides as capturing media for CO_2 from air have been widely discussed in the literature and most proposals include either a calcium hydroxide ($Ca(OH)_2$) or a alkali (sodium or potassium) hydroxide (NaOH,KOH) solutions as absorption liquid. The general reaction equation for metal hydroxide solutions used for capturing CO_2 is the following

$$2\ OH^- + CO_2 \rightarrow CO_3^{2-} + H_2O \qquad \Delta H_0 = -109.4\ \text{kJ/mol}\ .^{21} \qquad (1.1)$$

ΔH_0 is negative, therefore the reaction is thermodynamically favorable.

Evaporative water losses have to be taken usually into account for all these absorption processes. Note that in some reaction schemes (diss) indicates a complete dissociation of the substance in the given aqueous solution.

1.2.1.2.1 CO_2 capture with $Ca(OH)_2$

Dubey and coworkers[22] propose a very simple method for CO_2 capturing from air: CO_2 is transported over a sink filled with an aqueous solution of $Ca(OH)_2$ by natural airflow. The reaction equation for the CO_2 capturing can be summarized as:

$$CO_2 + Ca(OH)_2 \rightarrow CaCO_3 + H_2O \qquad (1.2)$$

114 kJ/mol are released. $CaCO_3$ will precipitate and can be collected periodically. $CaCO_3$ has to be recovered which can be done by calcination summarized by

$$CaCO_3 \rightarrow CaO + CO_2 \qquad (1.3)$$

Prior to the calcination $CaCO_3$ has to be dried. The drying energy could be provided by the heat of hydration when CaO is transformed into $Ca(OH)_2$ again.

$$CaO + H_2O \rightarrow Ca(OH)_2 \qquad (1.4)$$

The calcination reaction requires 179 kJ/mol, which can be considered as the energy penalty that has to be paid for recovering CO_2, and according to *Dubey and coworkers* it might come from the combustion of coal. A collection unit for CO_2 with the size of 1 m^2 sweep area and a wind velocity 3 m/s could collect 3.6 kg of CO_2 per hour assuming an extraction efficiency of 50 % and would cost around 22 $/t of CO_2. [22]

Nikuslshima and coworkers propose to use concentrated solar power for the calcination process.[23,24] With the combination of CO_2 release by decomposition of $CaCO_3$ with a CO_2 consuming dry reforming process, a possibility of coproduction of CaO and syngas according to

$$CaCO_3 + CH_4 \rightarrow CaO + 2\ CO + 2\ H_2 \qquad (1.5)$$

is given.[25] The overall required thermal energy input for such a system was estimated to be ~2.8 kJ per mol of CO_2 captured and per 4 moles of H_2 produced. This thermal energy is supplied by concentrated solar power.[23]

A major drawback of using $Ca(OH)_2$ as capturing solution is the low rate of CO_2 absorption due to the low solubility of $Ca(OH)_2$ in water, which is around 1.7 g/l (0.03 M).[26] In addition, the vapor pressure of water is high and therefore higher evaporative water losses can be expected.[15]

1.2.1.2.2 CO_2 capture with NaOH/KOH

Both sodium and potassium hydroxide show a very high solubility in water: NaOH has a solubility of 1260 g/l (31.5 M) [27] and KOH of 1130 g/l (20.1 M)[28] in water. The higher solubility of these two capturing liquids favors their use in comparison to $Ca(OH)_2$. In addition, NaOH solutions have a lower water vapor pressure compared to $Ca(OH)_2$ solutions and thus prevent water losses.[15,17] The feasibility of air capture with NaOH or KOH solutions is widely discussed in the literature for various types of absorber geometries.[17,29,30,31,32] The absorber geometries differ from various towers[33], spray absorbers[16] to hollow fiber membrane absorbers.[30,32] Most of the proposed systems include CO_2 capture in NaOH or KOH solutions and a subsequent CO_2 release from the carbonate solution either by acidification or by a thermal decomposition of carbonate. The main concern for all liquid absorbers is the evaporative water loss which should be as low as possible.

1.2.2 Release of CO_2 from carbonate solutions

As discussed above, metal hydroxide solutions seem to be the best candidate for capturing CO_2 from air and NaOH/KOH solutions seem to be favorable compared to $Ca(OH)_2$ for small to medium type installations. Due to this, possible ways of releasing concentrated CO_2 from Na_2CO_3 or K_2CO_3 solutions will be discussed here. All processes have in common that, in addition to the CO_2 release, the absorption liquid is regenerated using a thermochemcial or an acidification process as shown in Figure 1.2. By using an electrochemical acid generation the acidification can be carried out either inside or outside the electrochemical cell. For an outside acidification the acidification process and the acid generation are locally decoupled.

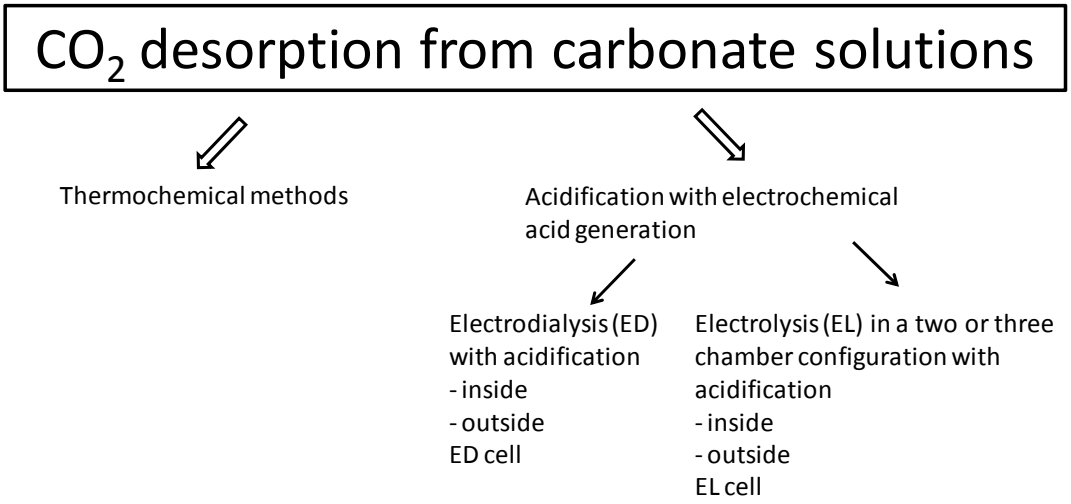

Figure 1.2 Overview over CO_2 desorption processes

1.2.2.1 Thermochemcial methods

1.2.2.1.1 Sodium-based thermochemical cycle

Nikulshina and coworkers[31] propose an all sodium based cycle for CO_2 absorption and release. They discuss 3 different thermochemical cycles (a–c). In cycle (a) CO_2 from atmospheric air (500 ppm CO_2) is captured with NaOH at 25 °C, where the following reaction takes place:

$$NaOH\,(s) + CO_2(g) \rightarrow NaHCO_3(s) \qquad (1.6)$$

The solid product $NaHCO_3$ is then thermally decomposed at 200 °C to Na_2CO_3 according to

$$2\,NaHCO_3(s) \rightarrow CO_2(g) + Na_2CO_3(s) + H_2O(g)\,. \qquad (1.7)$$

Pure CO_2 is delivered to the storage site and Na_2CO_3 is decomposed into Na_2O and CO_2:

$$Na_2CO_3 \rightarrow Na_2O + CO_2 \qquad (1.8)$$

Na_2O is directed to a reactor where it reacts with H_2O from reaction (1.7) to form NaOH at 700 °C. In cycle (b) the capturing of CO_2 and decomposition of $NaHCO_3$ into Na_2CO_3 is the same but instead of a thermal decomposition, the carbonate is steam-hydrolyzed into NaOH and CO_2 (reverse absorption reaction, endothermic). In cycle (c) CO_2 is absorbed in Na_2CO_3 according to

$$CO_2(g) + Na_2CO_3(s) + H_2O(g) \rightarrow 2\,NaHCO_3(s)\,. \qquad (1.9)$$

$NaHCO_3$ is thermally composed afterwards (1.7) and Na_2CO_3 and H_2O are recycled. For all three processes the inventory of NaOH (process cycle 1 and 2) or Na_2CO_3 (process cycle 3) is higher than for Ca-based sorbents.

1.2.2.1.2 Sodium- and Calcium- based thermochemcial cycles

A process using Na- and Ca- based thermochemical cycles is suggested by *Zeman and coworkers*[34], *Bacciochi and coworkers*[35] and *Keith and coworkers*[36]. The main idea is that CO_2 is absorbed in a NaOH solution and producing therefore dissolved sodium carbonate in an exothermic reaction. The removal of the carbonate ions is achieved by the reaction with $Ca(OH)_2$:

$$Na_2CO_3 + Ca(OH)_2(s) \rightarrow 2\ NaOH + CaCO_3(s) \qquad (1.10)$$

This calcination reaction is mildly exothermic (ΔH_0 = - 5.3 kJ/mol).[34] The precipitated calcite ($CaCO_3$) is filtered from the solution and thermally decomposed (1.3). In this step concentrated CO_2 and CaO are obtained. The lime hydration reaction (1.4) is exothermic (ΔH_0 = - 64.5 kJ/mol)[34] and is used for regeneration of $Ca(OH)_2$.The calcination reaction (1.3) is the only endothermic reaction in the process. According to *Zeman and coworkers*[37] the sum of all reaction enthalpies is zero and the only energy cost that has to be paid is the overcoming of the mixing energy (~ 20 kJ/mol).

1.2.2.2 Acidification of carbonate solutions with electrochemical acid generation

Contrary to the previous described thermochemical methods, in these processes CO_2 is released by acidification according to

$$CO_3^{2-} + 2\ H^+ \rightarrow H_2O + CO_2 \qquad (1.11)$$

The acid is generated either by an electrodialysis or an electrolysis process. In conjunction with the acid generation the absorption base is regenerated. In both electrochemical processes the acidification process is either done inside the electrochemical cell (Figure 1.3) or outside of the cell by using an additional stripper (Figure 1.4). The major drawback of acidification inside the electrochemical cell is the production of gas inside the cell which increases the overpotential.

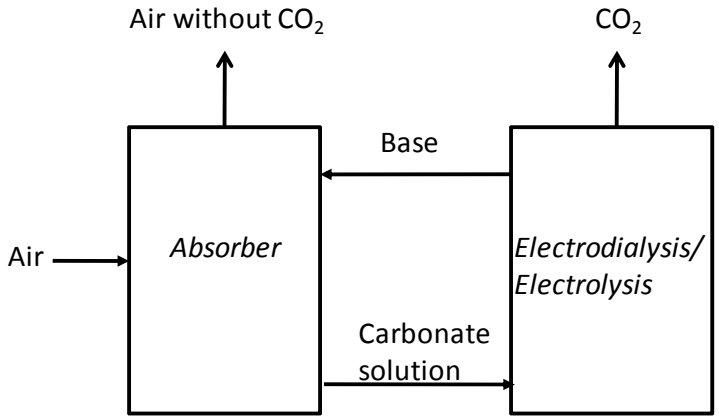

Figure 1.3 Schematic drawing of the acidification process inside the electrochemical cell

As shown in Figure 1.3 the carbonate solution (from the absorber) can be used as electrolyte solution for the electrodialysis or the electrolysis cell. Inside the electrochemical cell this solution is acidified thus CO_2 is released while the absorption base is regenerated. Figure 1.4 shows a schematic drawing of an acidification process outside an electrochemical cell in a stripper. In the stripper CO_2 is released and a salt solution is formed. The acid for the stripping is generated by an electrodialysis or an electrolysis process of the salt solution with simultaneous regeneration of the base.

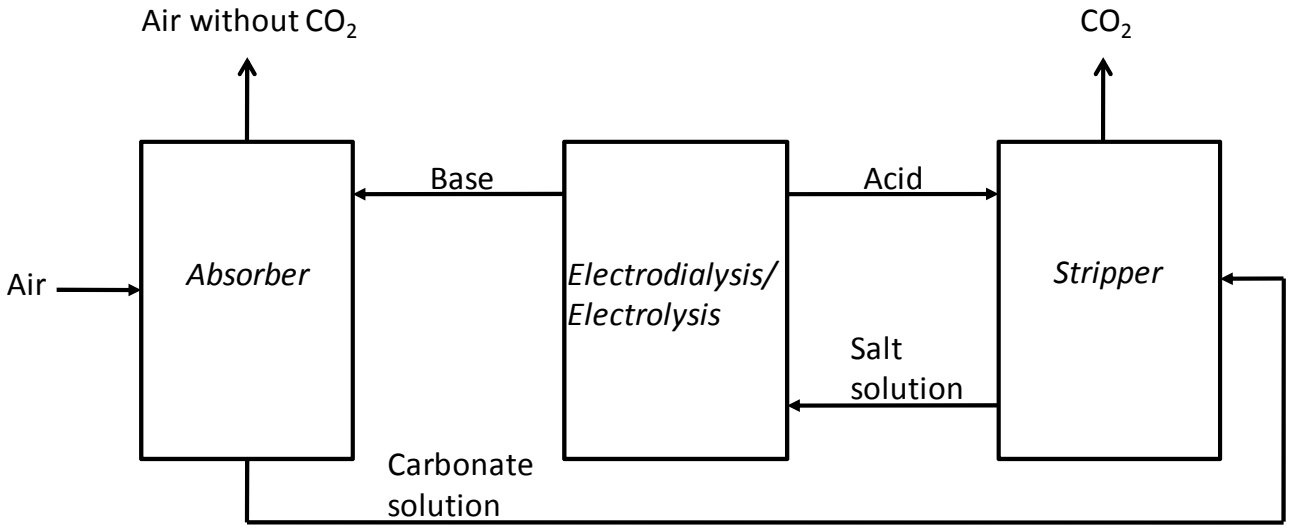

Figure 1.4 Schematic drawing of the acidification process outside the electrochemical cell

Both electrochemical processes (electrodialysis and electrolysis) for acid generation will be described in the following part. The electrodialysis process described in this chapter is based on an acidification outside the electrochemical cell. A possible acidification inside the electrochemical cell is described in Chapter 2 (2.2.2). For the electrolysis process both possibilities of acidification are described in the following and an additional possibility of acidification inside the cell (operating the electrolysis system under pressure) is described in Chapter 3 (3.4).

1.2.2.2.1 Electrodialysis

This electrochemical method to release CO_2 from a carbonate solution was proposed by *Specht and coworkers*[13]. Using a 1 M base solution (either NaOH or KOH) for the CO_2 capturing process results in the formation of a carbonate solution (see 1.1).The stripping acid as well as the absorption base are provided by an electrodialysis process of a sulfate salt. A potassium based cycle or a sodium based cycle are possible. As the solubility in water of

Na_2SO_4 is a factor of ~ 2 higher compared to K_2SO_4 (1.2 M for Na_2SO_4 ,0.6 M for K_2SO_4)[38,39] , *Specht and coworkers*[13] chose Na_2SO_4. Therefore the description of the process will be given here for the sodium based cycle (Figure 1.5). Air is enters the caustic soda scrubber column and CO_2 reacts with NaOH:

$$CO_2\ (g) + 2\ NaOH \rightarrow Na_2CO_3 + H_2O \tag{1.12}$$

The carbonate solution is transferred to the stripper column where CO_2 is released by acidification with sulfuric acid (H_2SO_4) according to the following reaction equation.

$$Na_2CO_3 + H_2SO_4 \rightarrow H_2O + CO_2 + Na_2SO_4 \tag{1.13}$$

As can be seen from the Hägg diagram in Figure 1.6, at $pH < 4$ CO_2 is in physical solution. The physical solubility of gases in water mainly depends on their partial pressure and on the temperature.[40] Therefore either increasing the temperature or decreasing the pressure releases gaseous CO_2 from the solution. The stripping acid, as well as the absorption base, are regenerated by an electrodialysis of a Na_2SO_4 solution.

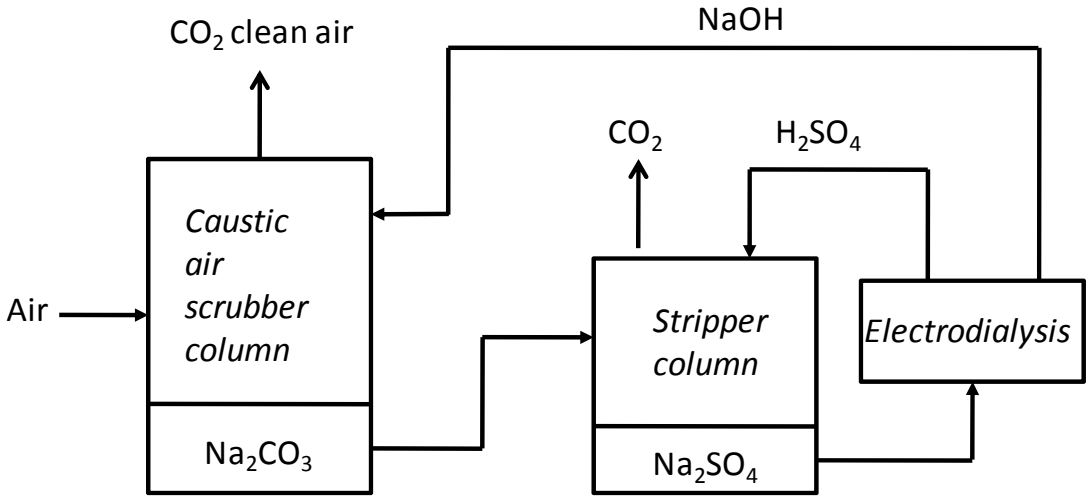

Figure 1.5 Schematic overview for the CO_2 recovery process based on *Specht et al*[13]

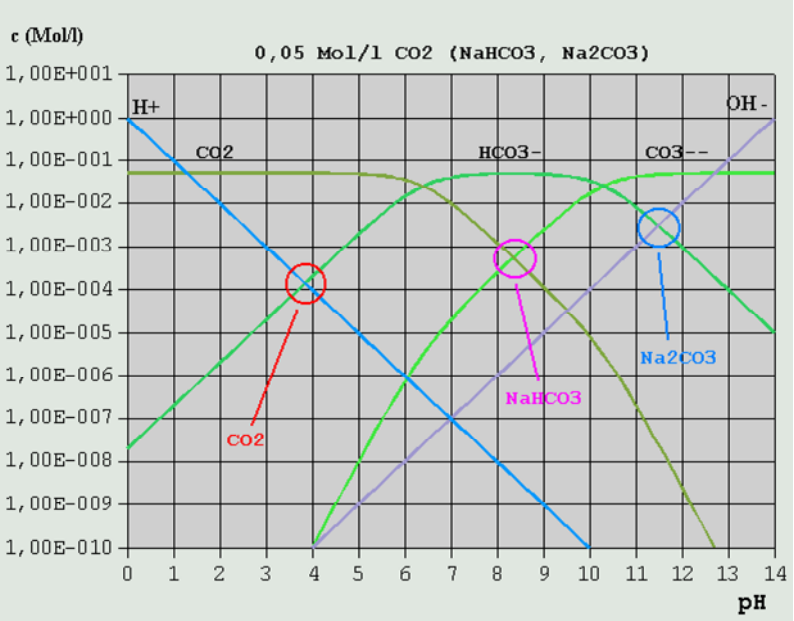

Figure 1.6 Hägg diagram for CO_2 and carbonates. Reprinted from Ref [41]

Electrodialysis processes for base and acid generation from a salt are well described in the literature.[42,43,44] An electrodialysis unit is an electrochemical cell that separates dissolved ions that make up the salt (Na^+ and SO_4^{2-}) to produce the corresponding acid and base, in this example sulfuric acid (H_2SO_4) and sodium hydroxide. This is done by water electrolysis, ion migration and ion exchange membranes (Figure 1.7).

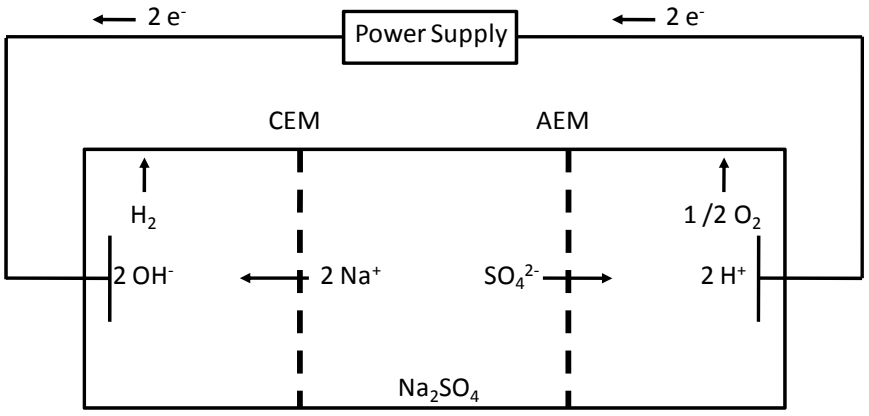

Figure 1.7 Schematic drawing of Na_2SO_4 splitting in a 3 compartment electrodialysis

In general, different ion exchange membranes are placed between 2 electrodes (anode and cathode). On the anode (positively charged electrode) water is oxidized to O_2

$$H_2O \rightarrow 2\,e^- + 2\,H^+ + \frac{1}{2}\,O_2 \qquad (1.\,14)$$

while protons are reduced on the cathode (negatively charged electrode) to hydrogen gas.

$$2\ H_2O + 2\ e^- \rightarrow H_2 + 2\ OH^- \qquad (1.15)$$

In the electric field, ions migrate towards the respective electrodes: anions to the anode and cations to the cathode. Ion selective membranes allow the migration of only one type of charged ion: only cations can pass through a cation exchange membrane (CEM) while anion exchange membranes (AEM) allow only the migration of anions. Figure 1.7 shows a scheme of a 3 compartment electrodialysis. A sodium sulfate (Na_2SO_4) solution is fed to the center compartment. Sodium ions can migrate across the CEM to the anode compartment and sulfate ions migrate across the AEM towards the cathode. Thus NaOH and H_2SO_4 are generated (both dissociated in aqueous solution). The overall reaction can be summarized as

$$H_2O + Na_2SO_4 \rightarrow NaOH + H_2SO_4 \qquad (1.16)$$

In the report by *Specht and coworkers*[11], an electrodialysis stack built up of bipolar (BPM) and cation exchange membranes (CEM) was used. A bipolar membrane consist of 2 ion exchange membranes (with opposite charge, AEM and CEM) in intimate contact (Figure 1.8) with the CEM ("+" label in Figure 1.8) side facing the anode and the AEM ("-" label in Figure 1.8) side facing the cathode. No ions can migrate through the BPM as always one of the membranes blocks the migration of ion with opposite charge. Only the diffusion of neutral species (e.g. H_2O) is possible. Note that the space between CEM and AEM in Figure 1.8 should represent the interface between these two membranes.

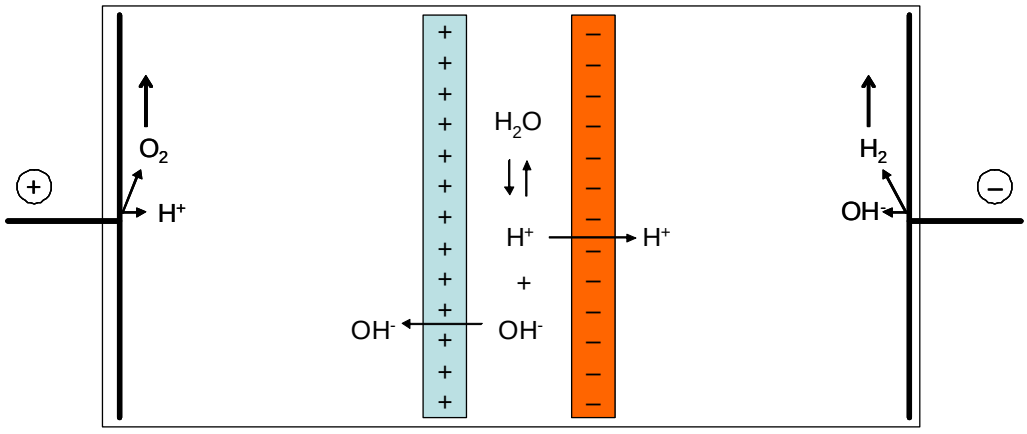

Figure 1.8 Working principle of a bipolar membrane. The "+" label represent the CEM and the "-" the AEM. Both membranes are in intimate contact. Reprinted with friendly permission from Ref [45].

At the interface of the 2 membranes building up the BPM, water is dissociated according to the autoprotolysis of water:

$$2\,H_2O \rightleftharpoons 2\,H^+_{aq} + 2\,OH^-_{aq} \qquad (1.17)$$

Only this dissociation enables the current flow over a BPM as the protons will migrate across the CEM to the cathode and the hydroxyl ions across the AEM to the anode respectively. The diffusion potential *e* under standard conditions can be calculated under a given concentration gradient over the membrane by

$$e = \pm(t_+ - t_-)\frac{RT}{nF}\ln\frac{(a_\pm)^1}{(a_\pm)^2}.^{40} \qquad \text{(eq. 1.2)}$$

In this equation t_+ *(*t_-*)* is the transfer number, *R* the ideal gas constant, *T* the temperature, *n* the ion charge, *F* the Faraday constant and $(a_\pm)$ is the mean activity. Using a CEM, the transfer number for negative ions (t_-) can be set to 0. As both transfer numbers sum up to one ($t_+ + t_- = 1$) t_+ is equal one for the CEM. The opposite is true for the AEM: in an ideal case, only negatively charged ions can migrate through the AEM membrane therefore $t_- = 1$ and $t_+ = 0$. Membrane potentials are additive and the free energy change from the interface of the two membranes to outside of the BPM is given by[46]

$$-\Delta G = nF\Delta E = RT\ln\left[\frac{(a_{H^+})^i(a_{OH^-})^i}{(a_{H^+})^o(a_{OH^-})^o}\right] \qquad \text{(eq. 1.3)}$$

where $(a_{H^+})^i$ ($(a_{OH^-})^i$) is the activity of H^+ (OH^-) inside the BPM (at the interface of the AEM and the CEM), $(a_{H^+})^o$ ($(a_{OH^-})^o$) is the activity of H^+ (OH^-) outside the BPM, *n* is the number of equivalents/mol of reactant, *ΔE* is the reversible electromotive force, *R* the ideal gas constant, *T* the temperature and *F* the Faraday constant . Only pure water is in the interior of the bipolar membrane thus its dissociation is given by K_W (water dissociation constant). At 25 °C

$$(a_{H^+})^i(a_{OH^-})^i = K_w = 10^{-13.995}\ mol^2/kg^2.^{47} \qquad \text{(eq. 1.4)}$$

For the generation solutions with $(a_{H^+})^o = (a_{OH^-})^o = 1$ the equation for the change in the free energy can be rewritten to

$$\Delta G = -F\Delta E = -RT\ln(a^i_{H^+}a^i_{OH^-}) \quad \text{or} \quad \Delta E = -\frac{RT}{F}\ln K_W \qquad \text{(eq. 1.5)}$$

since $n = 1$. For an ideal bipolar membrane, the theoretical potential for generation of acid and base is 0.83 V.[46] A simple formula for the theoretical potential calculation can be obtained by assuming $K_W = 10^{-14}$ mol^2/l^2. In addition $-\log(a_{H^+}) = pH$ and $-\log(a_{OH^-}) = pOH = 14 - pH$. Thus eq. 1.4 can be rewritten to

$$\Delta E = -\frac{RT}{F}\ln\left[\frac{10^{-14}}{10^{-pH_{Cathode}}10^{-(14-pH_{Anode})}}\right] = 0.059(pH_{Anode} - pH_{Cathode}) \qquad \text{(eq. 1.6)}$$

where pH_{Anode} is the pH value of the solution in the compartment facing the anode and $pH_{Cathode}$ for the solution in the compartment facing the cathode.

The water dissociation inside the bipolar membrane seems to be accelerated compared to aqueous solutions: acceleration factors of 10^6 – 10^7 are reported in the literature.[48,49] The reason for this enhancement is still not clear. The main explanations result in either a chemical reaction model or are based on the second Wien effect.[42] The chemical reaction model assumes reactions between ionic groups at the interface of the membranes with water[50]. The second Wien effect describes the influence of a high electric field on the dissociation rate constant (a high electric field can shift the equilibrium of a weak electrolyte towards the dissociated form)[51].

The working principle of an electrodialyis stack as used by *Specht and coworkers* [11] with alternating bipolar and cation selective membranes is depicted in Figure 1.9. In such type of electrodialysis unit, no pure acid and base can be generated but always a mixture of salt/acid or salt/base respectively.[13] For the generation of a stripping acid and an absorption base, it is not necessary to have pure products: only the pH difference is important. Thus ionic "impurities" from the salt do not matter. To simplify the following description only acid and base and not the mixtures with the salt are given.

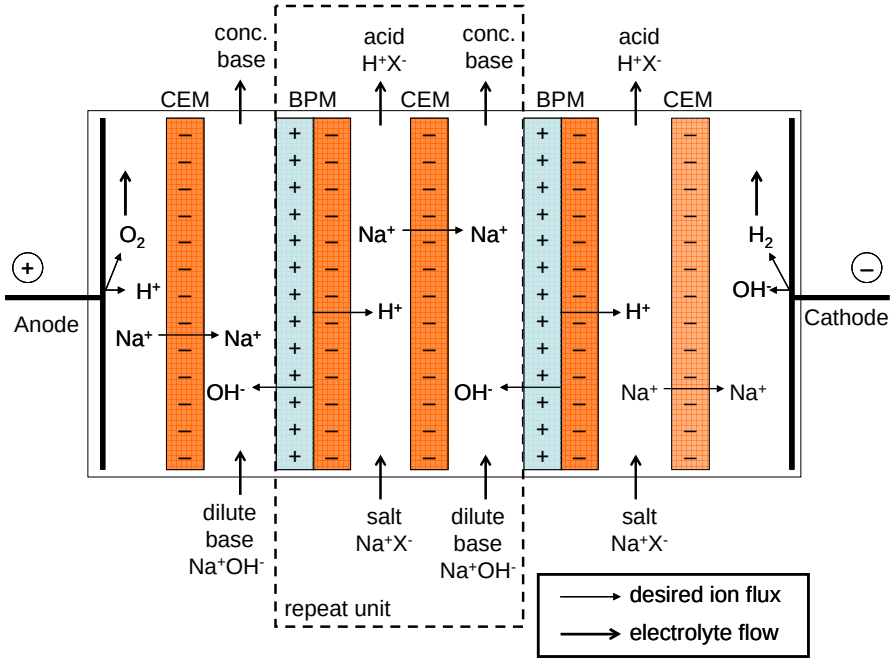

Figure 1.9 Working principle of an electrodialysis stack using bipolar and cation exchange membranes. Reprinted with friendly permission from Ref [45].

Due to the applied potential between the electrodes water is split into hydrogen and oxygen. The salt solution is fed to the dialysis stack in the compartments between BPM and CEM. A dilute base is the feeding solution for the compartments build up by CEM and BPM. As mentioned above, the only way to ensure a current flow over a perfect BPM is the dissociation of water molecules inside the BPM. In the electric field, Na^+ and H^+ ions migrate towards the cathode and OH^- ions towards the anode. Thus the dilute base will be concentrated and the salt solution is acidified. Usually an electroldialysis stack consists of many repeat units (alternating CEM and BPM). For this reason the amount of produced H_2 and O_2 is very small with respect to the produced acid and base.

An estimation for the thermodynamic potential for one repeat unit can be obtained by

$$\Delta E = 0{,}059\left(pH_{Anode} - pH_{Cathode}\right) + \frac{\Delta E_{el}}{x} \quad \text{(eq. 1.7)}$$ [45]

In eq. 1.7 ΔE_{el} is the necessary potential for the electrode reaction and x the number of repeat units. Under operation, current is flowing and each medium, although charges are moving, has a certain specific resistance: R_{ele} for the electrolytes, R_{CEM} for the CEM and R_{BPM} for the BPM. This can be summed up to

$$\Delta E_{operation} = 0{,}059\left(pH_{Anode} - pH_{Cathode}\right) + \frac{\Delta E_{el}}{x} + \left(R_{BPM} + R_{CEM} + R_{ele}\right) j \quad \text{(eq. 1.8)}$$

where j is the current density.[45]

In the report from *Specht and coworkers* [11], an electrodialysis stack from Berghof equipped with 6 CEM and 5 BPM was operated using CMH, CMX or CM1 from Tokuyama as CEM and Neosepta BP-1 as BPM. The maximum operating temperature of this bipolar membrane is around 45 °C and the maximum current density is 150 mA/cm^2. The voltage drop over one unit of CEM and BPM was found to be around 1.4 – 3.2 V at 50 – 100 mA/cm^2 depending on the used membranes. With the given setup, an 81 % integrated Faradaic efficiency at 45 % conversion was obtained. A main loss mechanism is the migration of H^+ instead of Na^+. This leads to a neutralization of OH^- and lowers therefore the efficiency. From the experiments it was concluded that around 280 kJ per mol of CO_2 are needed for the regeneration of the absorption and stripping solutions (at 50 mA/cm^2) using such an electrodialysis stack.
In the work of *Specht and coworkers*[11], methanol was synthesized from CO_2 captured from air. The main process steps are described above (Figure 1.5). In addition, high pressure water electrolyzers were used to generate H_2 for the fuel synthesis. A total energy demand of 1400 kJ per mol of methanol was calculated for the process using electrodialysis. The overall energetic efficiency for methanol synthesis from electricity, water and CO_2 from air was found to be ~ 46 %.

1.2.2.2.2 Electrolysis in a three or two chamber configuration

The main idea of this concept was described and studied by *Stucki and coworkers* .[12,52] They proposed to capture CO_2 from air with hollow fiber membranes filled with 0.5 M KOH. The absorption results predominantly in the formation of K_2CO_3. For the desorption of CO_2 from the carbonate solution and the simultaneous regeneration of KOH solution an acidification ,with electrochemical acid generation, is proposed. Three different electrochemical processes are described: Two and three chamber electrolysis of K_2CO_3 solutions (acidification inside the electrochemical cell) and two chamber electrolysis of K_2SO_4 solutions (acidification outside the electrochemical cell). The main advantage of all these three electrolysis processes is the production of hydrogen. In theory one mol H_2 per mol of desorbed CO_2 is generated. Thus the amount of hydrogen produced by the electrolyzer can be reduced.

1.2.2.2.2.1 Two chamber electrolysis with acidification inside the electrochemical cell

Figure 1.10 shows a schematic drawing of an electrochemical cell in which water electrolysis and CO_2 release are simultaneously performed. The cell is separated into two chambers by means of a CEM. The anolyte is K_2CO_3 from the absorber. At the anode water is oxidized and hydrogen is produced at the cathode. Due to the potential difference between anode and cathode cations migrate across the CEM from the anode to the cathode chamber. The

carbonate species are buffering between neutral and basic *pH*, depending on their concentration. As far more K^+ are present compared to H^+, mainly K^+ will be transported across the membrane. In the anode chamber K^+ is replaced by H^+ followed by the release of CO_2 from H_2CO_3:

$$H^+ + K_2CO_3 \rightarrow KHCO_3 + K^+ \quad (1.18)$$

$$H^+ + KHCO_3 \rightarrow H_2CO_3 + K^+ \quad (1.19)$$

$$H_2CO_3 \rightarrow H_2O + CO_2 \quad (1.20)$$

Together with the anode and cathode reactions (1.14 and 1.15) the total reaction equation for the two chamber electrolysis is the following

$$2H_2O + K_2CO_3 \rightarrow H_2 + \frac{1}{2} O_2 + CO_2 + KOH \quad (1.21)$$

Under the assumption of a 100 % efficiency for the K^+ transport across the membrane, H_2 and CO_2 are produced in equivalent amounts. As can be seen from (1.18) and (1.19) due to the acidification, first a bicarbonate ($KHCO_3$) solution is generated before CO_2 is released from the carbonic acid. The process must be optimized to minimize the carbonate concentration in the anolyte solution as non converted bicarbonate will be transferred to the cathode chamber (see Figure 1.10). The electrolyte solution in the cathode chamber is alkaline and therefore bicarbonate is neutralized to carbonate again. This decreases the overall efficiency of the process in respect of absorption liquid regeneration and CO_2 release. The product gases CO_2 and O_2 are generated in the same chamber and therefore a mixed gas stream leaves the cell. The gases have to be separated afterwards.

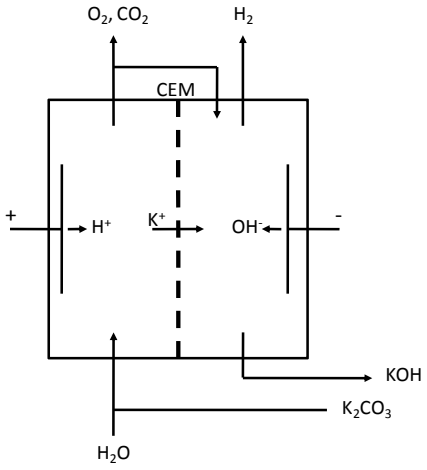

Figure 1.10 Two chamber electrochemical cell for electrolytic regeneration of absorption solution, stripping acid and hydrogen generation as proposed by *Stucki and coworkers*[52].

An electrochemical desorption cell was realized by a commercial available electrolysis cell from ElectroCell with an active area of 100 cm^2 and usually two cells were operated in a bipolar stack with j = 100 mA/cm^2. As CEM, Nafion 117 or Nafion 324 from DuPont were used. The electrolytes were usually kept at 70 °C. Different electrode configurations were realized towards a "zero gap" configuration were the electrodes are held in close contact to the membrane but separated by a metal spacer to avoid direct contact. In order to ensure a contact of the electrolyte soluiton with the membrane, holes were drilled into the electrodes. The holes of the electrodes where either matching each other or were displaced. As the $KHCO_3$ concentration is crucial for the process as mentioned above, the anolyte was chosen to be $KHCO_3$ and usually KOH was used as catholyte (both in aqueous solutions). Narrowing the gap resulted in decreased cell voltages but showed a reduced current efficiency for the transfer of K^+ most probably due to mass transfer limitations. More open electrode configurations (large holes, displaced) were found to perform better as they allow a better access of the electrolyte species. They found that the energy input for the best performing system for a stoichiometric mixture of CO_2 and H_2 (1:3) for methanol synthesis is around 1.4 MJ per mol of methanol.

1.2.2.2.2.2 Three chamber electrolysis with acidification inside the electrochemical cell

Another method for an electrochemical cell for CO_2 desorption from a carbonate solution and simultaneous regeneration of the absorption liquid proposed in the literature[53,52] is to use a three chamber geometry (Figure 1.11). The main idea is the same as previously described for the two chamber process with the difference that an additional CEM is used. Therefore O_2 and CO_2 are generated in different chambers and do not have to be separated afterwards which would be advantageous. However, an additional CEM causes an additional overpotential. Preliminary experiments carried out by *Stucki and coworkers* [52] showed that voltages > 4 V must be expected, which decreases the efficiency and therefore no further experiments were carried out.

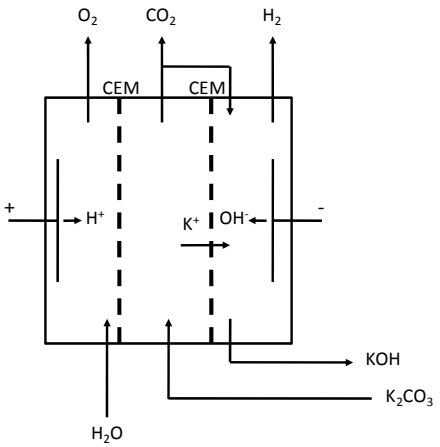

Figure 1.11 Three chamber electrochemical cell for electrolytic regeneration of absorbtion solution, stripping and hydrogen generation as proposed by *Stucki and coworkers*[52].

1.2.2.2.2.3 Two chamber electrolysis with acidification outside the electrochemical cell

Such process was described by The main idea of this process (Figure 1.12) is similar to the electrodialysis process described above. The carbonate solution from the absorber is neutralized with a $KHSO_4$ solution in order to release CO_2. During this neutralization reaction a K_2SO_4 solution is formed, which is used as electrolyte solution in a two chamber electrolysis process. Contrary to the bicarbonate process, the *pH* is stabilized at lower values to the sulfate/bisulfate buffer in the anode chamber. The KOH solution is recovered in the cathode chamber. From the $KHSO_4$ solution exiting the electrolysis cell, oxygen is separated prior to the CO_2 stripping process. From the KOH solution recovered from the cathode chamber, hydrogen is outgassed before it is transferred to the CO_2 absorber. Due to incomplete conversion of K_2SO_4 traces of it might be transferred to the absorber. Similar to the electrodialysis process, theses traces should not influence the process efficiency here.

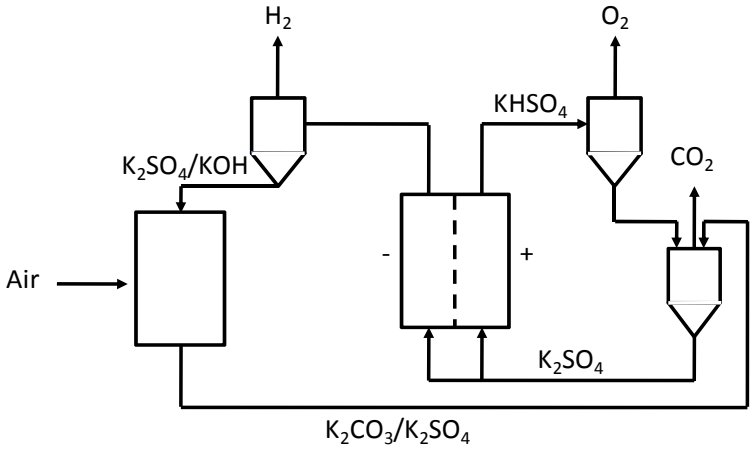

Figure 1.12 Schematic process overview for two chamber electrolysis using K_2SO_4 solutions as proposed by *Stucki and coworkers*[52]

Stucki and coworkers [52] tested the two chamber electrolysis process with 0.4 M K_2SO_4 as anolyte solution and KOH as catholyte in aqueous solution. The experimental setup was the same as previously described for the two chamber electrolysis using $KHCO_3$ and KOH as electrolytes. From their experimental data they concluded that, for a process shown in Figure 1.12, an efficiency of 60 % could be obtained depending on the degree of acidification of the sulfate solution. If the neutralization reaction is done with a 0.1 M $KHSO_4$ around 1 – 2 % O_2 impurities in the desorbed CO_2 can be expected.

1.2.3 Reduction of CO_2 into a Fuel

There are several possibilities for the reduction of CO_2 into a fuel as outlined in Figure 1.13. So called direct reduction processes include here electrochemical and photochemical methods. On the other hand CO_2 can be reduced to various fuels indirectly by using hydrogen gas or NADH with enzymes as catalysts.

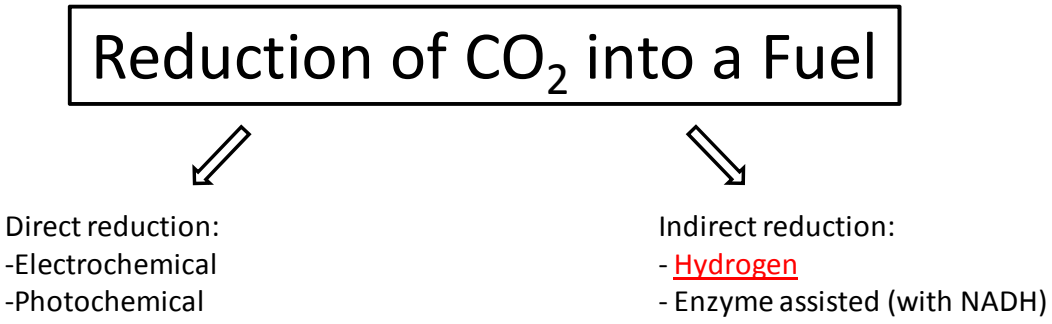

Figure 1.13 Overview of CO_2 reduction pathways

The direct reduction methods as well as the enzyme assisted reduction (using NADH) are still a topic of basic research. An overview over some literature reports is given in Chapter 5. On the other hand the reduction with hydrogen gas can be considered as industrial available and thus only this pathway will be discussed in this chapter. Currently around 110 Mt of CO_2 are used in the industry for synthesis of chemicals[54] such as urea, salicylic acid, cyclic carbonates and polycarbonates, where the largest CO_2 use is for the urea production,[55] but no fuels are produced industrially by reduction of pure CO_2 even if the possibilities are given. For the CO_2 reduction with hydrogen gas H_2 should be produced from carbon neutral sources. Water electrolyzers fulfill this requirement as water is split electrochemically into H_2 and O_2. An overview over state of the art water electrolyzers (including some basic considerations) is given in Appendix A.

1.2.3.1 Reduction with hydrogen

1.2.3.1.1 Methanol synthesis

The reaction equation for methanol synthesis is as follows:

$$CO_2 + 3\,H_2 \rightarrow CH_3OH + H_2O \quad . \qquad (1.22)$$

The reaction is exotherm ($\Delta H_R{}^0$ = -131.5 kJ/mol for liquid water and methanol and $\Delta H_R{}^0$ = -49.3 kJ/mol for gaseous products)[56]. Methanol is produced currently from CO and H_2 (syngas) using modified Cu-ZnO catalysts at 250 °C and pressures of 5 – 10 MPa. The thermodynamics for methanol production using CO_2 is thermodynamically not as favorable as if syngas is used. It seems like that even if syngas is used for methanol synthesis, the hydrogenated species on the catalyst surface is CO_2 (from CO by water gas shift reaction).[57] The usage of the $CuO/ZnO/ZrO_2$ catalysts currently used for syngas conversion are also active for the synthesis of methanol from CO_2 and H_2.[58] Addition of different oxide additives on the activity and structure of $CuO/ZnO/ZrO_2$ catalysts are under investigation in order to enhance the efficiency.[59] *Specht and coworkers*[11] used a commercially available catalyst form Südchemie AG for methanol synthesis from CO_2 and H_2 (80 bar, 260 °C) and report that in technical dimensions the process is feasible. In the literature a whole variety of catalyst for methanol synthesis at different parameters is described.[60] Mitsui Chemicals is building a pilot plant producing methanol from CO_2 and H_2 with an annual capacity of 100 t.[61] Methanol is a liquid hydrocarbon, which has advantages for distribution and it can be blended with gasoline/diesel to be used in internal combustion engines. It can be converted to various chemical products, especially interesting are the methanol-to-olefin (MTO) and the methanol-to-gasoline (MTG) process. In addition, in direct methanol fuel cells (DMFC) methanol is oxidized at the anode with air to CO_2 and water while producing electricity. Nobel laureate G. Olah therefore proposes the "Methanol Economy" beyond the area of abundant and cheap oil and gas.[62] However methanol has a disadvantage: it is corrosive and therefore distribution over the existing fuel structures like gas stations and pipelines is difficult.[15]

1.2.3.1.2 Methane synthesis

The methanation of carbon dioxide

$$CO_2 + 4\,H_2 \rightarrow CH_4 + 2\,H_2O \qquad (1.23)$$

is a strong exothermic reaction ($\Delta H_R{}^0$ = -252.7 kJ/mol for liquid and $\Delta H_R{}^0$ = -164.7 kJ/mol for gaseous water)[56]. Compared to other synthesis processes the CH_4 synthesis is very selective. The methanation is linked with the water gas shift reaction

$$CO + H_2O \rightarrow CO_2 + H_2 \quad . \tag{1.24}$$

The hydrogenation of CO_2 happens in two steps: a retro shift reaction followed by methanation of carbon monoxide

$$CO + 3\,H_2 \rightarrow CH_4 + H_2O \tag{1.25}$$

But a direct methanation of CO_2 can not be excluded. As the hydrogenation of carbon oxides is exothermic, low temperatures (200 – 400 °C) and higher pressures are preferred. Ni is often used as catalyst as it is highly selective for methane. [15] Other reported catalyst are based on Fe_2O_3, Co/Cu/K, RuO_2-TiO_2, Ni-Ru-Pt-Ir-Al_2O_3, Ni-La_2O_3-Ru dispersed on silica, Mo_2C, Fe_3C, WC and Ni particles in a ZrO_2 matrix.[60] Since natural gas and SNG (substitute or synthetic natural gas) mainly consist of methane, the distribution via the natural gas grid seems feasible. In addition natural gas vehicles are becoming available nowadays from a variety of car manufacturers.[63] The city of Vienna is currently subsidizing up to 3 000 € for taxis running on natural gas.[64]

1.2.3.1.3 DME synthesis

Dimethyl ether (DME) is the simplest of all ethers and is a colorless, non toxic and non corrosive gas. It is generally handled as a liquid and stored in pressurized tanks. It has a high cetane number (55 – 60) and thus it can be effectively used in diesel engines.[15,62] The production proceeds via methanol dehydration reaction using solid acids such as alumina or phosphoric acid modified γ-Al_2O_3.

$$2\,CH_3OH \rightarrow CH_3OCH_3 + H_2O \tag{1.26}$$

In countries like Japan, Korea and China, this is already an industrial process (~ 4 millon t DME per year are produced).[57] Alternatively, DME can be produced from syngas with special catalyst.

1.2.3.1.4 Other fuels

The conversion of CO_2 into fuels is a well known technology. Several other possible fuels synthesized from CO_2 are reported like formic acid, dimehtyl carbonate, etc.[58] Light olefins and liquid hydrocarbons can be obtained from hydrogenation of CO_2 over various kinds of iron based catalyst similar to the Fischer Tropsch (FT) chemistry of CO and H_2.[65] Due to the variety of products obtained, the FT based process seems to be only useful for a large scale production.

1.3 Summary and outline

Possible ways for recycling atmospheric CO_2 into of useful fuels were discussed in this chapter. The main process steps are capturing of CO_2 from air, subsequent release of pure CO_2 and its reduction into a fuel. The main focus was on the usage metal hydroxide solutions, like NaOH or KOH, as absorption liquid, thus forming carbonate solutions. From these carbonate solutions CO_2 can be desorbed either by thermochemical cycles or by acidification. Two possible electrochemical methods, electrodialysis and electrolysis, for acid generation and simultaneous absorption liquid regeneration were described. Thermochemical methods seem to be more interesting for large scale application (GW plants) whereas the methods based on acidification have advantages in smaller scale plants. Acidification of the carbonate solutions can be done either inside or outside the electrochemical cell. The pure CO_2 has to be reduced afterwards into a fuel. Reduction of CO_2 can be either done directly or indirectly. The industrially most mature way is the reduction with hydrogen gas. Hydrogen from non carbon based source can be obtained by using water electrolyzers. Several synthesis routes, including methane and methanol, were described.

Several researchers have already implemented CO_2 recycling processes and claim good efficiencies by using various strategies. Two very interesting ways were outlined by *Stucki and coworkers*[52] and *Specht and coworkers*. [13] Both of them used metal hydroxide based solutions for CO_2 capturing and acidifications methods for the CO_2 release. While *Stucki and coworkers* [52] suggest a two chamber electrolysis process for acid generation and absorption base regeneration, *Specht and coworkers* [13] use an electrodialysis process. As shown by *Specht and coworkers* [13], the main energy consuming parts in such a system are the water electrolyzer and the electrodialysis unit. Increasing the efficiency of these two processes will enhance the process efficiency.

A prototype for the "atmospheric CO_2 to fuel" process will be described in Chapter 2. The main aim of the work presented in this thesis was to increase the efficiency of such a process by increasing the CO_2 desorption efficiency. The two chamber electrolysis process seems to be advantageous over the electrodialysis due to simultaneously produced H_2. Therefore a systematic study on two chamber electrolysis of sulfate solutions was conducted in lab scale and is presented in Chapter 3. In addition a further operating possibility for the two and three chamber electrolysis systems is discussed in Chapter 3.

The state of the art water electrolyzers are the alkaline ones (see Appendix A). Even though they show good efficiencies they are operated under harsh conditions. Water splitting at neutral *pH* (like in nature) could be done at 1.23 V (calculated form thermodynamics). But

usually high overpotentials are observed. From the two half reactions, the oxidation of water is considered to be more difficult. Recent reports show that a catalyst for this reaction can be formed in situ upon electrolysis on various types of electrodes showing a Faradaic efficiency of 100 %.[66,67] The usage of such a catalyst could help to improve the process efficiency. As one focus was the implementation in either the two or three chamber electrolysis for CO_2 desorption, the formation as well as the stability of the catalyst was investigated by means of in situ spectroelectrochemistry. A possible implementation was found to be the three chamber electrolysis process with sodium sulfate as electrolyte and preliminary experiments were performed. The results are presented in Chapter 4.

In Chapter 5 an overview over other CO_2 reduction strategies is given and in Chapter 6 a final conclusion can be found.

1.4 References

[1] R.A. Kerr, *Science*, **317**, 2007, 437

[2] K. Richardson, W. Steffen, H.J. Schellnhuber, J. Alcamo, T. Barker, D.M. Kammen, R. Leemans, D. Liverman, M. Munasinghe, B. Osman-Elsha, N. Stern, O. Waever, *Synthesis report from Climate Change: Global Risks, Challenges & Decisions*, University of Copenhagen, 2009, www.climacongress.ku.dk

[3] S. Enthaler, *Chem.Sus.Chem.,***1**,2008, 801 -804

[4] Solomon, S., D. Qin, M. Manning, R.B. Alley, T. Berntsen, N.L. Bindoff, Z. Chen, A. Chidthaisong, J.M. Gregory, G.C. Hegerl, M. Heimann, B. Hewitson, B.J. Hoskins, F. Joos, J. Jouzel, V. Kattsov, U. Lohmann, T. Matsuno, M. Molina, N. Nicholls, J. Overpeck, G. Raga, V. Ramaswamy, J. Ren, M. Rusticucci, R. Somerville, T.F. Stocker, P. Whetton, R.A. Wood and D. Wratt, 2007: Technical Summary. In: *Climate Change 2007: The Physical Science Basis. Contribution of Working Group I to the Fourth Assessment Report of the Intergovernmental Panel on Climate Change* [Solomon, S., D. Qin, M. Manning, Z. Chen, M. Marquis,K.B. Averyt, M. Tignor and H.L. Miller (eds.)]. Cambridge University Press, Cambridge, United Kingdom and New York, NY,USA

[5] N.S. Lewis, D.G. Nocera, *P. Natl. Acad. Sci. USA.*, **103(43)**, 2006, 16729-15735

[6] http://www.ior.com.au/ecflist.html

[7] R. Priwasser, J. Felber, A. Kollmann, H. Steinmüller, R. Ticher, *Solar Fuel Endbericht*, 2009

[8] S. Fukuzumi, *Eur. J. Inorg. Chem.,* **9**, 2008, 1351-1362

[9] K.M. Kerry, I.G. Curcic, J. Gabriel, S.C.E. Tsang, *Chem.Sus.Chem.,***1**,2008, 893 -899

[10] http://co2now.org

[11] A. Bandi, M. Specht, T. Weimer, K. Schauber, *Energy Convers. Mgmt.,* **36(6-9)**, 1995, 899-902

[12] S. Stucki, A. Schuler, M. Constantinescu, *Int. J. Hydrogen Energy,* **20(8)**, 1995, 653-663

[13] M. Specht, A. Bandi, M. Elser, A. Heberle, U. Maier, K. Schaber, T. Welmer,*CO_2 Recycling zur Herstellung von Methanol, Endbericht*, 2001

[14] M. Specht, A. Bandi, M. Elser, F. Staiss, *Advances in Chemical Conversions for Mitigating Carbon Dioxide* in T.Inui, M. Anpo, K. Izui, S. Yanagida, T. Yamaguchi (Eds) *Studies in Surface Science and Catalysis*, Vol. 114, 1998, 363-366

[15] U. Zuberbühler, A. Bandi, M. Specht, *Screening of Methods of CO_2 Capture with Subsequent Fuel Synthesis in Remote Areas,* ZSW, 2009

[16] J.K. Stolaroff, D.W. Keith, G.V. Lowry, *Environ. Sci. Technol.*, **42**, 2008, 2728-2735

[17] J.K. Stolaroff, *Doctoral thesis: Capturing CO_2 from Ambient Air: a feasibility assessment,*Carnegie Mellon University Pittsburgh, 2006

[18] K.S. Lackner, *Eur. Phys. J. Special Topics,* **176**, 2009, 93-106

[19] R.V. Siriwardane, M.-S. Shen, E.P. Fisher, J.A. Poston, *Energy&Fuels*, **15**, 2001, 279-284

[20]http://www.chemgapedia.de/vsengine/vlu/vsc/de/ch/10/adsorption/anwendungen/anwendung_adsorption.vlu/Page/vsc/de/ch/10/adsorption/anwendungen/anwendungsprinzipien/druckwechseladsorption.vscml.html

[21] *Standard thermodynamic properties of chemical substances* and *Thermodynamic properties of aqueous systems* In D.R. Lide (Ed) *CRC Handbook of Chemistry and Physics,* electronic version 0.9, CRC Press LLC, 2002

[22] M.K. Dubey, H. Ziock, G. Rueff, S. Elliott, W.S. Smith, *Am. Chem. Soc. – Division of Fuel Chemistry Reprints*, **47(1)**, 2002, 81-84

[23] V. Nikulshina, D. Hirsch, M. Mazzotti, A. Steinfeld, *Energy*, **31**, 2006, 1379-1389

[24] V. Nikulshina, C. Gebald, A. Steinfeld, *Chem. Eng. J.*, **146**, 2009, 244-248
[25] M. Halmann, A. Steinfeld, *Energy Fuels*, **17**, 2003, 774-778
[26] Merck Chemicals, *Sicherheitsdatenblatt $Ca(OH)_2$,* Merck kGaA, Darmstatt, 2009
[27] *Physikalisch Chemische Eigenschaften: Kaliumhydroxid* in *BGIA Gestis Stoffdatenbank*: http://biade.itrust.de/
[28] *Physikalisch Chemische Eigenschaften: Natriumhydroxid* in *BGIA Gestis Stoffdatenbank*: http://biade.itrust.de/
[29] T. Weimer, K. Schaber, M. Specht, A. Bandi, *Energy Convers. Mgmt.*, **37(6-8)**, 1996, 1351-1356
[30] S.Stucki, A. Schuller, M. Costantinescu, *Int. J. Hydrogen Energy*, **20 (8)**,1995 , 653-663
[31] V. Nikulshina, A. Ayesa, M.E. Galvez, A. Steinfeld, *Chem. Eng. J.*, **140**, 2008, 62-70
[32] S. Atchariyawut, R. Jiraratananon, R. Wong, *Sep. Purif. Technol.*, **63**, 2008, 15-22
[33] L. Lackner, P. Grimes, H.J. Ziock, http://www.netl.doe.gov/publications/proceedings/01/carbon_seq/7b1.pdf
[34] F. Zeman, *Environ. Sci. Technol.*, **41**, 2007, 7558-7563
[35] R. Baciocchi, G. Storti, M. Mazzotti, *Chem. Eng. Process.*, **45**, 2006, 1047-1058
[36] D.W. Keith, M. Ha-Duong, J. Stoalroff, *Climatic Change*, **74**, 2006, 17-45
[37] F. Zeman, *Environ. Sci. Technol.*, **41**, 2007, 7558-7563
[38] *Physikalisch Chemische Eigenschaften: Kaliumsulfat* in *BGIA Gestis Stoffdatenbank*: http://biade.itrust.de/
[39] *Physikalisch Chemische Eigenschaften: Natriumsulfat* in *BGIA Gestis Stoffdatenbank*: http://biade.itrust.de/
[40] G.M. Barrow, Bearb: G.W. Herzog, *Physikalische Chemie,* Bohmann-Verlag, Wien, 1984
[41] http://www.wissenschaft-technik-ethik.de/wasser_ph.html#330
[42] S. Koter, A. Warszawski, *Pol. J. Environ. Stud.*, **9 (1)**, 2000, 45-56
[43] S.M. Davis, G.E. Gray, P.A. Kohl, *J. Appl. Electrochem.*, **38**, 2008, 777-783
[44] F.G. Wilhem, *PhD. Thesis: Bipolar Membrane Electrodialysis,* Universtiy of Twente, Twente University Press, 2001
[45] M. Egginger, G. Waldstein, A. Fuchsbauer, E. Portenkirchner, M. Kruijen, B. Meana Esteban, E. Avci, P. Thamyongkit, D. Egbe, K. Oppelt, P. Trefflinger, S. N. Sariciftci *,Solar Fuel Project overview*, LIOS, 2009
[46] K.N. Mani, *J. Membr. Science*, **58**, 1991, 117-138
[47] *Ionization constant of normal and heavy water* in D.R. Lide (Ed) *CRC Handbook of Chemistry and Physics,* electronic version 0.9, CRC Press LLC, 2002
[48] M. Hein, A. Grabowski, *Produktion von Säuren und Laugen mittels bipolarer Membranen"; Praktikum für Studenten der Technischen Biologie;* ZSW, 2003
[49] H. Strathmann, J.J. Krol, H.-J. Rapp, G. Eigenberger, *J. Membr. Sci.*,**125** ,1997, 123-142.
[50] J.Blaster, D.F. Stamatialis, M. Wessling, *Chem. Eng. Process.*, **43**, 2004, 1115-1127
[51] C.H. Hamann, W. Vielstich, *Elektrochemie I*, VCH Verlagsgesellschaft, 1985
[52] S. Stucki, M. Constantinescu, A. Schuler, *NEFF Projekt Nr. 467 Schlussbericht*, 1993
[53] M. Steinberg, Patent US 4197421, 1980
[54] M. Aresta, A. Dibenedetto, *Dalton Trans.*, **28**, 2007, 2975-2992
[55] H. Arakawa, M. Aresta, J.N. Armor, M.A. Barteau, E.J. Beckman, A.T. Bell, J.E. Bercaw, C. Creutz, E. Dinjus, D.A. Dixon, K. Domen, D.L. DuBois, J. Eckert, E. Fujita, D.H. Gibson, W. Goddard, D.W. Goodman, J. Keller, G.J. Kubas, H.H. King, J.E. Lyons, L.E. Manzer, T.J. Marks, K. Morokuma, K.M. Nicholas, R. Periana, L. Que, J. Rostrup-Nielson, W.M.H. Sachtler, L.D. Schmidt, A. Sen, G.A. Somorjai, R.C. Stair, B.R. Stults, W. Tumas, *Chem.Rev.,***101**, 2001, 953-996
[56] *Standard Thermodynamic Properties of Chemical Substances* in D.R. Lide (Ed) *CRC Handbook of Chemistry and Physics,* electronic version 0.9, CRC Press LLC, 2002

[57] G.A. Olah, A. Goeppert, G.K.S. Prakash, *J. Org. Chem.,* **74**, 2009, 487-498
[58] K.M.K. Yu, I. Curcic, J. Gabriel, S.C.E. Tsang, *Chem. Sus. Chem.,* **1,** 2008, 893-899
[59] J. Słoczynski, R. Grabowski, P. Olszewski, A. Kozłowska, J. Stoch, M. Lachowska, J. Skrzypek, *Appl. Catal. A: Gen*, **310**, 2006,127-137
[60] M.M. Halmann, *Chemical Fixation of Carbon Dioxide,*CRC Press, Inc. 2000, Chapter 5
[61] http://www.mitsuichem.com/release/2008/080825e.htm
[62] G.A. Olah, G.K.S. Prakash, *Beyond Oil and Gas: The Methanol Economy,* Wiley-VCH Verlag, Weinheim, 2006
[63] http://www.erdgasautos.org/erdgasautos/erdgasautos-modelle-opel-34.htm
[64] http://www.wien.gv.at/amtshelfer/umwelt/umweltschutz/foerderung-erdgastaxis.html
[65] J.S. Kim, S. Lee, S.B. Lee, M.J. Choi, K.W. Lee, *Catal. Today*, **115**, 2006, 228-234
[66] M.W. Kanan, D.G. Nocera, *Science*,**321**,2008,1072-1075
[67] Y. Surendranath, M. Dinca, D.G. Nocera, *J. Am. Chem. Soc.*, **131**, 2009,2615-2620

Chapter 2

The "Solar Fuel Alpha Prototype": An example of a working CO_2 recycling setup

The company Solar Fuel Technology GmbH & Co KG[1] was founded in the year 2007 with the main goal to develop technologies for converting CO_2 from air into a fuel. In the year 2008 the Linz Institute of Organic Solar Cells (LIOS)[2] at the JKU joined this project. In the same year it was decided that a demonstration plant, the so called "Solar Fuel Prototype" will be built by the ZSW[3] group in Stuttgart by order of Solar Fuel GmbH & Co KG. The working principle of the Prototype is based on the work by *Specht et al*[4]. To use renewable energy like wind or solar energy and water to convert carbon dioxide from air into a fuel, is the main concept.

2.1. Introduction

Different types of renewable energies can be converted electricity. This electricity drives the Solar Fuel Module to produce a CO_2 neutral fuel (Figure 2.1). One requirement is a pure CO_2 source. The Solar Fuel module can extract CO_2 from nearly any CO_2 containing gas source but the main application is to use atmospheric CO_2. After pure CO_2 is obtained it has to be reduced, which is done in the demonstration plant with H_2.

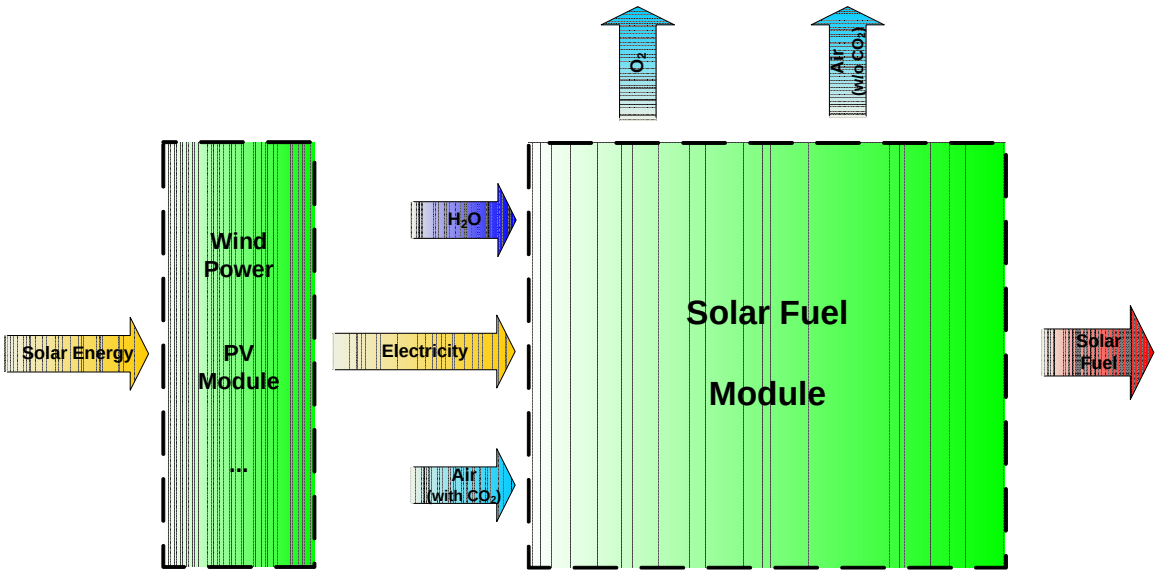

Figure 2.1 Simplified flow diagram showing the Solar Fuel concept. Reprinted with friendly permission from Ref. [5].

The main components of the prototype are an absorber for CO_2, an electrodialysis stack for CO_2 release, a water electrolyzer for H_2 generation and a fuel reactor. The fuel synthesized by the prototype is methane. Methane can be used as fuel in natural gas cars thus the prototype has the connectors to fuel such a vehicle. A detailed flow diagram of the Solar Fuel prototype is depicted in Figure 2.2. Water, air and a sodium hydroxide (NaOH) solution are fed to the absorber where CO_2 is converted into a sodium carbonate solution (Na_2CO_3). In the electroldialysis, CO_2 is released from the Na_2CO_3 solution by acidification and NaOH is recovered back. In the electrolysis unit (electrolyzer) water is split into H_2 and O_2 electrochemically. Hydrogen and carbon dioxide are transferred in stoichiometric amounts (4:1) to the methane reactor where the fuel is produced. Exhaust gases in the process are only CO_2 depleted air and O_2. The principles of the different steps were already described in Chapter 1 thus the main focus in this chapter is the technical description.[6] The prototype is built for a methane production of 20 m³ per day.

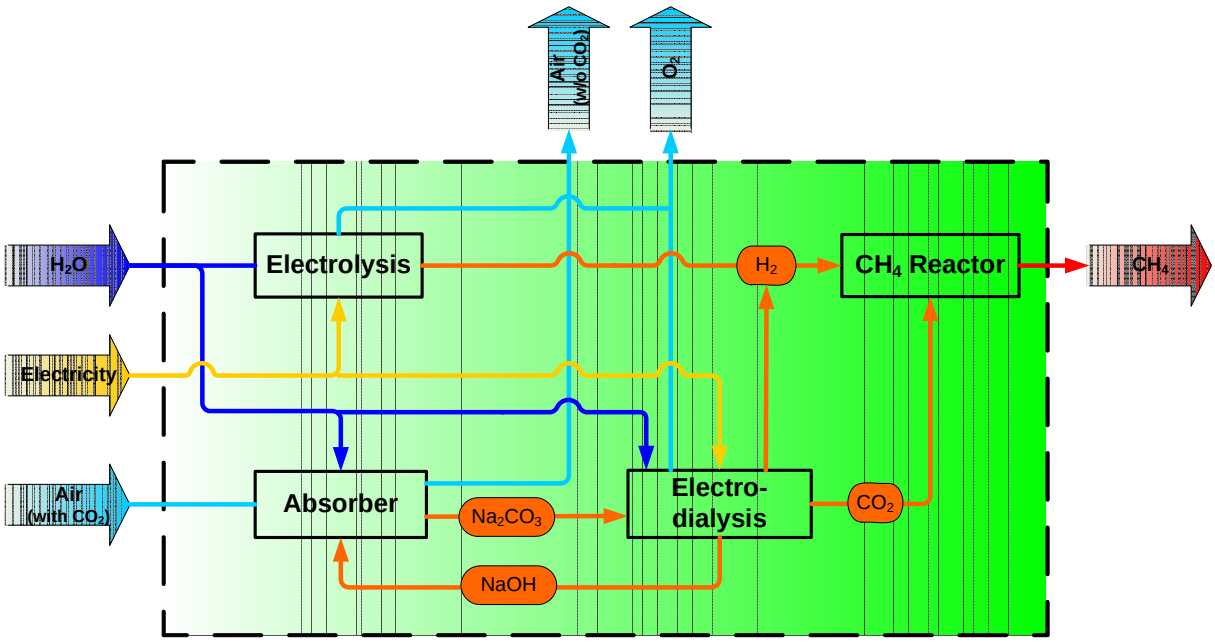

Figure 2.2 Detailed flow diagram of the Solar Fuel prototype. Reprinted with friendly permission from Ref. [5].

2.2. Description of the different parts of the prototype

2.2.1 Absorber

The usage of NaOH ensures a very low partial pressure of CO_2 over the absorption liquid which allows absorption. Before air enters the absorber, it is wetted in a humidifier to ensure a saturation of water in air. Due to the humidification, evaporative water losses in the absorber are minimized. In the absorber itself, air and aqueous NaOH solution flow in opposite directions. With a high surface area, a good conversion of CO_2 into Na_2CO_3 is achieved. The air flow is obtained by a fan. A nearly complete conversion is necessary as non converted NaOH causes losses in the electrodialysis. A 1 M NaOH solution is used as absorption base. In the flow of 0.5 M Na_2CO_3 (80 – 100 l/h) as transport liquid the NaOH concentration should be lower than 0.02 M. Note that a NaOH conversion of 95 % corresponds to 0.05 M NaOH.[6]

2.2.2 Electrodialysis

The main working principle of an electrodialysis was already described previously in Chapter 1: electricity is used in this electrochemical cell to split a salt into its corresponding acid and base. Contrary to the electrodiaylsis (ED) process described in Chapter 1 where a Na_2SO_4 was used as salt for the electrodialysis, the carbonate solution (Na_2CO_3) is fed directly into the ED

stack. H^+ ions, generated in the bipolar membrane (BPM), are used for acidification of the carbonate solution. In order to prevent gaseous CO_2 in the electrodialysis (causing an enhanced overpotential due to gas bubbles), the stack is operated under pressure, thus CO_2 stays in physical solution inside the ED stack and is released afterwards in a stripper. The electrodialysis is operated in a continuous "Feed and Bleed" mode. In the "Feed and Bleed" process a certain volume of electrolytes is continuously circulated through the electrodialysis stack and smaller volumes of base are withdrawn (Bleed) and of salts are added (Feed). A schematic drawing of the electrodialysis unit can be seen in Figure 2.3. As in one loop constantly liquid is withdrawn or added, respectively, a bypass from the acid to the storage base tank ensures the volume neutrality of the process.

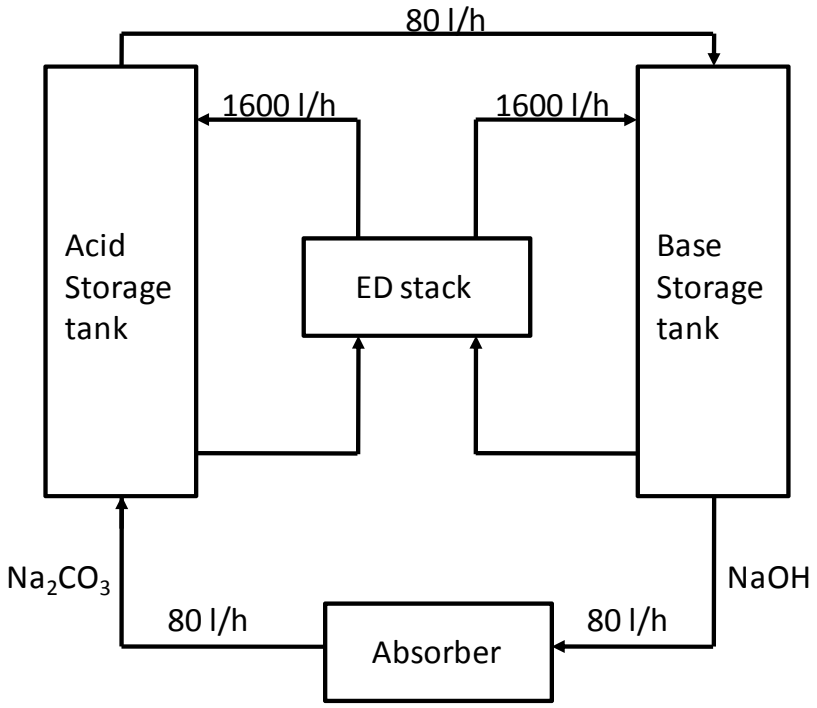

Figure 2.3 Schematic drawing of the Feed and Bleed electrodialysis process

Due to procedural reasons there is one more loop besides the two electrode compartments (electrode loop) for the gas/liquid separation. Acid, base and electrode loop have storage tanks of 100 l each. In the base loop ~ 1 M NaOH and in the acid loop a Na_2CO_3 solution with $pH < 4$ are circulated (1600 l/h each). The withdrawal of absorption base (80 l/h of 1 M NaOH) is carried out continuously at the exit of the base loop.The addition of the Na_2CO_3 solution from the absorption tower (80 l/h of 0.5 M Na_2CO_3) is done at the exit of the acid loop. Due to the acidification, CO_2 is released but stays in physical solution as the electrodialysis is operated at 2.5 bar. In a subsequent stripper CO_2 is released by decompression and removed by means of

underpressure. With a circulation of 1600 l/h in the acid loop a pressure difference of 0.85 bar is needed for the release of 40 mol_{CO2}/h. The CO_2 stripper is part of the acid loop of the electrodialysis thus unreleased CO_2 in the stripper does not influence the electrodialysis performance as the solution is compressed again before entering the stack. The electrodialysis stack is provided by Hescon GmbH and is a so called two chamber electrodialysis consisting of 80 membrane pairs (consisting of alternating CEM and BPM). The effective cell area is 560 cm^2. The operating temperature is limited to 40 °C due to the stability of the bipolar membranes.

The adjacent methane reactor requires a continuous and exact CO_2 dosing for a high product quality. Thus a buffer tank and a mass flow controller are installed. The O_2 content of the gas has to be monitored in order to prevent the formation of an ignitable mixture of hydrogen and oxygen gas in the reactor. The buffer tank is pressurized and has a volume of ~ 80 l. The CO_2 production of around 50 min can be stored in this tank.[6]

2.2.3 Water electrolyzer

Since alkaline electrolyzers are the technically most mature type, such an electrolyzer is implemented in the Solar Fuel prototype. As mentioned before, they operate either at ambient pressure or as pressurized systems. The electrolyte is usually a 20 – 40 % aqueous KOH solution. For the methane reactor pressurized hydrogen is needed, therefore a pressurized system is beneficial. Due to given process details, the electrolyzer should produce 4 Nm^3/h at a pressure of 10 bar. A commercial available alkaline electrolyzer G10 from ErreDue srl[7] is implemented in the Solar Fuel prototype. The maximum production rate of H_2 is 6 Nm^3/h with a pressure of 10 bar. The purity of the produced hydrogen is 99.3 – 99.8 %. [6]

2.2.4 Methane synthesis

The reactor converts CO_2 and H_2 into methane and water

$$4\,H_{2\,(g)} + CO_{2\,(g)} \rightleftharpoons CH_{4\,(g)} + 2\,H_2O_{\,(g)} \qquad \Delta H_R^0 = -164.7\ \text{kJ/mol}\ ^{8} \tag{2.1}$$

The reaction can be divided into a CO retro shift reaction (2.2) and the hydrogentation of carbon monoxide (2.3)

$$H_{2\,(g)} + CO_{2\,(g)} \rightleftharpoons CO_{\,(g)} + H_2O_{\,(g)} \qquad \Delta H_R^0 = -41.2\ \text{kJ/mol}\ ^{8} \tag{2.2}$$

$$3\,H_{2\,(g)} + CO_{\,(g)} \rightleftharpoons CH_{4\,(g)} + H_2O_{\,(g)} \qquad \Delta H_R^0 = -205.9\ \text{kJ/mol}\ ^{8} \tag{2.3}$$

From the standard reaction enthalpies it can be seen that all 3 reaction (2.1 – 2.3) are exothermic. Therefore the reactions are favored at lower temperatures. In addition, the volume

of reactants is higher than the volume of products under the assumption of ideal gases (more mol of reactants compared to products) thus higher pressures shift the equilibria to the product side. For economical reasons and due to the high selectivity, a Ni based catalyst is used, as both reactions, retro shift and CO hydrogenation, are catalyzed. A scheme of the methane synthesis part of the prototype is shown in Figure 2.4. The actual reactor consists of two reactors in order to ensure the right temperature profile. Thus to each reactor an oil thermostat is attached. Hydrogen and carbon dioxide are mixed before entering the reactor and preheated. Carbon and coke might deposit on the catalyst and deactivate it, therefore steam is added to the gas mixture if needed. Steam is created with the waste heat from the oil thermostat. Inside the reactor the temperature needs to be higher than 200 °C otherwise toxic nickel carbonyl compounds may be formed. The reactors are operated at 500 – 220 °C with a pressure < 10 bar. The catalyst is based on Ni. The methane/steam mixture leaving the reactor 1 and 2, respectively, is cooled and liquid water and methane are separated due to procedural reasons.[6]

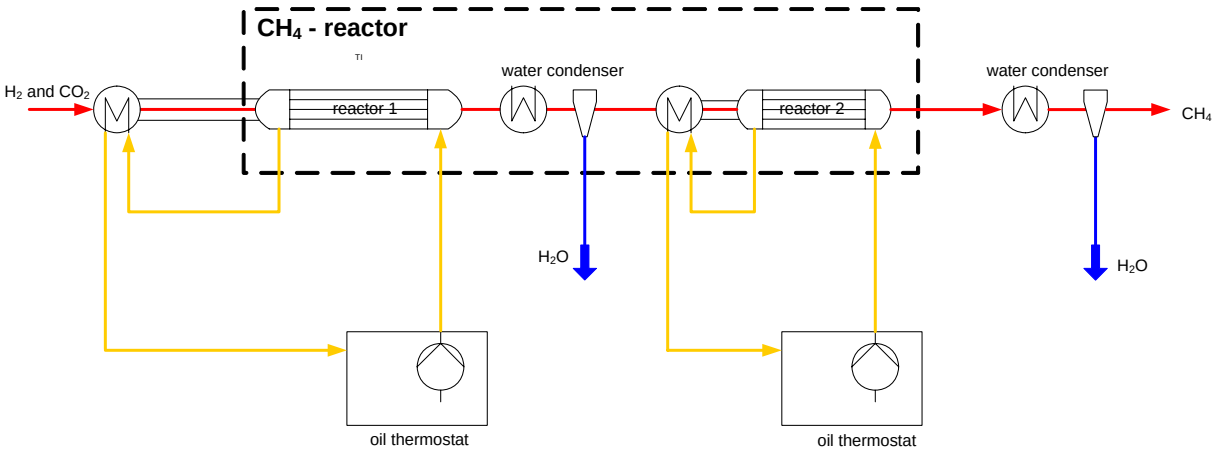

Figure 2.4 Schematic flow chart of the methane reactor

2.2.5 Car fuelling system

The fuelling system is a so-called "Fast fill" construction which allows a filling in approximately 5 min. This is achieved by using a high pressure buffer tank system. Most of the gas stations for natural gas vehicles use this system. On the contrary, "Slow fill" constructions directly pump the gas out of the gas grid into the tank of the car without a buffer tank in between. Thus more time is required for the fuelling using a "Slow fill" system and it is usually used in private fueling stations in companies.[9]

In order to make sure that the produced methane gas meets the demands of natural gas it has to be dried prior to storage under pressure. Non dried gas would cause icing of several parts because the gas is expanded (and thus cooled) during fuelling. After this cooling the methane

gas is stored in a buffer tank with 80 l volume. An additional drying of the gas is required to meet the quality standard for the fuelling of cars and this is done with water adsorption on molecular sieves. The gas has to be repressurized afterwards (~ 200 bar) by a compressor before storage in high pressure tanks (with 80 l each). The prototype is equipped with a standard fuel nozzle for natural gas cars and a burning torch in case no methane is needed.[6]

2.2.6 The containers

The Solar Fuel prototype consists of two containers with the size of ~ 6 x 2.5 x 2.9 m (L x W x H) each. A schematic drawing of them can be seen in Figure 2.5. One container is dedicated to the CO_2 production and the other one to the fuel synthesis. The CO_2 production container comprises the air humidifier (and a fan), the absorber tower including pumps, the electrodialysis with the CO_2 stripper and the compressor. The fuel synthesis container is divided into 2 parts: the components for the methane synthesis and the fuelling system. The methane synthesis section consists of the water electrolyzer, the methane reactor and chillers. The fuelling system contains all components for the processing of methane gas and the buffer tanks. The containers are placed parallel to each other and occupy a space of around 30 m^2. Each container has its own control panel and both are controlloed via a computer with LabVIEW software. As gases are produced, there are safety monitoring systems including monitoring of gases, fire detection and breakdown detection of the controlling software. In case of danger, the hardware is switched off. Both electrodialysis and water electrolyzer need pressured air for valve switching. A compressor for air is installed in the fuel synthesis container. Deionized water is needed for the water electrolyzer, the methane reactor and the electrodialysis stack. It is generated by a DI water cartridge installed in the fuel synthesis container and the quality is monitored.

The complete prototype was first operated in November 2009 at the ZSW in Stuttgart.[1]

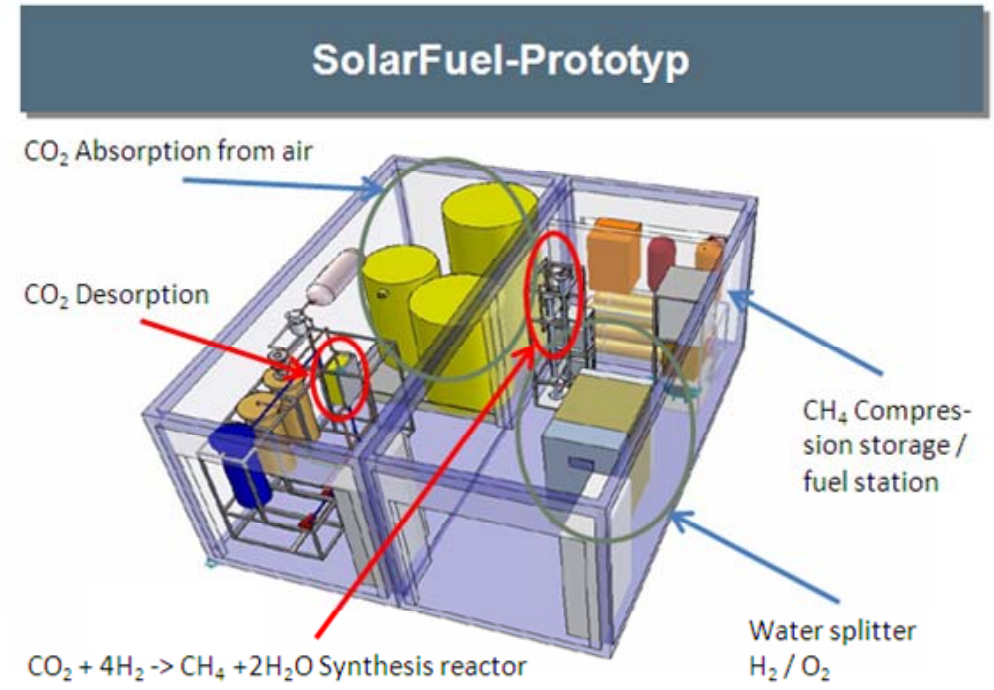

Figure 2.5 Schematic drawing of the Solar Fuel prototype**.** Thanks to the ZSW for providing the picture.

2.2.7 Flow charts of the Solar Fuel prototype

A flow chart of the whole Solar Fuel container is shown in Figure 2.6.

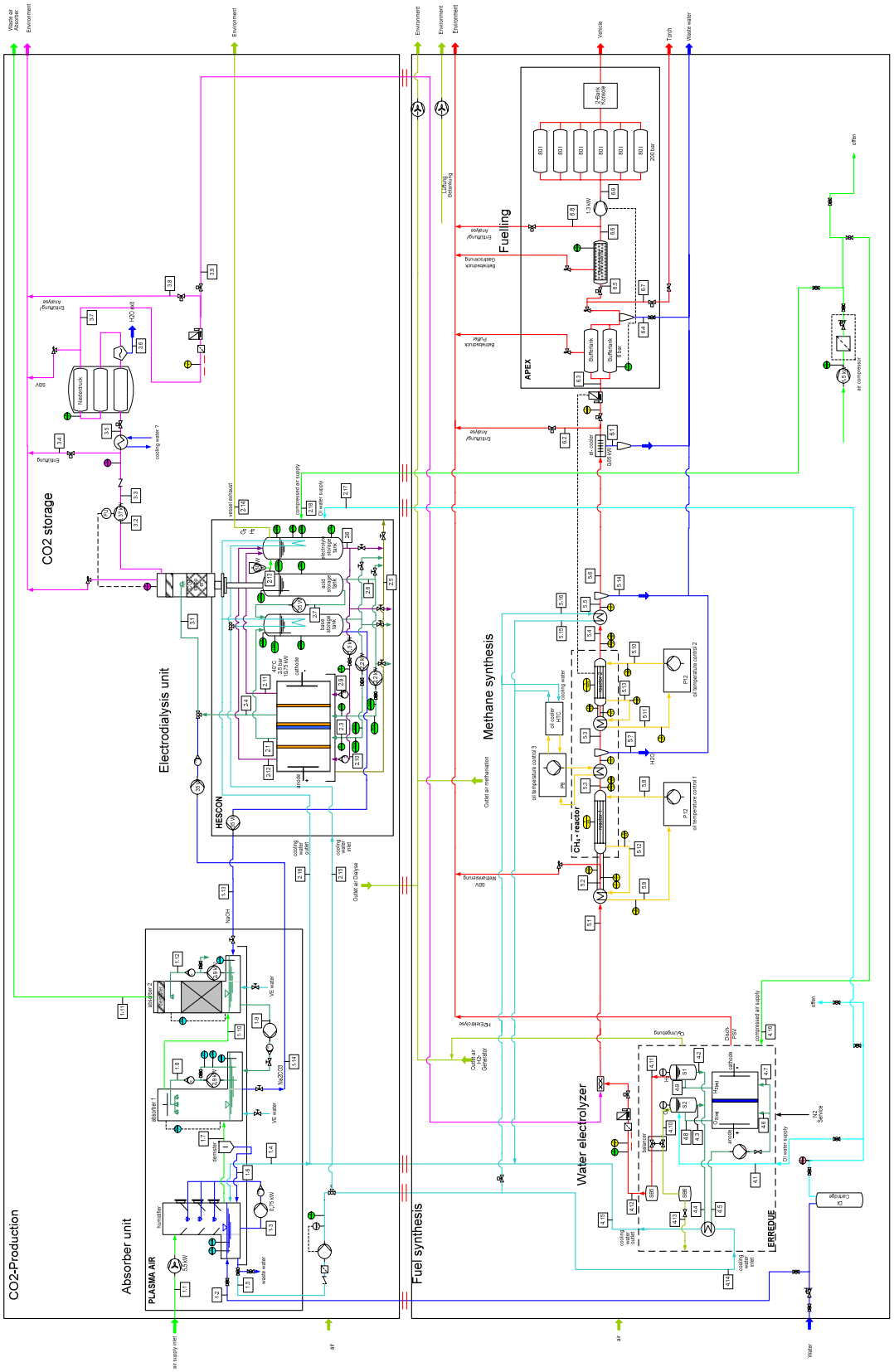

Figure 2.6 Flow chart of the Solar Fuel prototype. Thanks to E. Portenkirchner for providing the picture.

2.3 References

[1] http://www.solar-fuel.com/
[2] http://www.lios.at
[3] http://www.zsw-bw.de/index.html
[4]M. Specht, A. Bandi, M. Elser, A. Heberle, U. Maier, K. Schaber, T. Welmer,*CO_2 Recycling zur Herstellung von Methanol, Endbericht*, 2001
[5] M. Egginger, G. Waldstein, A. Fuchsbauer, E. Portenkirchner, M. Kruijen, B. Meana Esteban, E. Avci, P. Thamyongkit, D. Egbe, K. Oppelt, P. Trefflinger, S. N. Sariciftci *,Solar Fuel Project overview*, LIOS, 2009
[6] U. Zuberbühler, A. Bandi, M. Specht, F. Baumgart, B. Stürmer, B. Feigel, *Aufbau einer containerintegrierten Versuchsanlage zur CO_2 Absorption aus der Luft mit anschließender Kraftstoffproduktion CH_4*, Lastenheft, 2009
[7] http://www.erreduegas.it/en/
[8] *Standard Thermodynamic Properties of Chemical Substances* in D.R. Lide (Ed) *CRC Handbook of Chemistry and Physics,* electronic version 0.9, CRC Press LLC, 2002
[9] http://www.erdgasautos.at/tanken/

Chapter 3

Two and three chamber electrolysis

Release of concentrated CO_2 from the absorption liquid is a crucial point in terms of energy demand in a CO_2 recycling process like described in Chapter 2. In the prototype this is achieved by using an electrodialysis stack. The main working principle of the electrodialysis is the usage of bipolar and cation selective membranes. In the bipolar membranes H^+ and OH^- ions are generated due to autoprotolysis of water at the interface between an anion and a cation selective membrane (see Chapter 1). Hydrogen and oxygen generation are highly suppressed in the electrodialysis and the energy demand can only be assigned to the CO_2 release and the regeneration of the absorption base. Using a two chamber electrolysis process can result in a slightly higher energy demand but at the same time as CO_2 is released (or the stripping acid is generated) hydrogen is produced. This is advantageous as for methane synthesis four moles of hydrogen per mol of CO_2 are necessary. Thus using an electrolysis process as described below in this chapter has the potential to reduce the total energy demand.

3.1 Introduction

From the absorption tower a Na_2CO_3 solution is obtained from which CO_2 has to be released and the absorption liquid (NaOH) has to be recovered. The acidification process can be done inside the electrochemical cell in which the acid is generated or outside (Figure 3.1). An electrodialysis process with acidification outside the electrochemical cell was previously described in Chapter 1. The electrodialysis operated in the Solar Fuel prototype is an example of an acidification process outside the electrochemical cell (see 2.2.2).

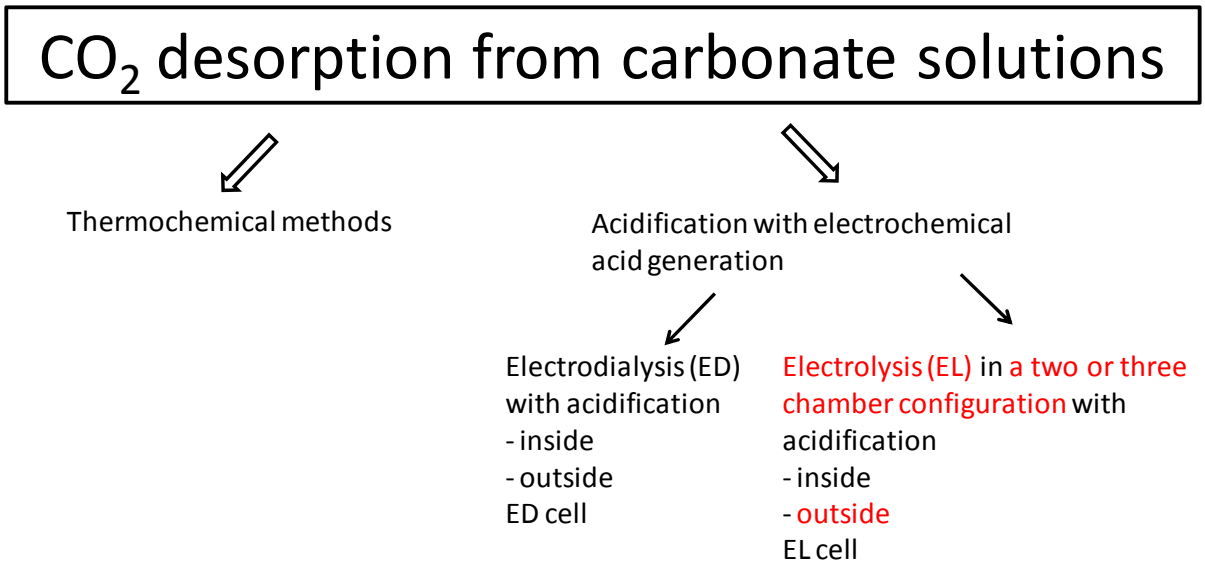

Figure 3.1 Scheme of different CO_2 desorption methods from carbonate solutions

Direct electrolysis of a carbonate solution would result in a mixture between CO_2 and O_2 and the two gases have to be separated afterwards. This is again energy demanding and a complicated processes.[1] Thus using a system in which CO_2 and O_2 are generated separately seems to be more promising and was already proposed in the literature.[2] The flow diagram in Figure 3.2 shows the main idea behind this process: As described before CO_2 is absorbed from the air using a NaOH solution. This generates a carbonate solution from which concentrated CO_2 is released by acidification (addition of a stripping acid). If sulfuric acid is used as an stripping acid the release of CO_2 results in the formation of a sodium sulfate solution which is afterwards used as electrolyte solution. Due to the electrolysis the stripping acid as well as the absorption liquid can be gained back.

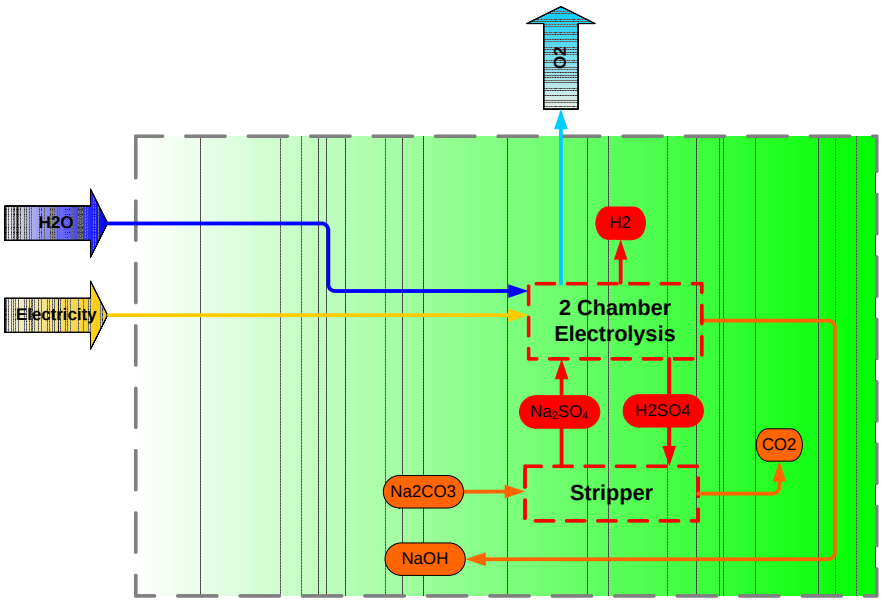

Figure 3.2 Flow diagram with using a two chamber electrolysis process of sodium sulfate solutions. Reprinted with friendly permission from Ref [3].

The electrolysis of sulfate solutions is the main part in this project idea and was therefore studied in detail. Electrolysis of sulfate solutions is not new and is studied well in literature as sodium sulfate is a by-product of many industrial processes (eg. pulp mills). Research focuses on the production of pure sulfuric acid and sodium hydroxide (caustic soda). For this reason usually three chamber systems with cation and anion selective membranes or bipolar membranes are used.[4,5] In the given process the stripping acid as well as the absorption liquid do not have to be as pure as possible because carrying over of some sodium sulfate will not influence the process much, as it is operated in a closed loop. We have focused on the studies of a two and three chamber electrolysis system. These two electrolysis systems will be described separately in the following part in more detail.

3.1.1 Two chamber electrolysis system

A schematic drawing of the two chamber electrolysis system can be seen in Figure 3.3. The electrolysis cell consists of two chambers that are separated from each other by means of a cation selective membrane. Each chamber contains an electrode: In one chamber the potential bias to the electrode is positive therefore this is the anode chamber where water is oxidized and O_2 and H^+ is generated. This leads to an acidification of the sulfate solution in this chamber. The other electrode has a negative potential bias therefore acting as cathode. On the cathode H^+ is reduced to hydrogen and OH^- is generated leading to an increase of the *pH* in

this chamber. Under the influence of the electric field cations (Na^+ or H^+) will migrate through the cation selective membrane towards the cathode to close the electric circle.

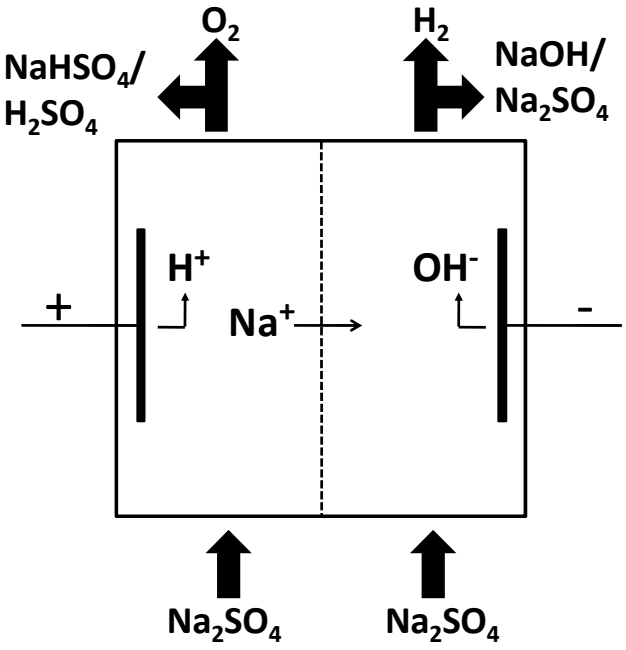

Figure 3.3 Schematic drawing of a two chamber electrolysis of a sodium sulfate solution

This process can be described in more detail as follows:

Due to the applied potential bias water is electrolyzed inside the cell. On the anode water is oxidized and on the cathode protons are reduced:

$$\begin{aligned} &\text{Cathode: } 2\,H_2O + 2\,e^- \rightarrow H_2 + 2\,OH^- \\ &\text{Anode: } \quad H_2O \rightarrow \frac{1}{2}\,O_2 + 2\,H^+ + 2\,e^- \\ &\overline{\qquad\qquad\qquad\qquad\qquad\qquad\qquad\qquad\qquad\qquad} \\ &\qquad 3\,H_2O \rightarrow H_2 + 2\,OH^- + \frac{1}{2}\,O_2 + 2\,H^+ \end{aligned} \tag{3.1}$$

The sodium sulfate salt is dissociated in water and does not take part in the water splitting reaction. Due to the electric field between the anode and the cathode positive ions migrate from the anode chamber towards the cathode chamber. This includes migration through the membrane. In an ideal case only Na^+ should be transported through the membrane but usually the permselectivity for cation exchange membranes is not perfect resulting in a migration of H^+ towards the cathode chamber and of of OH^- to the anode chamber in the electric field, respectivley. Membranes like Nafion® 324 are reinforced composites of two sulfonic films that differ in their equivalent weight and show therefore a barrier for OH^- diffusion through

the membrane if mounted correctly.[2,6] This process results in a buildup of a *pH* difference between anode and cathode chamber: The *pH* value in the anode chamber will decrease due to the production of protons whereas in the cathode chamber the pH value will be increased as OH^- ions are produced. Migration of H^+ or OH^- through the membrane can therefore be accounted as a loss mechanism as these ions will counterbalance the buildup of a *pH* difference. By monitoring the *pH* value in each chamber an estimation on how much Na^+ was migrating into the cathode chamber can be obtained.

The stripping solution (H_2SO_4) will be used afterwards to release CO_2 from the Na_2CO_3 solution according to:

$$H_2SO_4 + Na_2CO_3 \rightleftharpoons CO_2 + Na_2SO_4 + H_2O \tag{3.2}$$

The whole process can be summarized as follows:

$$\begin{aligned} 3\ H_2O &\rightarrow H_2 + 2\ OH^- + \frac{1}{2}\ O_2 + 2\ H^+ \\ Na_2SO_4 + 2\ H^+ &\rightarrow H_2SO_4 + 2\ Na^+ \\ \underline{H_2SO_4 + Na_2CO_3} &\underline{\rightarrow CO_2 + Na_2SO_4 + H_2O} \\ 2\ H_2O + Na_2CO_3 &\rightarrow CO_2 + 2\ NaOH + H_2 + \frac{1}{2}O_2 \end{aligned} \tag{3.3}$$

Thus in theory per mol H_2 produced one mol of CO_2 is released and two moles of NaOH are regenerated. This process splits two moles of water. The produced NaOH can be used in the absorber to form Na_2CO_3.

3.1.2 Three chamber electrolysis process

Figure 3.4 shows a schematic drawing of the three chamber process: It is comparable to the two chamber process with one additional chamber due to the use of one additional membrane. In the middle chamber no electrodes are immersed in the electrolyte solution. Two different types of membranes can be used separate to the middle chamber from the anode compartment: A cation selective or a bipolar membrane. The electrode reactions are the same as in the two chamber electrolysis (3.1). Using a cation selective membrane results in a similar process as in the two chamber geometry: Protons generated in the anode compartment move towards the middle compartment through the membrane. This leads to an acidification of the middle compartment and mainly sodium ions migrate through the second cation selective membrane towards the cathode chamber. Due to the cathodic reaction the alkalinity of the solution in the respective chamber is increased. By using a bipolar membrane to separate anode and middle compartment the working principle is different. As bipolar

membranes consist of an anion and a cation selective membrane in close contact to each other, no ions can migrate through the membrane because either the anion or the cation selective membrane is blocking the ion movement. But neutral species like H_2O can diffuse into the membrane. At the interface of these two membranes autoprotolysis of water into H^+ and OH^- takes place. If the bipolar membrane is mounted correctly into an electrochemical cell (cation exchange membrane facing the cathode and anion selective membrane facing the anode, respectively) H^+ and OH^- can migrate in the electric field from the interface inside the membrane towards the respective electrodes. The migration of these ions ensures the electric contact over the membrane.[7,8,9] Therefore the bipolar membrane is acting similar to a "salt bridge" connecting two electrochemical half cells. This setup was here mainly used to determine the potential drop over bipolar and cation selective membranes.

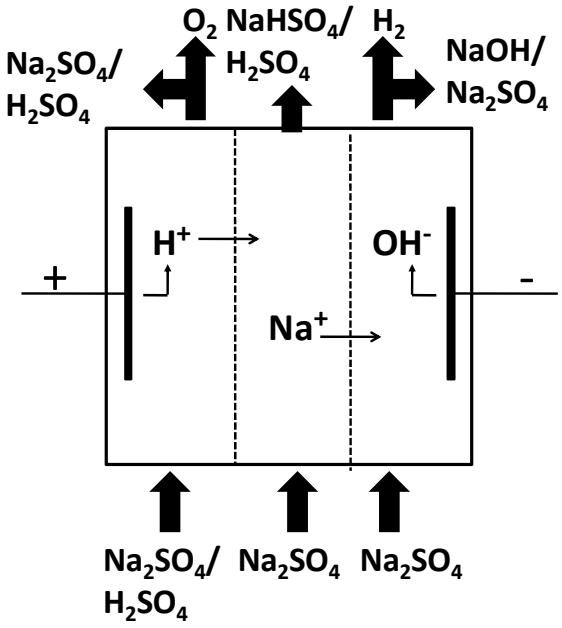

Figure 3.4 Schematic drawing of a three chamber electrolysis of sodium sulfate solutions.

3.2 Experimental

For testing the two and three chamber electrolysis process a Micro Flow Cell from ElectroCell[10] was used. As anode DSA (dimension stable anode, from ElectrocCell) and as cathode Pt/Ti (platinized Titania, form ElectroCell) was used unless stated otherwise. Figure 2.4a shows a picture of the different components of the Micro Flow cell: The cell consist of 2 PTFE end frames which have each 2 inlets and 2 outlets for the electrolyte. This means in total 4 chambers in the cell can be built where each chamber has an own in- and outlet. The

two end frames are more or less identical with one exception: One end frame has four recessed holes that allow the insertion of four guide pins. The four guide pins (PTFE) are mounted into the other end frame. These guide pins allow the proper alignment of the gaskets and the electrodes. Stainless steel endplates (2 pieces) provide additional mechanical support for the cell and the inlet and outlet holes are numbered on each plate. The cell assembly hardware consists of 60 mm long head bolts and nuts which are used to tighten the cell by screwing together. The actual chambers of the cell are build up by flow frames (PTFE) and gaskets (Viton). Inside the gasket usually a PVDF flow mesh is placed to guarantee turbulence flow conditions inside the chamber. There are 3 different types of gaskets: end frame gaskets with four holes, electrode gaskets which have a center cut corresponding to the active area and 2 diagonal cut holes and membrane gaskets with only the active area cut out without holes. The holes in the gaskets and the flow frames ensure the electrolyte solution flow.

To build a two chamber (see Figure 3.5b) cell one end frame with guide pins is placed on top of an end plate. An end frame gasket is put on top of this and the first electrode is added on top. The next step is building of the flow chamber itself which consists of the following parts: an electrode gasket, a flow frame with a flow mesh and a membrane gasket. On top of the membrane gasket the membrane is laid and completes the first chamber. Then the second chamber is built in mirror image way: membrane gasket, flow frame with flow mesh and an electrode gasket. This is followed by the second electrode, an end frame gasket and the second end frame with an end plate. The cell is then pressed together and tightened by screwing the screw bolts on the 6 screws and appropriate tube fittings are inserted into the designated inlet and outlet holes. Usually the cell was tightened using a torque wrench (~ 0.6 Nm).

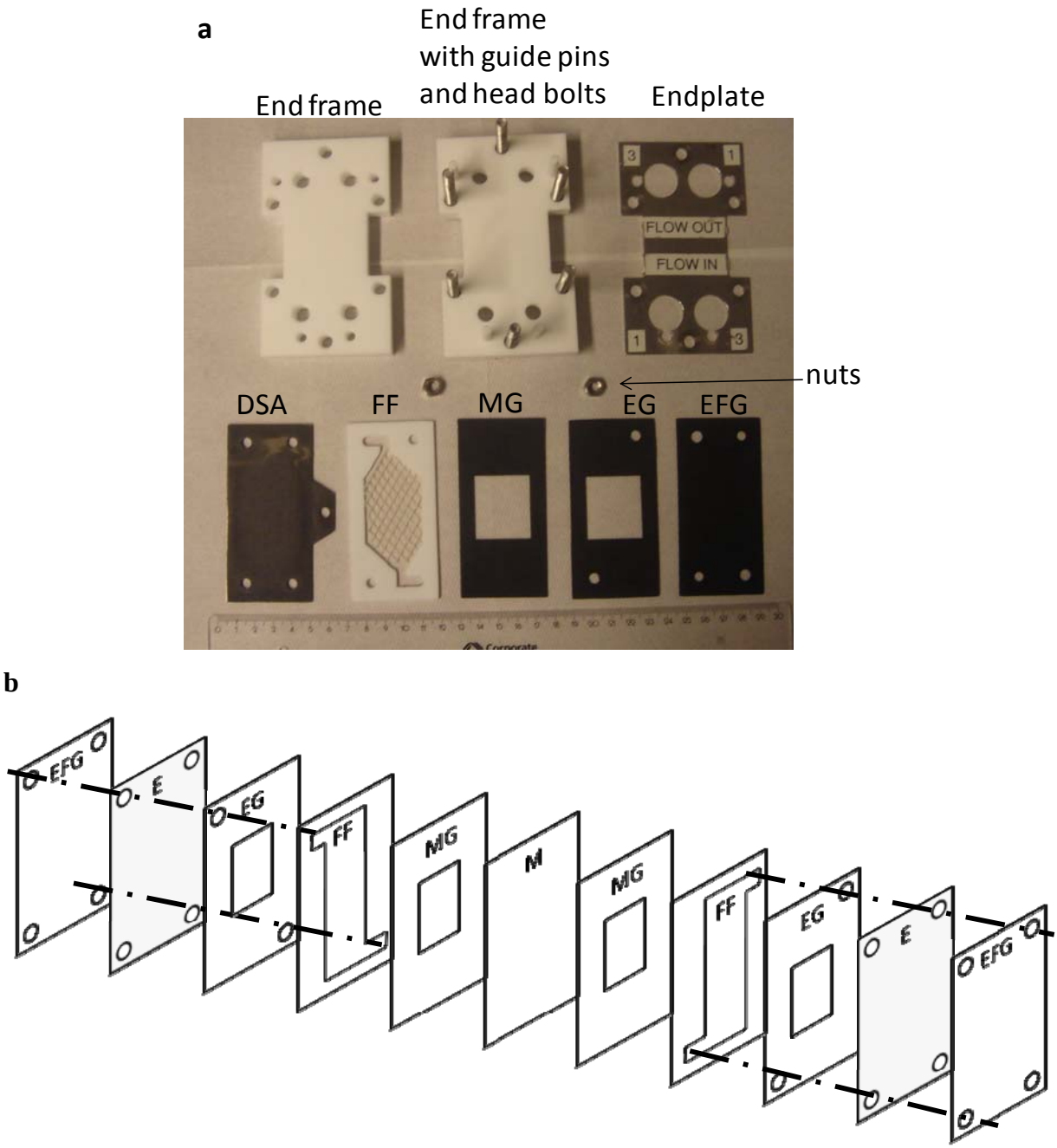

Figure 3.5a Picture of different components and **b** schematic drawing of two chamber Micro Flow Cell from ElectroCell: EFG = end frame gasket, E = electrode, EG = electrode gasket, FF = flow frame with flow mesh, MG = membrane gasket, M = membrane

If the cell is built using the standard cell components form ElectroCell the gap between the electrodes can be calculated by adding the different thickness of the cell components (without the membrane):

flow frame:	2	mm
electrode gasket:	0.8	mm
membrane gasket:	1.1	mm

This results in a total gap between the electrodes of 7.8 mm for the standard configuration of a two chamber cell. The active area of such a cell is 10 cm^2. The gap between the electrodes was varied by exchanging some parts deviating from the standard cell components of ElectroCell:

- A homemade 1 mm thick flow frame
- An electrode gasket was used as flow frame (cut in the same way as the standard flow frame).
- An electrode gasket was used as flow chamber.

As the Viton gasket were not performing in a proper way (leakage of the cell was observed) after some time of usage a new Viton sheet with the thickness of 1 mm was bought and the gasket were cut out of it. Due to theses variation the gap between the electrodes was different between the experiments and thus the actual gap and a short description of the flow chamber will be always stated in the subsequent results and discussion part. In addition the active area was expanded to 14.2 cm^2 if an electrode gasket as flow chamber was used. Therefore the active area will as well be stated in the subsequent section.

The first chamber of a three chamber cell is built in the same way as described above. In order to ensure an electrolyte flow in the middle chamber all four inlet and outlet holes have to be used on one end frame. Thus one inlet/outlet combination ensures the electrolyte flow in the chamber close to the electrode and the other combination is used to circulate the electrolyte through the middle chamber. Due to this the electrode gasket has to have 4 holes and both membrane and membrane gasket have to have 2 holes. The assembly of such type of cell is depicted in Figure 3.6.

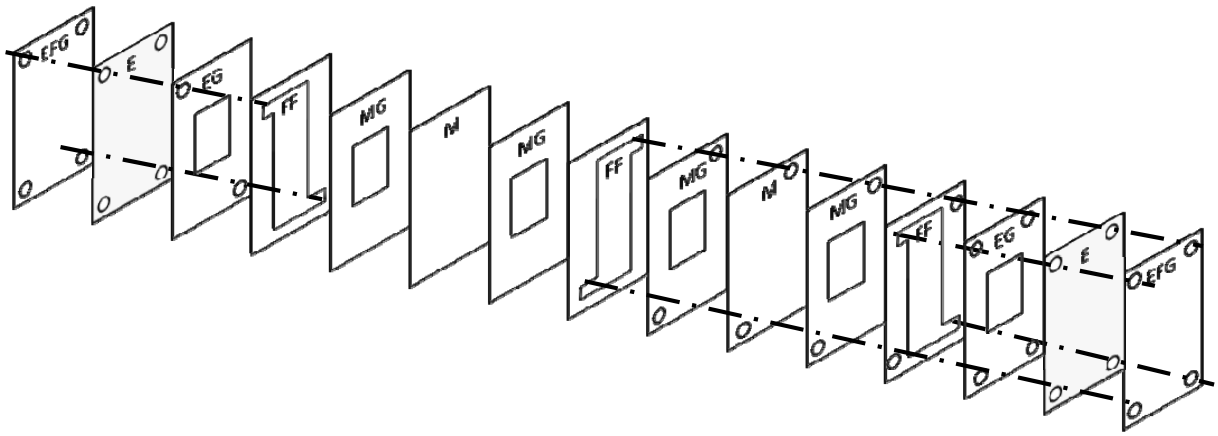

Figure 3.6 Schematic drawing of three chamber Micro Flow Cell from ElectroCell: EFG = end frame gasket, E = electrode, EG = electrode gasket, FF = flow frame with flow mesh, MG = membrane gasket, M = membrane

As membrane for both processes mostly Nafion 324 was used. In addition two membranes from Hescon were tested: a bipolar electrodialysis membrane (Typ BP-1E) and a cation exchange membrane (Typ CMB).

The voltage/current source was either a Keithly 2700 Multimeter/Data acquisition system or a IPS IMP83 PC-10 Potentiostat/Galvanostat connected to a scan generator (ELCM-KIT 003 from IPS) and a computer. The experiments were carried out either in a potentiostatic or galvanostatic mode, respectively. In potentiostatic experiments usually a voltage difference of 3 V between anode and cathode was applied. Galvanostatic electrolysis usually was performed with a current density of 100 mA/cm^2. Exceptions will be stated in the results and discussion part below. Due to the experimental setup (cables, crocodile clamps) an error of 5 – 10 % can be expected for the measured potential values in the galvanostatic experiments. Flow experiments were carried out using a Medorex TU 200 peristaltic pump with different flow rates. With this pump 3 liquids can be pumped at the same time.

With the standard assembly configuration from ElectroCell the first experiments were carried out statically (no flow), meaning the cell was filled first with the electrolyte, the flow was stopped and electrolysis was performed for a certain time. The anolyte solution in this experiments was usually a 0.6 M K_2SO_4 (by dissolving stoichometric amounts of K_2SO_4 min. 99 % from Sigma in 18 MΩ water) and the solution in the cathode chamber was either 18 MΩ water or KOH (by dissolving stoichometric amounts of KOH pellets puriss., p.a. min. 99 % from Fluka in 18 MΩ water, pH = 9 – 11). Further experiments were carried out under flow conditions. Parameters like flow rate, temperature and different concentrations of K_2SO_4 as anolyte were tested. As the prototype is operating with NaOH as absorption liquid, Na_2SO_4

(puriss. from Sigma Aldrich) was used later on. The first flow experiments were performed in such a way, that the electrolyte solution was pumped once through the cell once. With higher flow rates both electrolyte solutions were recirculated, thus the pass through the cell more than once. If the temperature was higher than room temperature the electrolyte solutions were heated up outside the cell in a beaker under stirring. Therefore the actual temperature inside the cell might be a bit lower but high deviations are not expected as the tubing was not very long. Usually the pump was calibrated to a flow rate before the experiment and using larger gaps (standard configuration from ElectroCell) the actual flow through the cell was as calibrated. Implementing smaller gap configurations it was observed that the actual flow through the cell might be 25 % different. Thus sometimes a flow rate with ± 25 % will be given in the subsequent results part. For accurate flow rates using a small gap configuration of the two chamber electrolysis cell the calibration of the peristaltic pump was done through the cell.

pH values were measured using a Profitrode connected to a 826 pH mobile readout unit (both from Methrom). If electrolysis was carried out at eleveated temperatures the solution were cooled down to room temperature prior to measurement.

3.3 Results and Discussion

3.3.1 Two chamber electrolysis

3.3.1.1 Two chamber electrolysis using K_2SO_4 as electrolyte

In this set of experiments a two chamber cell with a gap of 7.8 mm and an active area of 10 cm^2 was used. The electrodes were DSA as anode and Pt/Ti as cathode, respectively. As catholyte solution 0.4 M K_2SO_4 was used and the anode compartment was filled with either 18 MΩ H_2O or a KOH solution with a certain pH value (*pH* = 9 – 11). Both compartments were filled from up to down and electrolysis was initiated after the pump was switch off by applying 3 V. Thus electrolysis was performed under stationary conditions. After a certain time electrolysis was stopped and the electrolyte solutions were pumped out of the cell and the pH value was measured. The results are depicted in Figure 3.7. It can be seen that independently of the solution in the anode chamber *j* is rising to a certain maximum value and is decreasing afterwards towards the end of the experiments. The highest current density was reached using KOH with a pH of 1 as anolyte solution (~ 3 mA/cm^2).

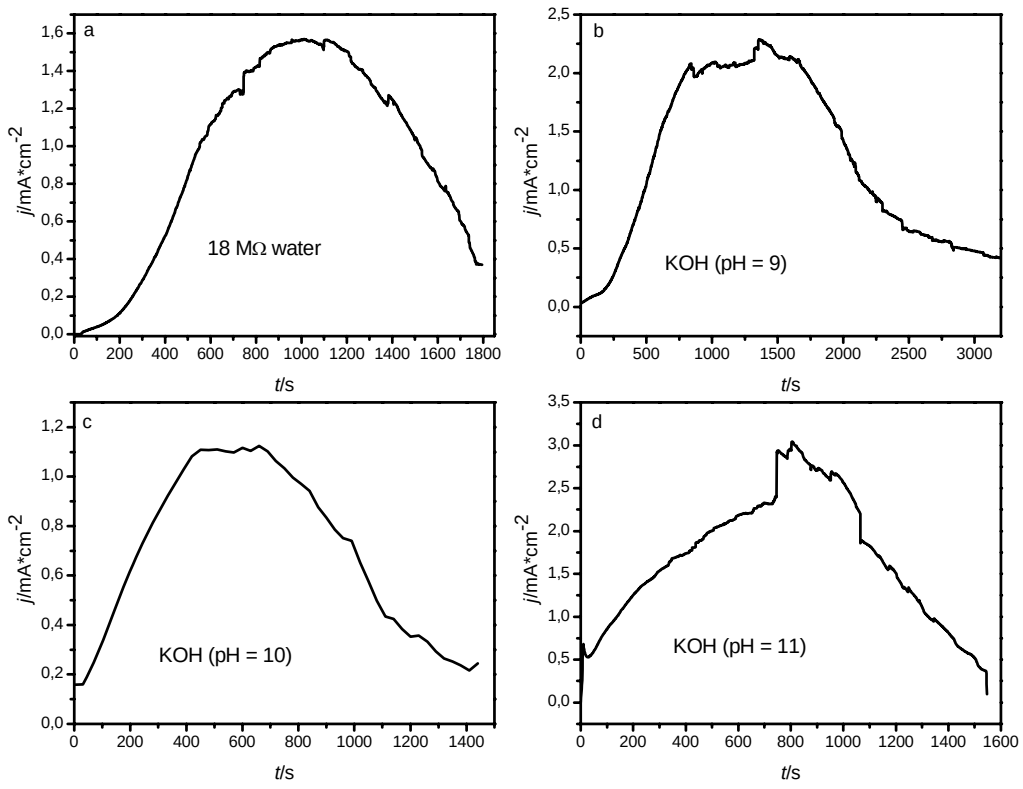

Figure 3.7 Current density profiles of two chamber (gap: 7.8 mm) potentiostatic electrolysis with 0.4 M K_2SO_4 in the cathode and **a** 18 MΩ water or KOH with a pH of **b** 9 **c** 10 **d** 11 in the anode chamber. Potential difference: 3 V.

The *pH* values are summarized in Table 3.1. The general trend is as expected: The *pH* value of the anolyte solution is decreased after electrolysis due to produced H^+ at the anode whereas the *pH* value of the catholyte solution is higher after electrolysis due to OH^- generated at the cathode.

Table 3.1 *pH* of the solutions in the anode (0.4 M K_2SO_4) and cathode (H_2O, KOH) chamber before and after electrolysis

pH **Anolyte solution before electrolysis**	***pH*** **Anolyte solution after electrolysis**	***pH*** **Catholyte solution before electrolysis**	***pH*** **Catholyte solution after electrolysis**
6.1	2.9	7	11.4
6	2.8	9	11.6
6.1	4	10.1	11
6.1	2.7	11	11.7

In addition the concentration of the anolyte in solution was varied between 0.4 and 0.6 M. The highest concentration at 20 °C in water of K_2SO_4 is around 0.6 M as the solubility of the salt in water at this temperature is 111.1 g/l[11]. The results are shown in Table 3.2. One can see that with the highest concentration the highest current density can be reached.

Table 3.2 Starting conditions and final conditions of electrolyte solutions (anolyte: K_2SO_4; catholyte = KOH) and maximal reached current density (applied potential difference: 3 V)

Starting conditions		**Final conditions**		
c*(K$_2$SO$_4$) / *pH	***pH*** **catholyte solution**	***pH*** **anolyte solution**	***pH*** **catholyte solution**	**maximal** ***j*/mA*cm^{-2}**
0.4 M / 6	7	3	11	1.8
0.4 M / 6	9	2.8	11.6	2.2
0.4 M / 6	10	4.4	11	1.1
0.4 M / 6	11	2.7	11.7	3.1
0.5 M / 6.2	11	2.8	11.8	3.2
0.6 M / 6.3	11	3	11.5	3.4

Even if the experiments are carried out under stationary conditions the electrolysis works much better if the cell is filled in the other way (from down to up) as can be seen in Figure 3.8. The current density is significantly higher as in case if the cell is filled in the opposite way and the current density profile looks different: The current density has a maximum in the beginning and decays afterwards to a certain more constant value. Two types of current densities are observed in such type of experiments are usually observed: capacitive and Faaradaic current density. A capacitive current (density) does not involve any electrochemical reaction but is due to the charging of the electrode and the electrolyte solution near the electrode surface.[12] Such a current (or current density) is seen if the potential of one electrode is changing. A current due to an electrochemical process is referred as Faradaic current. Thus in Figure 3.8 in the very beginning a capacitive current density is observed (usually shorter than 1 s). Then the current density decays slowly to a rather constant value. This decay can be assigned to Faradaic currents due to reduction of dissolved oxygen in the electrolyte solution and to the establishment of stationary conditions inside the cell. The rather constant current density after around 10 min is the Faradaic current density under stationary conditions. Such current density profiles are very common in electrolysis processes and indicate that filling of the cell is very important even if the experiment itself is carried out under stationary conditions. A possible reason might be that if the cell is filled from up to down not the whole

chamber volume is filled with electrolyte. A further indication that the electrolysis is working much better are the *pH* values: The starting *pH* of both electrolytes solutions was 6.1. After electrolysis *pH* of the anolyte solution was found to be 1.8 and for the solution in the cathode chamber a value of 13 was obtained.

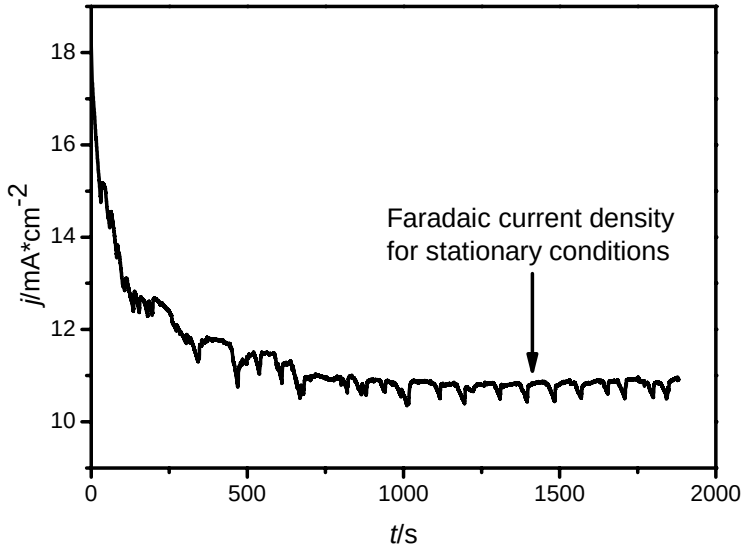

Figure 3.8 Current density profile of stationary two chamber electrolysis (gap: 7.8 mm) of 0.6 M K_2SO_4. Cell filled from down to up. T = 25 °C, 3 V applied.

Using same electrolyte solutions (0.6 M K_2SO_4) and performing electrolysis under flow conditions (20 ml/min) over 30 min nearly the same behavior as under stationary conditions can be seen (Figure 3.9). In this case a much faster decay to a rather constant current density profile is observed. A possible explanation is that due to the flow conditions the stationary conditions inside the cell are established much faster. The current density after 30 min is around 12.5 mA/cm^2 which is 1 mA/cm^2 higher compared to the stationary experiment. The higher current density can be explained by the flow conditions itself: Due to the constant flow of the electrolyte solutions through the compartment, the produced gas bubbles (H_2 and O_2) are removed faster from the cell. This increases the current density as it makes the electrochemical process more efficient according to a lowering of the overpotential (gas bubbles are non conductive). In this type of experiments the electrolyte solutions were pumped through the cell one time and collected afterwards in a beaker. The *pH* value of these collected solutions was measured. After 30 min a *pH* of 2.1 in the anolyte solution and of 12.8 in the catholyte solution was observed. These values are comparable to the ones of stationary electrolysis experiments.

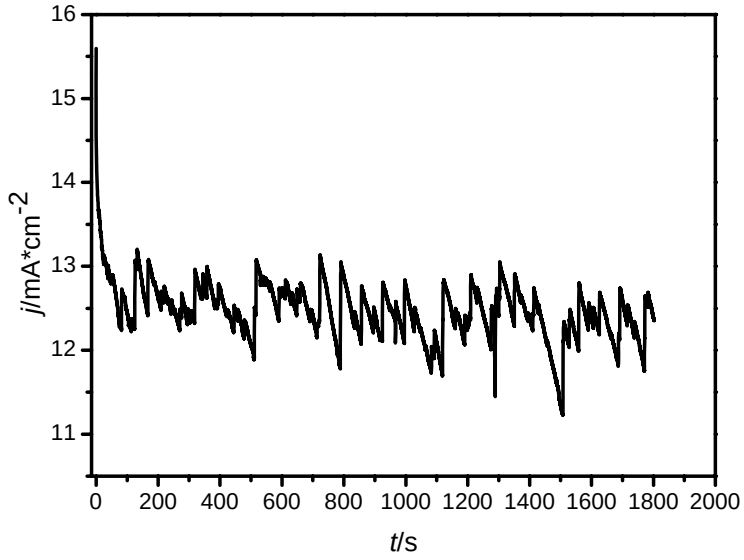

Figure 3.9 Current density profile of two chamber electrolysis (gap: 7.8 mm) of 0.6 M K_2SO_4 under flow conditions (20 ml/min). T = 25 °C, 3 V applied.

In further experiments the concentration of the catholyte, the temperature and the flow rates were varied. The results of the flow dependence are depicted in Figure 3.10. Current density and *pH* were measured after 30 min of electrolysis of a 0.6 M K_2SO_4 at 25 °C. As can be seen the current density is rising with higher flow rates. This is here assigned to a better removal of gas bubbles from the cell with higher flow rates. In addition the *pH* difference between catholyte and anolyte solution is smaller for higher flow rates. This is due to a shorter residence time of the electrolytes inside the two chamber cell. A *pH* of 11 – 12 for the absorption liquid and of around 2 – 3 for the stripping acid should be fine for absorption or stripping, respectively.

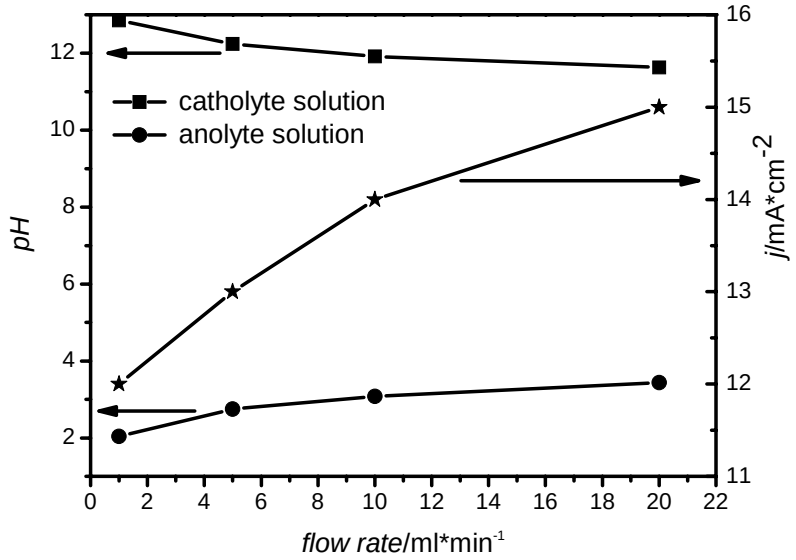

Figure 3.10 Flow rate dependence of two chamber electrolysis (gap: 7.8 mm) of 0.6 M K_2SO_4 (*pH* = 6.3). Squares: *pH* of catholyte solution, dots: *pH* of anolyte solution, stars: current density after 30 min of electrolysis (3 V applied, T = 25 °C).

Figure 3.11 shows the concentration dependence of the catholyte on the *pH* and on *j*. The anolyte solution was a 0.6 M K_2SO_4. As can be seen with a flow rate of 1 ml/min at room temperature the highest current density (~ 12 mA/cm^2) can be obtained if both electrolyte solutions have a concentration of 0.6 mol/l. This suggests that operating the electrolysis cell close to the solubility edge of K_2SO_4 should give the best results. Again the *pH* values of catholyte and anolyte solution are in the expected region and should be fine for absorption and stripping.

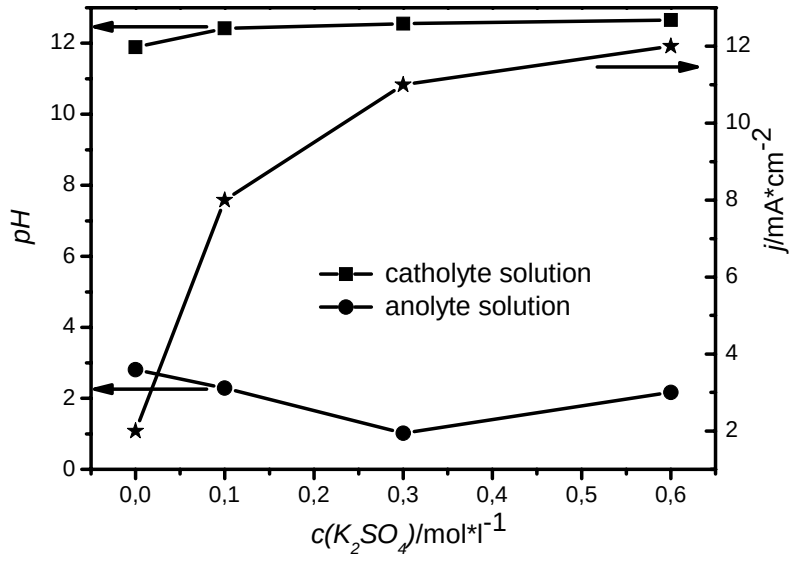

Figure 3.11 Concentration dependence of two chamber electrolysis (gap: 7.8 mm) with 1 ml/min flow of K_2SO_4 solutions. Squares: *pH* of catholyte solution, dots: *pH* of anolyte solution, stars: current density after 30 min of electrolysis (3 V applied, T = 25 °C).

The last parameter varied was the temperature. As the previous results suggest that higher concentration of K_2SO_4 in both compartments and higher flow rates give the highest current density, the experiment was performed with 0.6 M K_2SO_4 as electrolyte solution and a flow rate of 20 ml/min (see Figure 3.12). The current density is steeply rising with higher temperature and is at 90 °C a factor of 2 higher than at room temperature. The *pH* at this temperature of the catholyte solution has the highest value and of the anolyte solution the lowest value, respectively. These results suggest that operating the 2 chamber electroylysis of K_2SO_4 at elevated temperatures, higher concentration of the electrolytes in solution and at higher flow rates should give the best results.

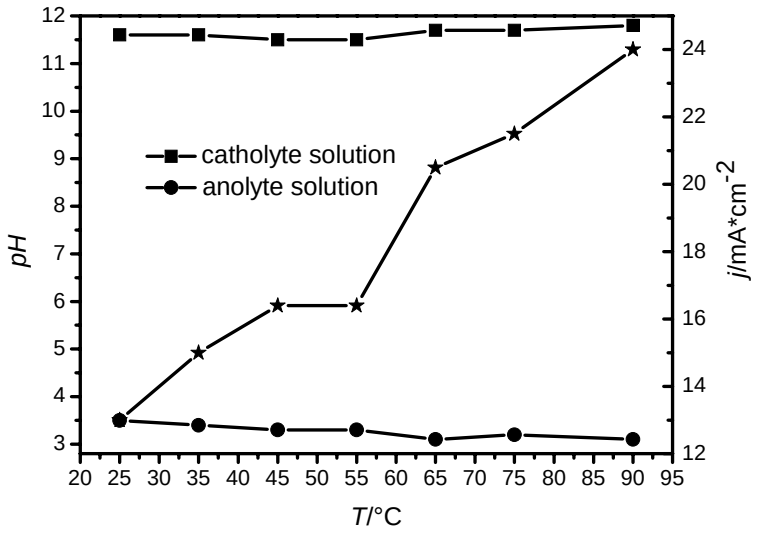

Figure 3.12 Temperature dependence of two chamber electrolysis (gap: 7.8 mm) with 20 ml ml/min flow of 0.6 M K_2SO_4 (*pH* = 6.2). Squares: *pH* of catholyte solution, dots: *pH* of anolyte solution, stars: current density after 30 min of electrolysis (3 V applied)

3.3.1.2 Two chamber electrolysis using Na_2SO_4 as electrolyte

As the prototype (see Chapter 2) is operating with sodium based solution the electrolyte was changed from K_2SO_4 to Na_2SO_4. Flow rate, temperature and concentration dependence on the performance of a two chamber electrolysis were tested.

The temperature dependence measurements were carried out using a 0.6 M Na_2SO_4 solution as initial electrolyte solution for both compartments in a two chamber electrolysis cell (gap: 7.8 mm). The temperature was varied in the range between 25 and 95 °C. In this set of experiments a flow rate of 20 ml/min was used like in case of K_2SO_4 as electrolyte. Electrolysis was carried out for 30 min by applying a potential difference of 3 V. *pH* and *j* values given in Figure 3.13 are taken after 30 min electrolysis time. The same trend is observed as already described above for K_2SO_4 as electrolyte: By increasing the temperature the current density is significantly enhanced and the *pH* difference between catholyte and anolyte solution is as well increasing. *pH* and *j* are comparable to the results obtained using K_2SO_4.

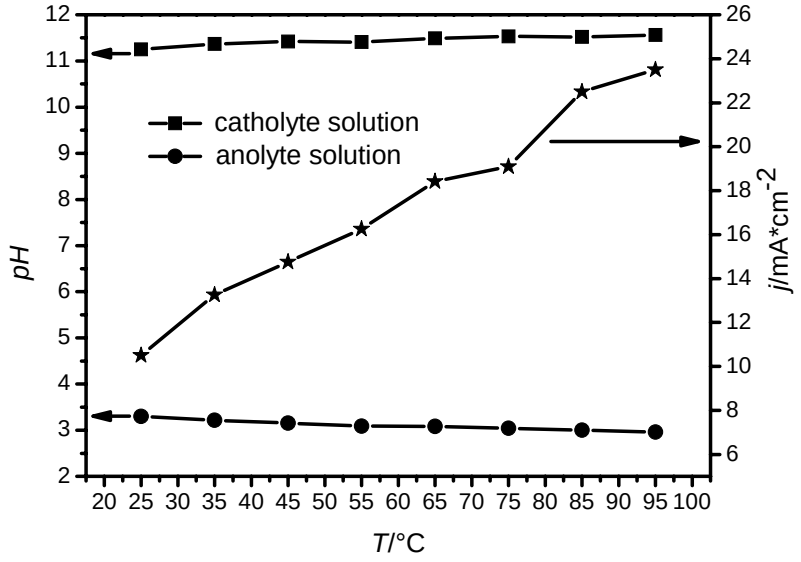

Figure 3.13 Temperature dependence of two chamber electrolysis (gap: 7.8 mm) of with 20 ml ml/min flow of 0.6 M Na_2SO_4 (*pH* ~ 6). Squares: *pH* of catholyte solution, dots: *pH* of anolyte solution, stars: current density after 30 min of electrolysis (3 V applied)

The temperature dependence of the rate constant *k* of a chemical reaction very often follows the Arrhenius law:

$$k = Ae^{-\frac{E_A}{RT}} \qquad \text{(eq. 3.1)}$$

where *A* is a prefactor, *R* the ideal gas constant, *T* the temperature (in K) and E_A the activation energy of the reaction.[13,14] To calculate E_A usually a plot of ln*k* against *1/T* is used according to:

$$\ln k = -\frac{E_A}{R}\frac{1}{T} + const \qquad \text{(eq. 3.2)}$$

From the slope of a linear fit in this type of plot E_A can be extracted.

The temperature dependence of the current density for both electrolytes (see Figure 3.12 and Figure 3.13) indicates an Arrhenius like behavior. Thus ln*j* was plotted versus *1/T* according to:

$$\ln j = -\frac{E_A}{R}\frac{1}{T} + const \qquad \text{(eq. 3.3)}$$

The Arrhenius plots for the 0.6 M K_2SO_4 and 0.6 M Na_2SO_4 are shown in Figure 3.14. Indeed an Arrhenius like behavior can be seen for both electrolytes. From the slope of the linear fit E_A can be obtained:

$$E_A = -slope*R \qquad \text{(eq. 3.4)}$$

For the 0.6 M K_2SO_4 and 0.6 M Na_2SO_4 E_A values of 8.45 kJ/mol and 10.04 kJ/mol are obtained, respectively. This suggests a lower activation energy for the potassium electrolyte solution compared to the sodium one.

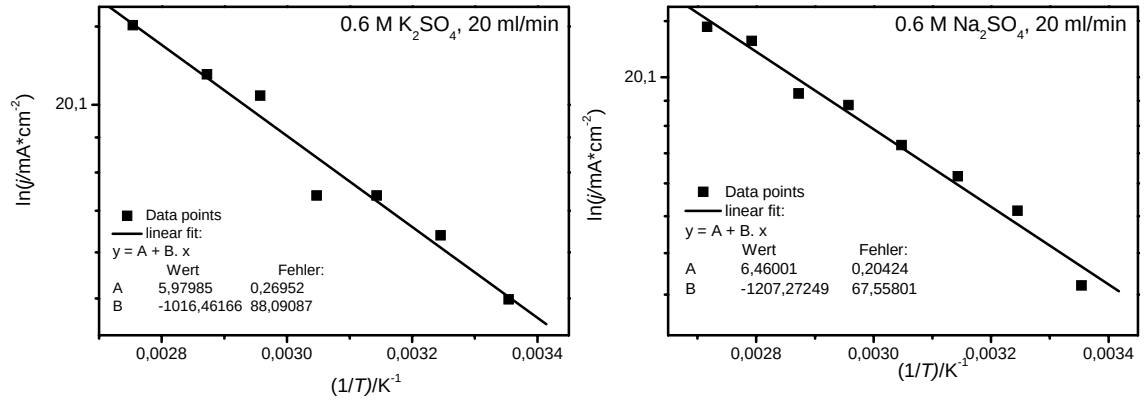

Figure 3.14 Arrhenius plots of the temperature dependence of the current density for Na_2SO_4 and K_2SO_4 electrolyte solutions.

As it was indicated by the temperature dependence measurements that higher temperatures increase the efficiency (higher *j*) of the given two chamber electrolysis processes the concentration dependence measurements were carried out at elevated temperature (55 °C). The flow rate was 20 ml/min. The gap of the two chamber electrolysis cell was 7.8 mm and a potential difference of 3 V between the electrodes was applied. *pH* and *j* values shown in Figure 3.15 are taken after 15 min of electrolysis. Increasing the concentration of the initial electrolyte increases both parameters. The maximum solubility of Na_2SO_4 in water at room temperature (170 g/l[15]) is higher than in case of K_2SO_4 therefore the solubility edge is at around 1.2 M concentrations.

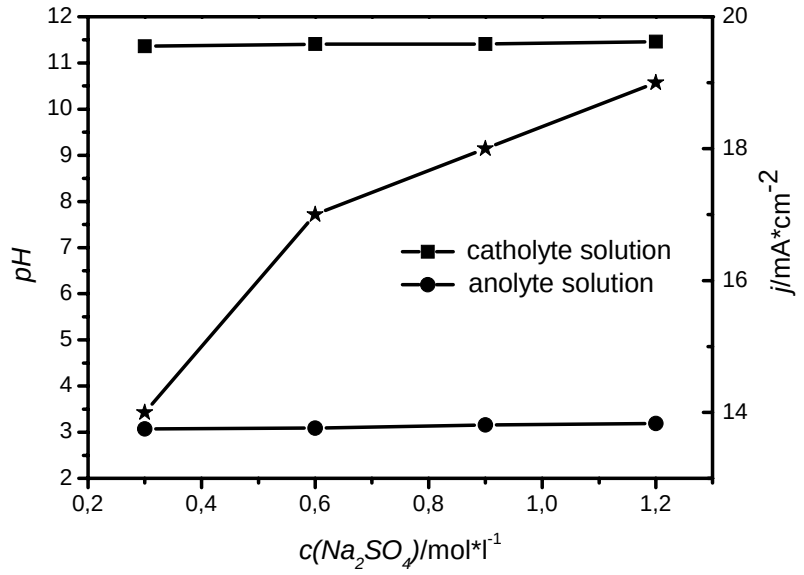

Figure 3.15 Concentration dependence of two chamber electrolysis (gap: 7.8 mm) with 20 ml/min flow of Na_2SO_4 solutions. Squares: *pH* of catholyte solution, dots: *pH* of anolyte solution, stars: current density after 15 min of electrolysis (3 V applied)

For the flow rate dependence the starting electrolyte solution was chosen to be a 1 M Na_2SO_4 solution for both chambers in the two chamber electrolysis cell (gap: 7.8 mm). The temperature was 55 °C. The flow rate was varied in the range of 10 – 100 ml/min. For 15 min a potential difference of 3 V was applied between the electrodes. The experiment was carried out twice under the same conditions with two different membranes: once using a Nafion 324 and once using a Nafion 424 membrane respectively. The results are depicted in Figure 3.16. One can see that for both membranes *j* is rising with higher flow rates. In case of Nafion 324 the current densities are a bit higher for every flow rate compared to Nafion 424 but the difference is not very pronounced. In addition the *pH* difference between anolyte and catholyte solution is decreasing with increasing flow rate for both membranes in a rather comparable way. A similar behavior was already previously described for K_2SO_4 solutions and the flow rate dependence of *j* suggests that with higher flow rates gas bubbles are more effective removed from the cell. A shorter residence time of the electrolytes inside the cell is a possible reason for the given *pH* dependence.

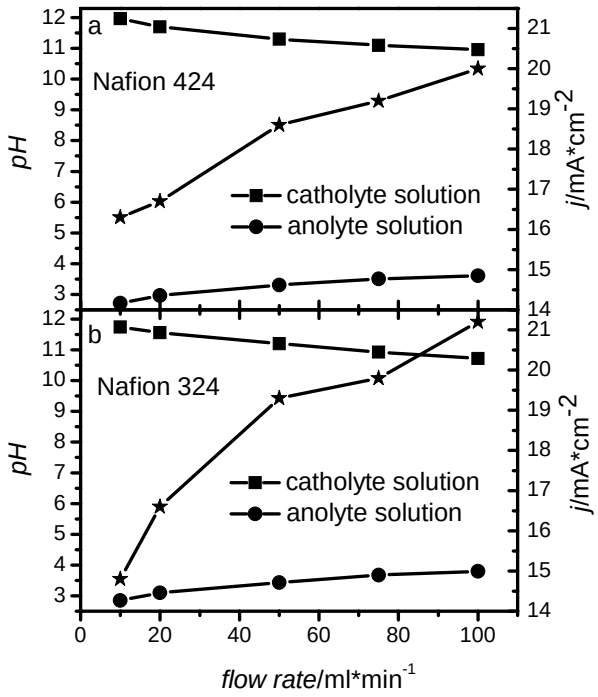

Figure 3.16 Flow rate dependence of two chamber electrolysis (gap: 7.8 mm) of 1 M Na_2SO_4 (*pH* = 5.7) using **a** Nafion 424 or **b** Nafion 324 as cation selective membrane. Squares: *pH* of catholyte solution, dots: *pH* of anolyte solution, stars: current density after 15 min of electrolysis (3 V applied).

As indicated by the previous measurements that higher flow rates increase the efficiency (higher *j*), but due to the shorter residence time the *pH* values of the anolyte solution are not as low (or as high for the catholyte solution) as with lower flow rates. A new set of experiments was performed recirculating both electrolyte solutions (one cycle for each electrolyte solution). Due to the recirculation the solutions pass through the cell more than one time. The total electrolyte solution amount passing through the cell is determined by the volume and the flow rate. The experiments were performed using a two chamber electrolysis cell with a gap of 7.8 mm. As initial electrolyte solution a 1 M Na_2SO_4 was used for both chambers and the reservoir (1 l) for both solutions was kept at 55 °C. The flow rate was varied in the range of 20 – 800 ml/min. Figure 3.17 shows the current density profile as well as the measured *pH* values during 60 min of electrolysis for a recirculation flow of 100 ml/min. The *pH* values of the catholyte solution are increasing during the time of the experiment and the ones for the anolyte solution are respectively decreasing. This is due to the recirculation: Both electrolyte solutions pass through the cell ~ 6 times in 1 h and by every

passage the acidity of the anolyte solution and the alkalinity of the catholyte solution are increased.

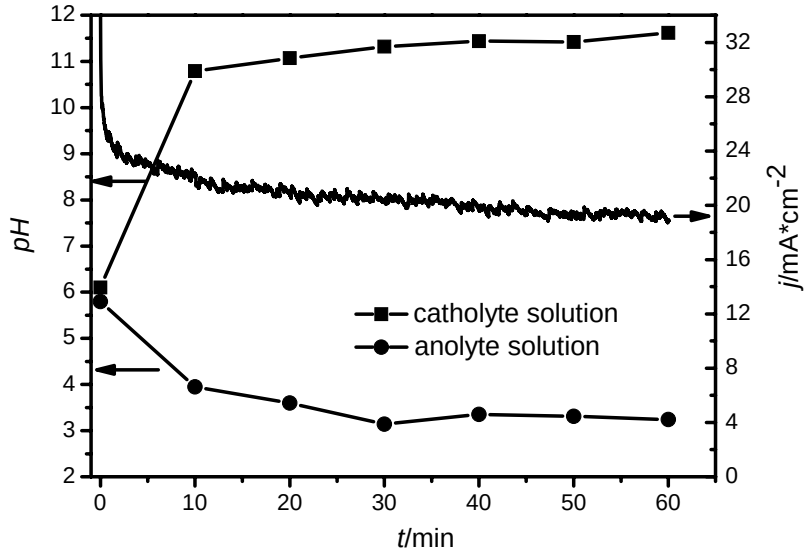

Figure 3.17 Two chamber electrolysis (gap: 7.8 mm) of 1 M Na_2SO_4 with recirculation (100 ml/min, T = 55 °C) of both soluitons. Squares: *pH* of catholyte solution, dots: *pH* of anolyte solution, solid line :current density during 60 min of electrolysis (3 V applied).

Figure 3.18 shows the dependence of *j* and the *pH* values of both electrolyte solutions on the flow rate for the above described two chamber electrolysis under recirculation conditions (all values after 1 h of electrolysis). As expected the highest flow rate (800 ml/min) gives the highest current density (23.4 mA/cm^2). With this flow rate the solutions passed through the cell ~ 48 times. As can be seen the *pH* values do not differ very much for different flow rates. The *pH* of the anolyte solution is found to be in the range between 2.7 – 3.3 and the one of the catholyte solution between 11.5 – 12. A possible explanation is that with higher flow rates the residence time is decreased if the flow rate is higher leading to a roughly constant *pH* profiles.

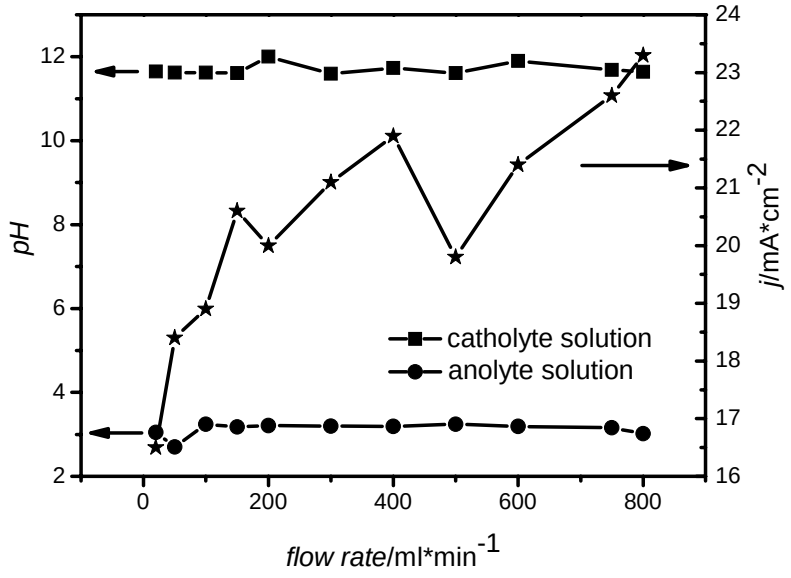

Figure 3.18 Flow rate dependence of two chamber electrolysis (gap: 7.8 mm) of 1 M Na_2SO_4 (*pH* ~ 5.9, T = 55 °C). Squares: *pH* of catholyte solution, Dots: *pH* of anolyte solution, stars: current density after 1h of electrolysis (3 V applied)

Therefore a longer electrolysis time results in higher *pH* values of the solution in the cathode chamber and in lower values for the anolyte solution respectively. For this reason a two chamber electrolysis (gap: 7.8 mm) experiment was performed for 11 h in total. The electrolysis had to be stopped 2 times but the electrolytes were kept and reused and the 2 chamber cell was not disassembled between the consecutive electrolysis experiments. As initial electrolyte solution a 1 M Na_2SO_4 solution was used for both chambers. The flow rate was 750 ml/min and the solutions were kept at 55 – 60 °C. The *pH* values as well as the *j* profile over time of electrolysis are depicted in Figure 3.19. Indeed as expected the *pH* of the anolyte solution decreased during the experimental time down to a value of 2.25 and during the same time the *pH* value of the solution in the cathode chamber increased to 12.45. The current density after 11 h was around 20 mA/cm^2.

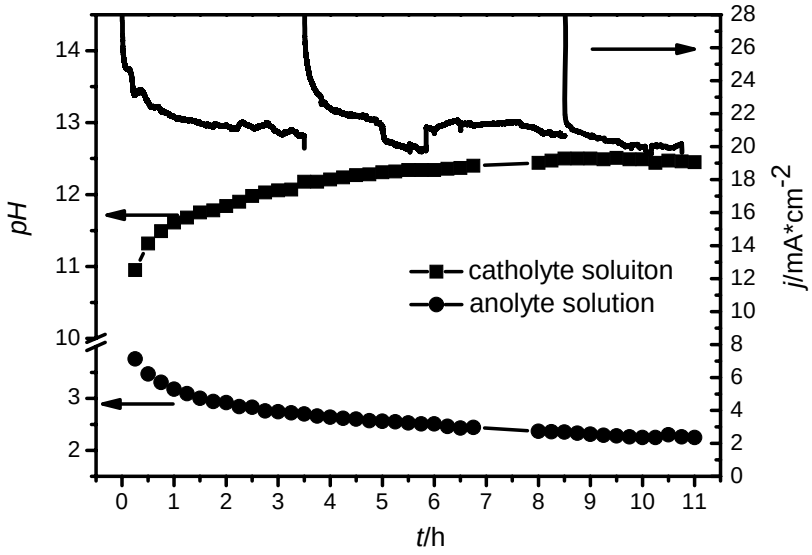

Figure 3.19 Two chamber electrolysis (gap: 7.8 mm) of 1 M Na_2SO_4 with recirculation (750 ml/min, T = 55 °C) of both solutions. Squares: *pH* of catholyte solution, Dots: *pH* of anolyte solution, solid line current density during 11 h of electrolysis (3 V applied)

Literature reports [1,2] indicate that reducing the gap between cathode and anode decreases the overpotential. This overpotential is due to the fact that the reactions are taking place on the electrode surface and the resistance of the electrolyte solutions mainly determines the total resistance of the electrolysis cell. For this reason a smaller gap should increase the current density in potentiostatic experiments. Thus in further experiment parts of the Micro Flow Cell were modified in order to reduce the gap. In the first experiments the flow frame was exchanged by an electrode gasket that was cut into the same shape as a flow frame. This resulted in an actual gap of 5.4 mm. A further gap reduction was achieved by using only the mentioned cut electrode gasket meaning that no further gaskets were used. Therefore this gasket acted as electrode gasket, flow frame and membrane gasket in one piece. This reduced the gap down to 1.6 mm and by the same time the active area was increased to ~ 14.2 cm^2. Note that all the given gaps do not contain the membrane thickness but just the thicknesses of gaskets and flow frames. 1 h electrolysis was performed using 7.8 mm, 5.4 and 1.6 mm gap two chamber electrolysis cells, respectively. The starting electrolyte solution was for every experiment a 1 M Na_2SO_4 solution in both chambers and 3 V potential difference was applied for 1 h. The temperature of the solutions was set to 55 – 60 °C and the flow rate was 400 or 800 ml/min (± 25 % for the 1.6 mm gap cell). The results for this experimental set are summarized in Table 3.3. The *pH* dependence suggests that the process is more efficient for smaller gaps but on the other hand the current density shows a different dependence. The

highest *j* was reached with the 5.4 mm gap (for 800 ml/min flow rate) which is counter intuitive.

Table 3.3 *pH* values of anolyte and catholyte solution and *j* after 1 h of electrolysis in a 2 chamber cell (3 V applied) for different gaps (*d*) with different active areas (*A)*

d/mm	*A*/cm^2	*flow rate*/ml*min^{-1}	$pH_{anolyte\ solution}$	$pH_{catholyte\ solution}$	*j*/mA*cm^{-2}
7.8	10	800	3.02	11.64	23.3
5.4	10	800	2.95	11.73	23.4
1.6	14.2	800	2.86	11.83	21.9
7.8	14.2	400	2.6	12.15	17.9
1.6	14.2	400	2.6	12.11	19.3

From Table 3.3 it can be seen that there are some variation in the obtained current densities. Comparing the two results with a flow rate of 400 ml/min it can be seen that the smaller gap cell seems to perform better. Especially the error in the flow rate for smaller gaps might explain the deviations.

Flow rate and temperature dependence for a 1.6 mm two chamber cell under recirculation conditions of a 1 M Na_2SO_4 (initial concentration for both chambers) were tested as well. The results are plotted in Figure 3.20. For the temperature dependence a flow rate of 800 ml/min was used and for the flow rate dependence a temperature of 55 – 60 °C was used. Note that all flow rates might have a 25 % error. The results show the same trend as previously described: Higher flow rates and higher temperatures enhance *j*.

From all the parameters that have been tested (concentration, temperature, flow rate and gap between the electrodes) the gap between the electrodes seems to have the smallest influence on the efficiency of the given process.

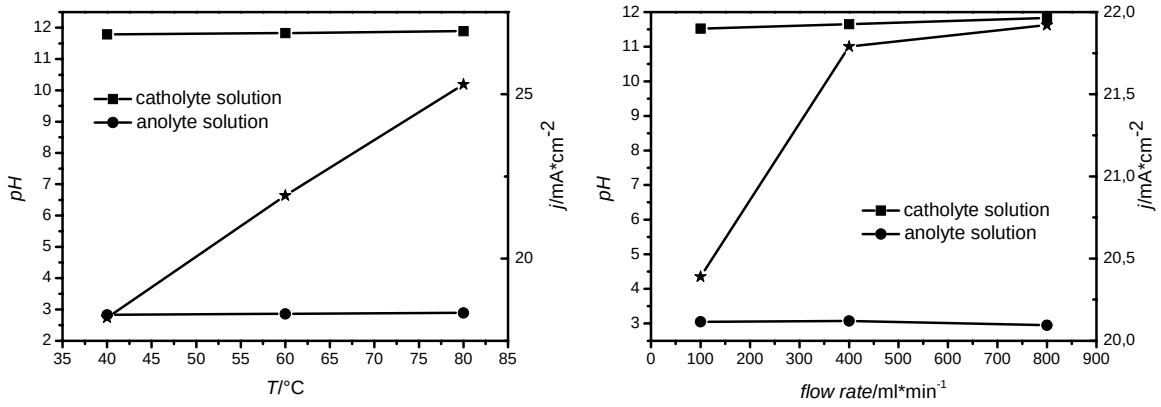

Figure 3.20 Temperature dependence and flow rate dependence of two chamber electrolysis cell (gap: 1.6 mm) of 1 M Na_2SO_4 with recirculation of both electrolyte solutions. Squares: *pH* of catholyte solution, dots: *pH* of anolyte solution, stars: current density after 1 h of electrolysis (3 V applied).

As indicated by all previous experiments the best working two chamber electrolysis should have a small gap and the initial electrolyte should have a high concentration. In addition higher flow rates and temperatures improve the performance. In order to compare the results to previous results from the literature[2] and to the electrodialysis from the prototype galvanostatic experiments with a current density of 100 mA/cm^2 were performed. For these experiments a two chamber cell with a gap of 1.6 mm was used. The flow rate was 800 ml/min (± 25 %) and the temperature was set to 80 °C. Over the time of 3 h every 15 min the *pH* values of the catholyte and anolyte solution were measured. The potential profile and the *pH* values are depicted in Figure 3.21. The potential difference between anode and cathode has a value of ~ 3.6 V after 3 h of galvanostatic electrolysis. Due to the experimental setup an error of around 5 – 10 % for the measured voltage value can be expected. The *pH* values follow the same trend as already described before: the acidity of the anolyte solution as well as the alkalinity of the catholyte solution are increasing and reach a final value of 2.1 for the anolyte and of 12.5 for the catholyte solution, respectively. The experiment was repeated a second time with the same experimental conditions and a potential difference of around 3.5 V was measured after 3 h of galvanostatic electrolysis. *pH* of the anolyte solution was measured to be 1.8 and the one of the catholyte solution to be 12.1. The results of both experiments are in good agreement with each other and seem to be reproducible.

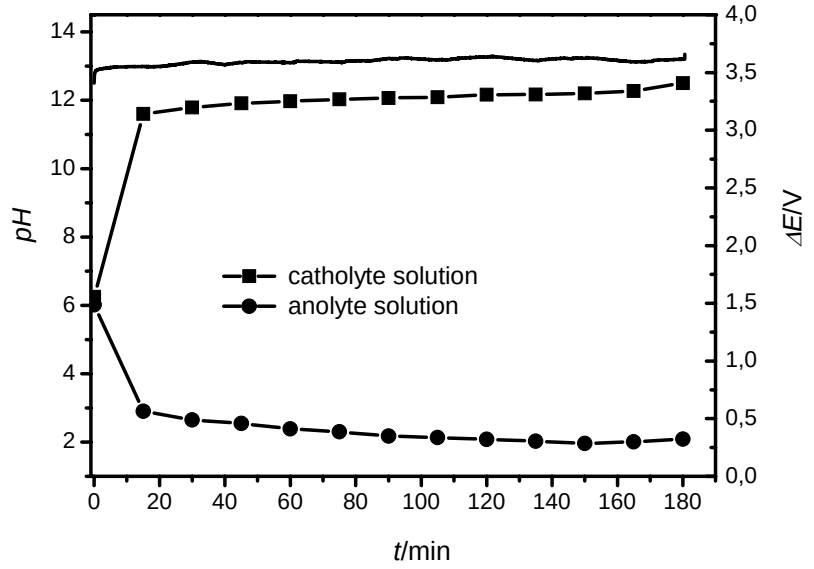

Figure 3.21 Two chamber electrolysis (gap: 1.6 mm) of 1 M Na_2SO_4 with recirculation (800 ml/min ± 25 %, T = 80 °C) of both solution. Squares: *pH* of catholyte solution, dots: *pH* of anolyte solution, solid line : potential difference between anode and cathode during 3 h of electrolysis (100 mA/cm^2 applied).

The flow dependence of the small cell was as well tested with the same experimental conditions (T = 80 °C, 1 M Na_2SO_4). This was done in one experiment were the flow rate was switched during a galvanostatic electrolysis (100 mA/cm^2) in a two chamber cell (gap:1.6 mm). The results are depicted in Figure 3.22. The lines indicate the time when the flow rate was changed. Increasing the flow rate decreases the potential difference whereas a decrease in the flow rate cause the opposite effect.

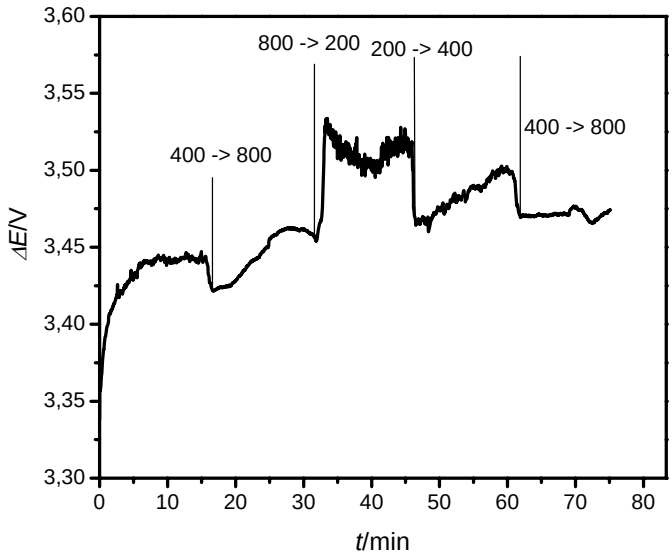

Figure 3.22 Potential traces for two chamber electrolysis (gap: 1.6 mm) of 1 M Na_2SO_4 with recirculation (T = 80 °C) of both electrolyte solutions. The lines indicate the time of changing the flow rates (± 25 % error possible for the given flow rates, numbers in the diagram represent the flow rates).

The influence of the gap was compared to an experiment with the same conditions using a two chamber cell with a gap of 7.8 mm. The potential difference trace as well as the *pH* values are shown in Figure 3.23. Increasing the gap leads to a slightly higher potential value after 3 h of galvanostatic electrolysis (~4 V). The spikes in the potential trace can be assigned to bad contacts of the used crocodile clamps and the electrodes. Even if the gap is by a factor of 4.9 higher the increase in the potential difference is only around 300 mV higher. This indicates another time that the gap between the two electrodes does not seem to have a high influence on the efficiency of the investigated process compared to other parameters like temperature or flow rate.

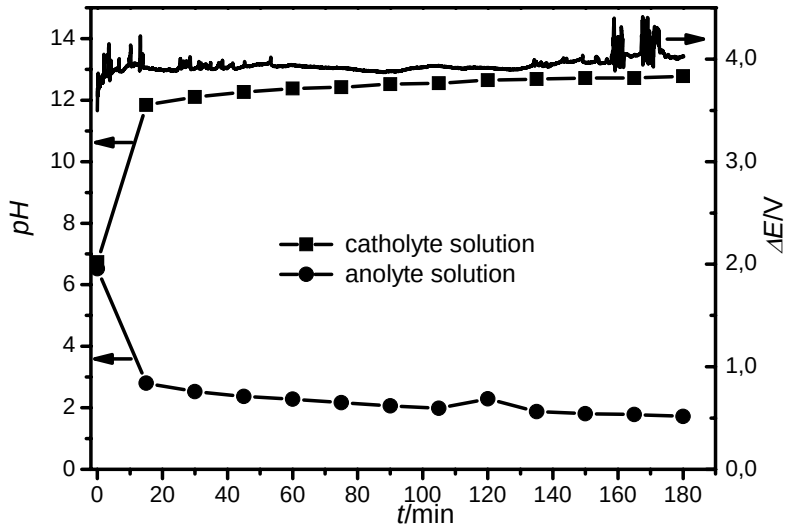

Figure 3.23 Two chamber electrolysis (gap: 7.8 mm) of 1 M Na_2SO_4 with recirculation (800 ml/min ± 25 %, T = 80 °C) of both electrolyte solution. Squares: *pH* of catholyte solution, dots: *pH* of anolyte solution, solid line: potential difference between anode and cathode during 3 h of electrolysis (100 mA/cm^2 applied)

Two chamber electrolysis cells with different gaps will have different cell volumes. Therefore by using the same flow rate the actual flow velocity of a flow element will be different. 3 different gaps of the two chamber electrolysis cell were realized: 8, 6 and 2 mm. The flow rates were chosen in such a way that the flow velocity was 0.028 m/s for all gaps: 200 ml/min flow rate per chamber for the 8 mm gap, 150 ml/min per chamber for the 6 mm gap and finally 50 ml/min per chamber for the 2 mm gap. Larger gap cells have a larger electrolyte volume and therefore if the other parameters are the same the main difference between these cells under operating conditions is due to the resistance of the electrolyte, as the distance between the electrodes is increased. In this experiment the pump was calibrated with the electrolyte solutions pumped through the cell at the experimental temperature (60 °C), thus a more accurate flow rate can be given. 100 mA/cm^2 were applied for 15 min and the electrolytes were recirculated during the electrolysis. The anolyte solution was 1 M Na_2SO_4 with H_2SO_4 (*pH* ~ 1.5) and the catholyte solution a 1 M Na_2SO_4 with NaOH (*pH* ~ 12.6). The obtained potential traces are shown in Figure 3.24. If the electrolyte solutions are pumped with the same flow velocity no big difference between the different gaps especially for the two smaller gaps is observed.

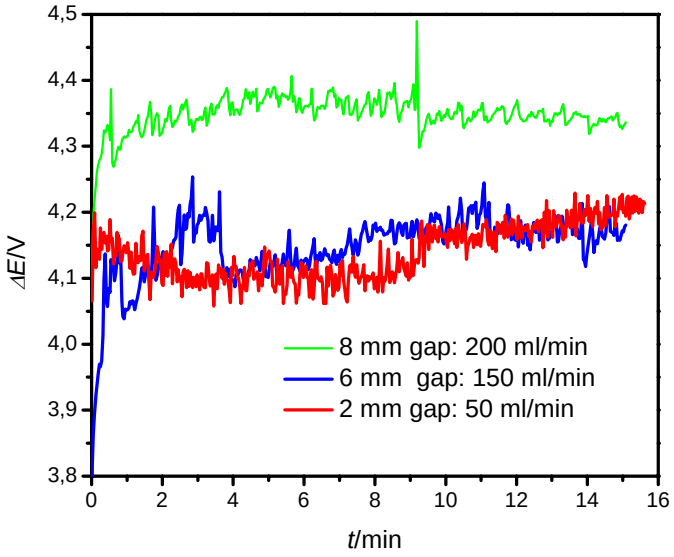

Figure 3.24 Potential profiles of two chamber electrolysis with different gaps and constant flow velocity (0.025 m/s). Green line: 8 mm gap, blue line: 6 mm gap, red line: 2 mm gap. Anolyte solution (was 1 M Na_2SO_4 with H_2SO_4; *pH* ~ 1.5) and catholyte solution (1 M Na_2SO_4 with NaOH; *pH* ~ 12.6) were recirculated. 100 mA/cm^2 were applied for 15 min. T = 60 °C

A further cation selective membrane (CMB) was compared to Nafion 324 in a two chamber electrolysis with recirculation (400 ml/min) of both electrolyte solutions (initial concentration for both chambers: 1 M Na_2SO_4). The CMB membrane does not have an additional hydroxyl barrier. The temperature was set to 60 °C and 100 mA/cm^2 were applied for 60 min. The results are shown in Figure 3.25. One can see that both membranes show a similar performance. In addition the *pH* values do not differ significantly: 2.2 for the anolyte solution and 12.5 for catholyte solution after 60 min. This indicates that the addition hydroxyl barrier of the Nafion membrane does not seem to have a significant influence on this electrolysis process.

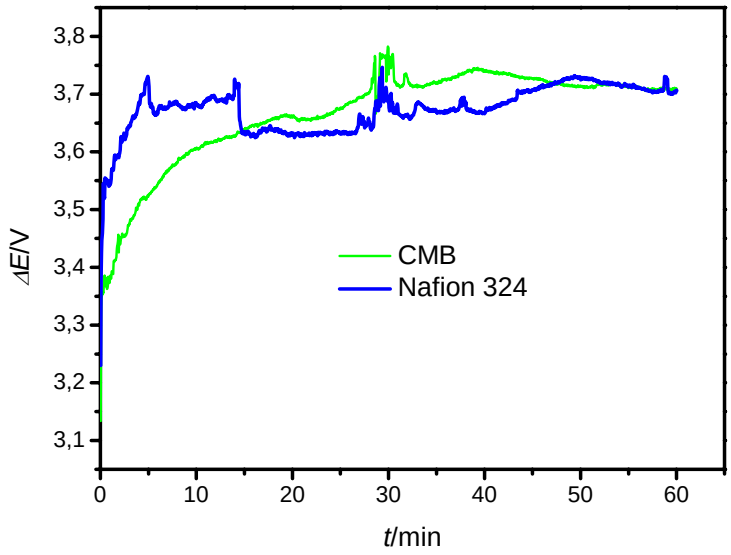

Figure 3.25 Potential profiles of two chamber electrolysis (2 mm gap) with 2 different membranes. Green line: CMB membrane; blue line: Nafion 324 membrane. Recirculation (400 ml/min) of electrolyte solutions (initial concentration for both chambers: 1 M Na_2SO_4). T= 60 °C . 100 mA/cm^2 were applied for 60 min.

As cathode material up to now only Pt/Ti was used. Pt electrodes are costly compared to other electrode materials: For example a Pt/Ti electrode for the Micro Flow Cell costs around 495 $ at ElectroCell whereas the price for electrodes made from stainless steel or Ni is around 90 $ or 105 $, respectively. On the other hand Pt catalyzes the reduction of protons and therefore nearly no overpotential is observed. In commercial alkaline electrolyzers nowadays Ni and stainless steel are widely used as they show small overpotentials and Ni shows good corrosion stability in the used media[16]. For this reason Ni (from ElectroCell) and stainless steel (homemade electrode) were as well tested in the 2 chamber electrolysis process. In this experiment the electrolyte solution (anode chamber: 1 M Na_2SO_4 with H_2SO_4;*pH* ~ 2 ; cathode chamber: 1 M Na_2SO_4 with NaOH ;*pH* ~ 12.6) were recirculated with 400 ml/min at 60 °C. A 2 mm gap cell was used in this set of experiments and electrolysis was carried out in a galvanostatic way for 15 min (100 mA/cm^2). The potential difference traces are depicted in Figure 3.26. Ni and stainless steel show rather comparable potential profiles but the potential difference if using Pt/Ti is around 0.2 V lower. For this process Ni and stainless steel show the expected higher overpotential compared to Pt/Ti.

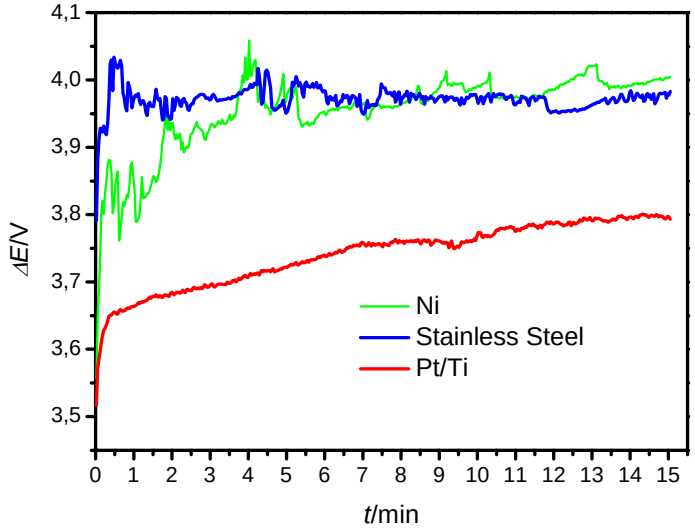

Figure 3.26 Potential profiles of two chamber (2 mm gap) electrolysis with 3 different cathode materials. Green line: Ni, blue line: stainless steel, red line: Pt/Ti. Anolyte solution (1 M Na_2SO_4 with H_2SO_4; *pH* ~ 2) and catholyte solution (1 M Na_2SO_4 with NaOH; *pH* ~ 12.6) were recirculated. 100 mA/cm^2 were applied for 15 min. T = 60 °C

3.3.1.3 Comparison with other systems

3.3.1.3.1 PSI system

The best operation system was a two chamber electrolysis cell with a gap of 1.6 mm. If the electrolytes are recirculated with a flow rate of 800 ml/min (± 25 %) and kept at a temperature of 80 °C a galvanostatic electrolysis (100 mA/cm^2) resulted in a potential difference of around 3.6 V. A similar system was already investigated by *Stucki and coworkers*.[2] Different to the above described experiments, they used a so called "zero gap cell", where the electrodes were in direct contact with the membrane. This means that the distance between anode and cathode was just the membrane thickness. As the electrolyte solution was "behind" the electrodes, holes were drilled into the electrodes to enable an exchange of the electrolyte in the membrane and the evolution of the produced gas. In their study the feed solution for the anode compartment (in total ~ 5 l) contained KOH and K_2SO_4 (0.4 M) while a KOH solution (also ~ 5 l) was fed into the cathode compartment. Both solutions were recirculated through the respective compartments. The temperature of the electrolyte solutions was adjusted to 70°C. The active area of the cell was 100 cm^2. Platinised Ti or Ti with an IrO_2/Ta_2O_5 as anode and as cathode Ni or platinised Ni was used. In the experiments a constant current density of 100 mA/cm^2 was applied for 300 min. Two cells were usually mounted in series and the cell voltage for one cell was afterwards calculated by the mean of the two cell voltages. During

this time the voltage increased from 3 to ~ 4.3 V . Nafion 324 was used as cation selective membrane.[2] A comparison of the results from the PSI study and the here above described system (LIOS system) can be seen in Table 3.4. The LIOS system has a lower potential difference between anode and cathode (~ 0.7 V difference) compared to the PSI system reported in the NEFF project summary.

Table 3.4 Comparison of parameters and results from the LIOS and the PSI[2] system for electrolysis of a sulfate solution

	LIOS	PSI
Electrolyte Solution (Anode// Cathode chamber)	1 M Na_2SO_4 // 1 M Na_2SO_4	K_2SO_4 (0.4 M) // KOH
Electrolyte volume	1 l	5 l
Temperature	~ 80°C	70°C
Current density	100 mA/cm^2	100 mA/cm^2
Gap	1.6 mm	thickness of the membrane
Active area	14.2 cm^2	100 cm^2
Membrane	Nafion 324	Nafion 324
Anode material	DSA for oxygen evolution	platinised Ti or Ti coated with IrO_2/Ta_2O_5
Cathode material	platinised Ti	Ni or platinisied Ni
Electrolyte flow	800 ml/min (± 25 %)	unknown
Voltage at t = 0 min	3.1 V	~ 3.1 V
Voltage after 180 min	3.5 -3.6 V	~ 4.3 V

From these results it seems to be feasible to implement two chamber electrolysis system into the process of methane synthesis using CO_2 from air.

3.3.1.3.2 Electrodialysis system of the Solar Fuel Prototype

As already previously described the prototype is using an electrodialysis stack to regenerate the absorption base and to release CO_2. In order to compare these two systems (eletrodialysis, two chamber electrolysis LIOS system) the energy demand for producing one mol or one m^3 of CH_4 was chosen as the comparative value.

The power demand for the LIOS system can be calculated by

$$P = U \cdot I = 3.6\ \text{V} \cdot 1.4\ \text{A} = 5.04\ \text{W} \qquad \text{(eq. 3.5)}$$

where U is voltage and I current. As 100 mA/cm^2 were used for the experiments and the active was 14.2 cm^2 I is equal to 1.4 A. Assuming an electrolysis time of 1 h gives an energy demand of 5.04 Wh. From the charge passed through the numbers of electrons N_e can be calculated as follows

$$Q = I \cdot t = 1.4\ \text{A} \cdot 3600\ \text{s} = 5040\ \text{C}$$
$$N_{e^-} = \frac{Q}{e} = \frac{5040\ \text{C}}{1.602 \cdot 10^{-19}\ \text{C}} = 3.15 \cdot 10^{22} \qquad \text{(eq. 3.6)}$$

For water splitting two moles e^- are needed to produce one mol H_2 and two moles H^+. According to the reaction equation for the acidification of sodium sulfate two moles H^+ corresponds to one mol released CO_2. This means that two moles e^- are needed to produce one mol H_2 and one mol CO_2 at the same time in theory. From this n for H_2 and CO_2 can be calculated by

$$\frac{3.15 \cdot 10^{22}}{2} = 1.573 \cdot 10^{22}$$
$$n_{H_2/CO_2} = \frac{N_{e^-}}{N_A} = \frac{1.573 \cdot 10^{22}}{6.022 \cdot 10^{23}\ \text{mol}^{-1}} = 0.026\ \text{mol} \qquad \text{(eq. 3.7)}$$

This leads to a total energy demand for the two chamber electrolysis of

$$\frac{5.04\ \text{Wh}}{0.026\ \text{mol}} = 192.9\ \frac{\text{Wh}}{\text{mol}_{H_2/CO_2}} \qquad \text{(eq. 3.8)}$$

The prototype uses an electrodialysis to regenerate the washing solution and to release CO_2. The production of hydrogen at the electrode is negligible in this case.. Preliminary experiments at ZSW testing an electrodialysis stack with an active membrane area of 57 cm^2 showed that about ~ 2.4 V per cell have to be applied to achieve a current density of 70 mA/cm^2.[17] The stack consisted of 5 cells. It is assumed that a potential of 2.5 – 3 V is necessary to achieve a current density of 100 mA/cm^2, which is the current density of the LIOS two chamber electrolysis. With this an energy demand of $134.6 - 161.5\ \frac{\text{Wh}}{\text{mol}_{CO_2}}$ for the electrodialysis system can be calculated. This value is lower than the energy demand of the two chamber electrolysis, but the LIOS two chamber system produces not only CO_2, but additionally one mol of H_2 per mol CO_2. Therefore, the energy demand for an additional mol of H_2 has to be added to the energy demand of the electrodialysis. For the fuel synthesis reaction

$$CO_2 + 4\ H_2 \rightarrow CH_4 + 2\ H_2O \qquad (2.5)$$

per mol CO_2 four moles H_2 are required. Assuming a Faradaic efficiency of 100 % for the H_2 production in the two chamber system one mol H_2 is already generated and does not have to be produced by an additional water electrolyzer. Today's water electrolyzer operate with an efficiency of around 66 %. [18] An efficiency of 70 % for the electrolyzer corresponds to 1.76 V for the H_2 production (from thermodynamics 1.23 V are need). From this an energy demand

of 94.76 $\frac{\text{Wh}}{\text{mol}_{H_2}}$ can be calculated. Therefore the total energy demand for using the electrodialysis system an be calculated as the demand for the CO_2 release plus 4 times the energy demand of the electrolyzer, whereas for the two chamber electrolysis system the value for the electrolyzer has to be taken into account only 3 times. The calculation for the total energy demand for both systems per mol CH_4 is given in Table 3.5.

Table 3.5 Calculation of the total energy demand for the electrodialysis and for the 2 chamber electrolysis system

	Electrodialysis system	Two chamber electrolysis system
Energy demand for CO_2 release	134.6 – 161.5 $\frac{\text{Wh}}{\text{mol}_{CO_2}}$	192.7 $\frac{\text{Wh}}{\text{mol}_{CO_2/H_2}}$
Energy demand for electrolyzer	379 $\frac{\text{Wh}}{4\ \text{mol}_{H_2}}$	284 $\frac{\text{Wh}}{3\ \text{mol}_{H_2}}$
Total energy demand	513.6 – 540.5 $\frac{\text{Wh}}{\text{mol}_{CH_4}}$	476.4 $\frac{\text{Wh}}{\text{mol}_{CH_4}}$

Assuming an ideal gas the volume of 1 mol gas can be calculated to 0.0245 m^3 (T = 25 °C, p = 1 atm) . This leads to an energy consumption for the electrodialysis system of 20.9 – 22 $\frac{\text{kWh}}{\text{m}^3_{CH_4}}$ and to 19.4 $\frac{\text{kWh}}{\text{m}^3_{CH_4}}$ for the 2 chamber electrolysis system. This shows that the two chamber electrolysis system has the potential to increase the overall efficiency of the CO_2 from air to fuel process. *Specht and coworkers*[19] report a value of 280 $\frac{\text{kJ}}{\text{mol}_{CO_2}}$, which corresponds to ~ 78 $\frac{\text{Wh}}{\text{mol}_{CO_2}}$ This value is lower than the herein used value for the comparison, but the current density reported in *Specht and coworkers*[20] was a factor of 2 lower (50 mA/cm^2). It can be assumed that this value will increase if the electrodialysis is operated at 100 mA/cm^2.

3.3.2 Three chamber electrolysis

3.3.2.1 Three chamber electrolysis using Na_2SO_4 as electrolyte

Using a three chamber system that has the same gap between the electrodes (membrane thickness not taken into account) as a two chamber system allows estimating the potential drop over a membrane if the same flow velocity in both system is guaranteed. Thus the same volume per time should be present and the potential drop over the electrolyte solutions is assumed to be similar for both configurations.

For this reason preliminary measurements with a three chamber electrolysis cell were performed to verify the working principle. A three chamber cell was built with a gap of 12 mm between the electrodes and an active area of 10 cm^2 where all the compartments are separated from each other by means of a Nafion 324 membrane. The initial electrolyte solution of the anode chamber was a 0.5 M Na_2SO_4 solution with H_2SO_4 (*pH* ~1). For the middle and the cathode chamber the initial electrolyte solution was a 1 M Na_2SO_4 solution. All solutions had a temperature of 60 °C and were recirculated through the respective compartments. The flow rate was 200 ml/min (calibrated with flow through cell). Electrolysis was performed by applying 100 mA/cm^2 for 1 h (Figure 3.27). After 1 h of electrolysis a potential difference of around 4.6 V was observed. From *pH* values recorded after every 15 min the expected trend is visible: The *pH* values in the anode chamber do not change significantly with electrolysis time whereas in the middle chamber an increase in the acidity and in the cathode chamber in the alkalinity is observed. The potential is higher compared to all above shown galvanostatic two chamber electrolysis experiments. The main reason for this is the rather large gap and an additional membrane.

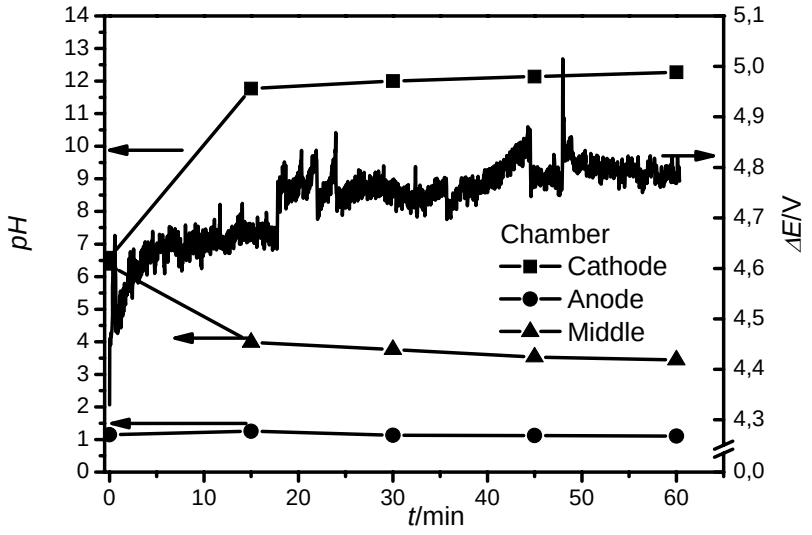

Figure 3.27 Three chamber electrolysis (gap: 12 mm) of sodium sulfate solution with recirculation (200 ml/min, T = 60 °C) of all solutions. Initial electrolyte solution concentrations for the different chambers: Anode: 0.5 M Na_2SO_4 solution with H_2SO_4 (*pH* ~1), Cathode and Middle: 1 M Na_2SO_4. Squares: *pH* of catholyte solutions, dots: *pH* of anolyte solution, triangles: *pH* of electrolyte solution in the middle chamber. Solid line: potential difference between anode and cathode during 1 h of electrolysis (100 mA/cm^2 applied)

Using the same electrolyte concentrations as described above different parameters were varied. A summary of the results is shown in

Table 3.6. The same trend as for the two chamber electrolysis is observed: Higher flow rates and higher temperatures improve the process (lower potential difference between the electrodes for the same current density). Cells with a gap of 12 mm had an active area of 10 cm^2 whereas cells with a smaller gap (9 mm) had an active area of 14.2 cm^2. In all experiments the calibration of the pump was done by pumping the solutions through the cell. For experiments with cells of a gap of 9 mm the highest flow rate that could be reached was 200 ml/min. A possible explanation for this is a higher flow resistance for the smaller gap.

Table 3.6 Comparison of different three chamber electrolysis: different gaps (*d*), different temperatures and flow rates

d/mm	*T*/°C	*flow rate*/ml*min^{-1}	pH_{Anode}	pH_{Middle}	$pH_{Cathode}$	ΔE/V
12	60	200	1.1	3.4	12.4	4.6
12	80	200	1.1	3.2	12.6	4.4
12	80	800	1	3	12.7	4.2
9	60	200	1	3.2	12.3	4.7
9	80	200	1	2.9	12.5	4.5

The main purpose of the three chamber electrolysis experiments was to estimate the potential drop over either a Nafion 324 membrane or a bipolar membrane. For a determination of this factor for a Nafion 324 membrane a galvanostatic two chamber electrolysis was compared with a 3 chamber process under similar experimental conditions: The gap for both cells was 9 mm and the same flow velocity (0.018 m/s) was ensured. Thus a flow velocity of 150 ml/min per chamber for the 2 chamber and 100 ml/min per chamber for the three chamber electrolysis was chosen. All membranes used in the two cells were Nafion 324. The electrolyte solutions were recirculated through the chambers and kept at a temperature of 60 °C. For the two chamber electrolysis the initial concentration for both electrolyte solutions was 1 M of Na_2SO_4 . The same concentration was used for the middle and the cathode chamber in case of the 3 chamber process. The anolyte solution for the three chamber configuration was 0.5 M Na_2SO_4 solution adjusted to *pH* ~1 (with H_2SO_4). Both cells had an active area of 14.2 cm^2 and electrolysis was performed with 100 mA/cm^2. The comparison is depicted in Figure 3.28 and shows that in the three chamber electrolysis the voltage is ~ 0.5 V higher compared to the two chamber process. The *pH* values of catholyte solution are identical. In addition the difference in the *pH* between anolyte solution in the two chamber setup and electrolyte solution in the middle chamber (three chamber system) are very similar. The main contribution to the higher voltage is the electric resistance of the additional membrane (Nafion 324). In the literature[21] an area sheet resistance of 4 – 5 Ωcm^2 is assumed for cation exchange membranes. A current density of 100 mA/cm^2 leads therefore to a potential drop of around 0.4 – 0.5 Ω for one of these membranes. This is in very good agreement with the 0.5 V difference between the two and three chamber electrolysis presented here.

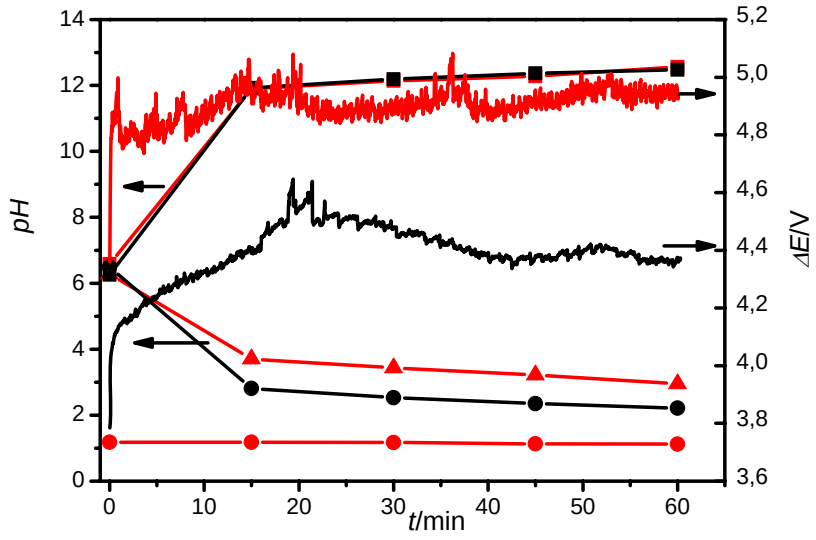

Figure 3.28 Comparison of a two chamber (black line and symbol) and a three chamber (red line and symbols) electrolysis with recirculating solutions (T = 60 °C,100 mA/cm^2 for 1 h). Squares: *pH* of catholyte solution, dots: *pH* of anolyte solution, triangles: *pH* of electrolyte solution in the middle chamber, solid line: potential difference between anode and cathode.

The voltage drop over a bipolar membrane is assumed to be much higher: For a current density of 100 mA/cm^2 values of 1.1 – 1.3 V [22] and area sheet resistances up 12 - 22 Ωcm^2 [21] are reported in the literature. For an estimation of this voltage drop, a bipolar membrane purchased from Hescon was used for separating anode and middle chamber. The other experimental conditions like current density, temperature, flow rate etc. were the same as above described for the Nafion membrane. Figure 3.29 shows a comparison of the voltage difference between the electrodes for these two membranes during galvanostatic electrolysis. A value of around 0.9 V higher for the bipolar membrane compared to the Nafion 324 is observed. Together with the estimated voltage drop of around 0.5 V for the Nafion 324 this leads to a voltage drop of around 1.4 V over this type of bipolar membrane. This result is in good agreement with the literature.

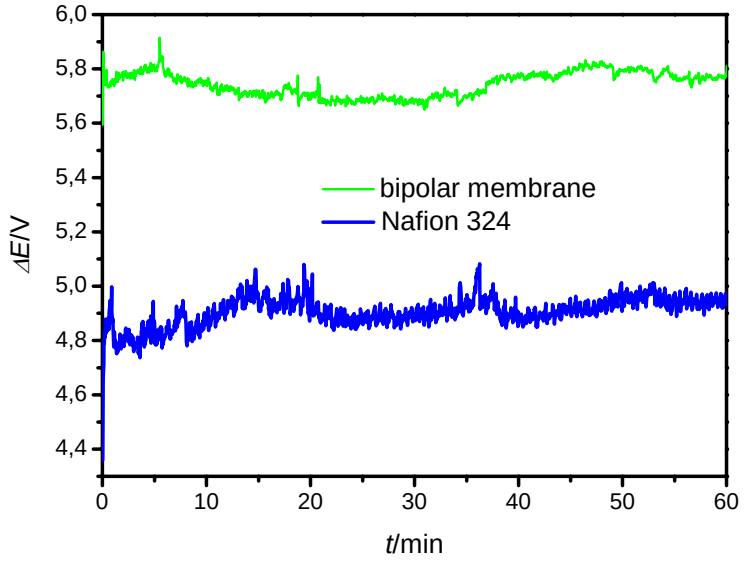

Figure 3.29 Comparison of the voltage traces for 2 three chamber electrolysis processes with different membranes separating anode and middle chamber. Green line: bipolar membrane; blue line: Nafion 324

The usage of a three chamber electrolysis system for the sulfate splitting does not seem to be energetically favorable over the two chamber system as higher potential difference between the electrodes are present due to one additional membrane. Especially bipolar membranes lead to a much higher energy consumption.

3.4 Outlook: Three and two chamber electrolysis of carbonate solutions under pressure

Three and two chamber electrolysis processes using Na_2SO_4 solutions were already discussed above and in Chapter 1 (1.2.2). Due to higher overpotentials observed for the three chamber geometry, mainly due to an additional membrane, compared to the two chamber electrolysis of a this system does not seem to advantageous. Using directly the carbonate solution from the absorber as feed solution for a three chamber process was previously discussed in the literature.[2,23] The main advantage compared to a two chamber electrolysis of a carbonate solution is the separate release of O_2, CO_2 and H_2 but on the cost of a higher resistance due to an additional membrane. Furthermore, CO_2 release directly in an electrolysis system enhances the overpotential as another gas is produced. This problem can be solved by operating a three

chamber electrolysis system under pressure in a “Feed and Bleed” mode as previously described for the electrodialysis in Chapter 2 (2.2.2). Thus CO_2 will be in physical solution inside the electrolysis unit and released afterwards in a stripper by reduction of the operating pressure. In addition as hydrogen is already produced under pressurized conditions the energy costs for hydrogen compression, which is needed for fuel synthesis, can be saved. A schematic drawing of such a process is shown in Figure 3.30. Between middle chamber (B) and cathode chamber is a cation selective membrane. The separation between anode chamber (A) and middle chamber (B) can either be a cation selective membrane, an anion selective membrane or a bipolar membrane. The pumps P1 – P3 together with the valves V1 – V3 are used for pressure generation. In the cathode chamber (C) hydrogen and the absorption base are generated. One part of the base is removed (“Bleed”, 1) and transferred to the absorber for CO_2 absorption. The carbonate solution leaving the absorber is fed to the middle chamber (“Feed”, 2). The protons that migrate from the anode chamber (3) through the membrane into the middle chamber are used to release CO_2 in this chamber. As the electrolysis cell is operated under pressure CO_2 is in physical solution. After reducing the pressure (valve V2) gaseous CO_2 is obtained. In order to ensure volume neutrality in the tanks for the loops B and C, some solution form loop B has to be transferred to loop C.

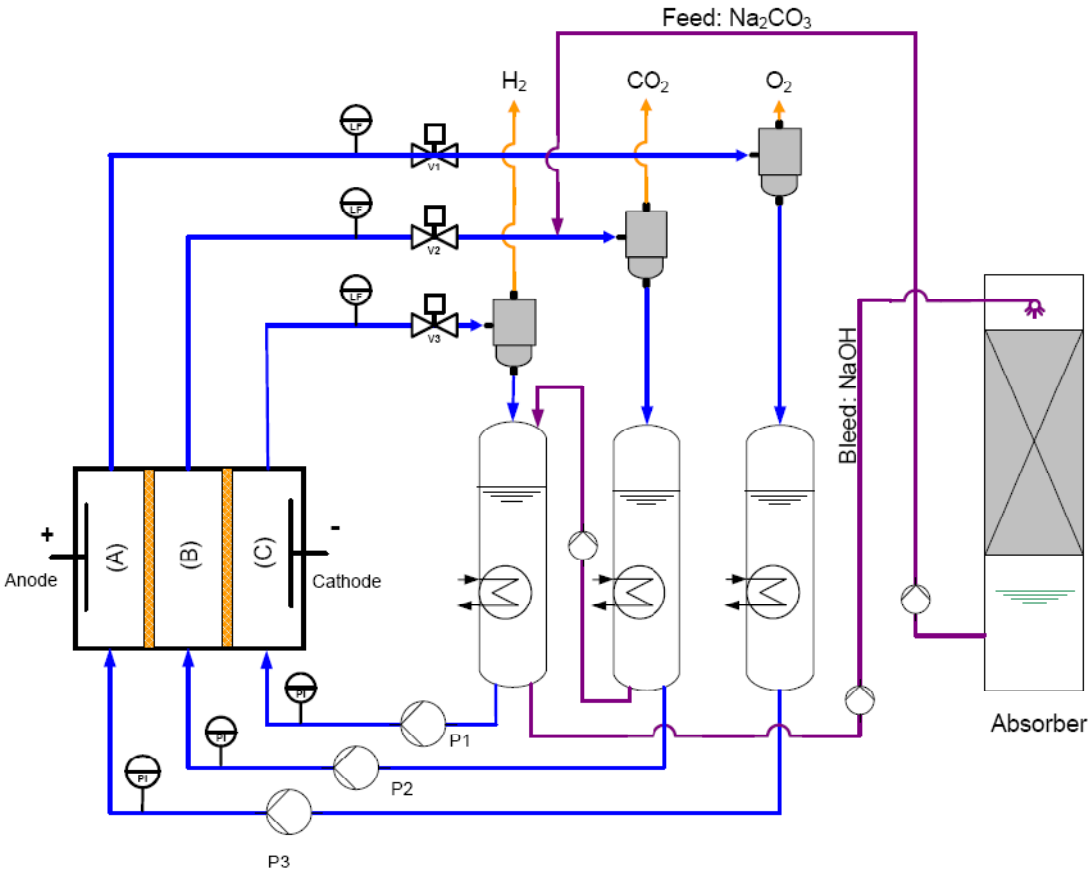

Figure 3.30 Schematic drawing of a three chamber electrolysis process operated under pressure using a Na_2CO_3 solution**.** Thanks to M. Kruijen for providing the picture.

A two chamber electrolysis cell using Na_2CO_3 as electrolyte has the disadvantage of simultaneous production of CO_2 and O_2 in the anode chamber. By operating such a system as well under pressure (like shown in Figure 3.31) this can be avoided. Due to the pressure in the electrochemical cell (established through pumps P2 and P3 and the valves V1 and V2) CO_2 is in physical solution. After reducing the pressure (V5) CO_2 is obtained as gas. The "Feed and Bleed" principle is similar to the above described 3 chamber process under pressure. The separation between anode and cathode chamber (B and C) is done by means of a cation selective membrane. The two chamber electrolysis system of carbonate solutions has to be tested especially in terms of complete O_2 degassing prior to the CO_2 release.

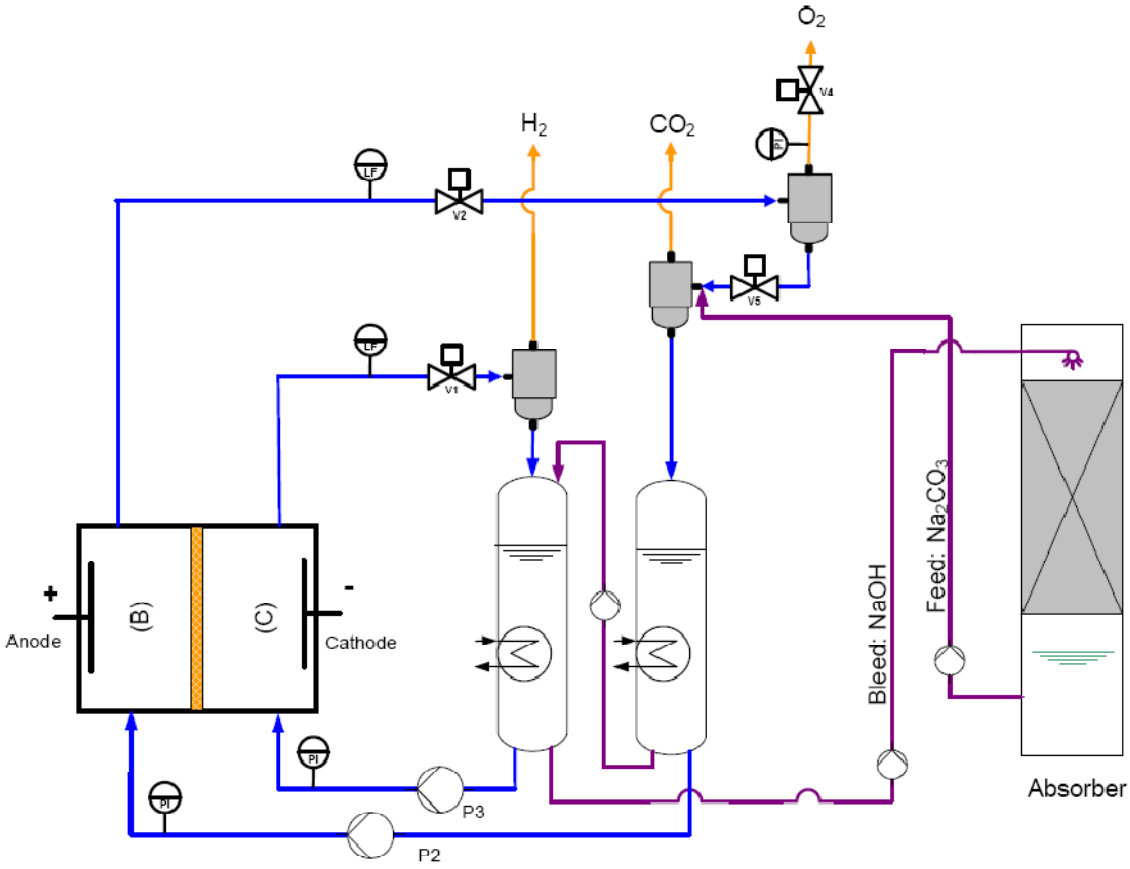

Figure 3.31 Schematic drawing of a two chamber electrolysis process operated under pressure using a Na_2CO_3 solution**.** Thanks to M. Kruijen for providing the picture.

3.5 Summary

Two chamber electrolysis of sodium sulfate solutions is an interesting method from the energetic point of view for generation of stripping acid, absorption liquid and hydrogen gas simultaneously. As shown in this chapter the electrolysis process performs better if operated with higher electrolyte concentrations, elevated temperature, larger flow rates and smaller gaps between the electrodes. Temperature dependence measurements showed an activation energy of around 10 kJ/mol for a 0.6 M Na_2SO_4 solution and therefore elevated temperatures to improve the efficiency of the given process. Larger flow rates enhance the transport of the produced gas (O_2 and H_2) out of the electrolysis cell. This decreases the overpotential of the process as gas has a high electric resistance. As the gap between the electrodes determines how much electrolyte is present in the electrolysis flow cell, decreasing this gap results in lower overall overpotentials. Compared to the influence of the temperature and the flow rate a weaker dependence of the electrolysis performance on the gap was found. *pH* values of anolyte and catholyte solution confirmed the working principle of the process. Due to the applied voltage difference between anode and cathode water is split at the electrodes: H_2 and OH^- are produced at the cathode while O_2 and H^+ are produced at the anode. Mainly Na^+ migrates through the cation selective membrane and thus the anolyte soluiton is acidified while the *pH* of the catholyte solution increases. The best operating parameters were found to be as follows: A two chamber electrolysis with a gap of 1.6 mm was operated with 100 mA/cm^2. Both electrolyte solutions were recirculated through the chambers and kept at a temperature of 80 °C. Using DSA and Pt/Ti as electrodes resulted in a voltage of 3.6 V after 3 h of electrolysis. In an estimation on the energetics, these operating conditions result in a total energy demand of 19.7 $\frac{\mathrm{kWh}}{\mathrm{m}^3_{CH_4}}$ which was found in an first estimation to be lower than an electrodialysis process. Thus a two chamber electrolysis is promising to increase the overall efficiency of the prototype module. In the near future an upscaling process is necessary for a better comparison between the energy demand for an electrodialysis and a two chamber electrolysis. Preliminary measurements with a three chamber configuration show higher overpotentials compared to the two chamber process and does not seem to be favorable for implementation if using a Na_2SO_4 electrolyte solution. An outlook on electrolysis systems with acidification inside the cell was as well described (carbonate as electrolyte). The main idea is to operate either a two or a three chamber system under pressure, thus CO_2 will stay in physical solution and will not lead to further overpotentials caused by gas bubbles.

3.6 References

[1] S.Stucki, A. Schuller, M. Costantinescu, *Int. J. Hydrogen Energy*, **20 (8)**,1995 , 653-663
[2] S. Stucki, M. Constantinescu, A. Schuler, *NEFF Projekt Nr. 467 Schlussbericht*, 1993
[3] M. Egginger, G. Waldstein, A. Fuchsbauer, E. Portenkirchner, M. Kruijen, B. Meana Esteban, E. Avci, P. Thamyongkit, D. Egbe, K. Oppelt, P. Trefflinger, S. N. Sariciftci *,Solar Fuel Project overview*, LIOS, 2009
[4] J. Jörissen, S. M. Breitner, C. Funk, *J. Memb. Sci.,* **213**, 2003, 247-261
[5] S.M. Davis, G.E. Gray, P.A. Kohl, *J. Appl. Electrochem.*,**38**, 2008, 777-783
[6] DuPont Nafion perfluorinated membranes, Product information, 3/18/02
[7] K.N. Mani, *J. Membr. Science*., **58,** 1991,117 - 138
[8] S. Koter, A. Warszawski, *Pol. J. Environ. Stud.*, **9 (1)**, 2000, 45 - 56
[9] F.G. Wilhem, *PhD. Thesis: Bipolar Membrane Electrodialysis,* University of Twente, Twente University Press, 2001
[10] *ElectroCell Micro Flow Cell Instruction Manual*, ElectroCell A/S, Tarm, Denmark
[11] *BGIA Gestis Stoffdatenbank*: http://biade.itrust.de
[12] C.H. Hamann, W. Vielstich, *Elektrochemie*, 4. Auflage, Wiley-VCH Verlag, 2005
[13] P.W. Atkins, *Physikalische Chemie,* dritte Auflage*,* Wiley-VCH Verlag, 2001
[14] G.M. Barrow, *Physikalische Chemie,* 6. berichtigte Auflage, Bohmann-Verlag, 1984
[15] *BGIA Gestis Stoffdatenbank:* http://biade.itrust.de
[16] C.A. Grimes, O.K. Varghese, S. Ranjan In *Light, Water, Hydrogen The Solar Generation of Hydrogen by Photoelectrolysis*, Springer Science+Business Media, LLC,2008,Chapter 2
[17] U. Zuberbühler, personal communication
[18] B. Liptak, *Post Oil Energy Technology: The World's First Solar – Hydrogen Demonstration Plant*, CRC Press, Taylor & Francis Group, LLC, 2009
[19] M. Specht, A. Bandi, M. Elser, A. Heberle, U. Maier, K. Schaber, T. Welmer,CO_2 *Recycling zur Herstellung von Methanol, Endbericht*, 2001
[20] M. Specht, A. Bandi, M. Elser, A. Heberle, U. Maier, K. Schaber, T. Welmer,CO_2 *Recycling zur Herstellung von Methanol, Endbericht*, 2001
[21] M. Hein, A. Grabowski, *Produktion von Säuren und Laugen mittels bipolarer Membranen"; Praktikum für Studenten der Technischen Biologie;* ZSW, 2003
[22] J.L. Gineste, G. Pourcelly, Y. Lorraine, F. Persin, C. Gavach, *J. Membrane Sci*., **112**,1996,199-208
[23] M. Steinberg, Patent US 4197421, 1980

Chapter 4

Studies on an In Situ Electrodeposited Cobalt Based Catalyst for Water Oxidation

Electrochemical water splitting is of high interest for the CO_2 into fuel process (see Chapter 1 and 2) as both electrochemical acid generation (either by electrodialysis or electrolysis) and water electrolyzers are based on this principle. From the two half reactions the oxidation is considered to be more complex. Therefore there is a high interest in catalysis for this reaction and a very active field of research exists. In 2008 a catalytic material was introduced by *Kanan and Nocera*[6] that is obtained in situ upon electrolysis in a neutral *pH* buffer containing Co^{2+} ions. Details on the formation as well as the working mechanisms of the catalyst are not fully understood yes. To get more information in situ spectroelectrochemical techniques to study the formation as well as the stability of the catalyst different electrolytes were preformed. In general, in situ spectroelectrochemical techniques combine electrochemistry and spectroscopy: while electrochemical measurements are performed changes in the spectroscopic behavior of species of interest are investigated. The spectroscopic properties of the catalyst film in two different regions of the electromagnetic spectrum were measured: in the UV-Vis region by means of in situ UV-Vis absorption and in the IR region by FTIR Attenuated Total Reflection (FTIR-ATR). Special emphasis in these studies was on a possible implementation of the catalyst either in electrolysis processes (two or three chamber geometry) of sulfate solutions.

4.1 Introduction

As described previously (Chapter 1 and Chapter 2) one CO_2 reduction pathway is hydrogenation. A carbon – neutral source of hydrogen is the electrolysis of water if electric energy is obtained from carbon free sources.[1] Electrochemical splitting of water can be divided into 2 half reactions as can be seen below (ε^0 are the standard electrode potentials for the half reactions[2]):

$$\begin{aligned} 2H_2O &\rightleftharpoons O_2 + 4H^+ + 4e & \varepsilon^0 &= 1.229\ V \\ 4H^+ + 4e^- &\rightleftharpoons 2H_2 & \varepsilon^0 &= 0\ V \\ \hline 2H_2O &\rightarrow 2H_2 + O_2 & \Delta E^0 &= -1.229\ V \end{aligned} \qquad (4.1)$$

From the reaction scheme above one can see that ΔE^0 for the reaction is negative which goes along with $\Delta G > 0$. This means that the overall reaction will not occur spontaneously and energy has to be applied to the system. In electrochemical water splitting the energy is supplied to the system by applying a potential difference between the two electrodes. The minimum potential difference that is need under standard conditions is 1.229 V.

Of the two half cell reactions the oxidation of water is considered to be more complex because this reaction requires four electrons coupled to the removal of four protons as well as the formation of a relatively weak bond between two oxygen atoms.[3] Commercially, water splitting is done with electrolyzers that are very efficient, operating at 1 A/cm^2. But this high current density comes with a price: harsh operating conditions and high engineering costs.[4] On the other hand neutral water is oxidized at Pt electrodes and there are reports on some precious metal oxides that show electro catalytic oxidation of water in neutral or weak acidic solutions.[5] In the year 2008 a new water oxidizing catalyst was reported that electrodeposits in situ on various types of electrodes from an electrolyte solution containing Co^{2+} ions and a neutral *pH* phosphate electrolyte (Pi).[6,7] The catalyst was shown to be amorphous and can grow up to thickness of around 3 µm upon the passage of 40 C/cm^2. Further studies revealed that the catalyst can be obtain from other Co^{2+} containing electrolyte solutions as well and shows a Faradaic efficiency of around 100 % for the oxidation of water.[8] A crucial point for the electrodeposition of the catalyst seems to be the proton accepting ability of the electrolytes: If the electrolyte is exchanged to poor proton accepting systems (eg. sulfate electrolytes) a much higher amount of Co^{2+} has to be added to the electrolyte (~ 10 – 100 fold higher) in order to ensure a film formation and Faradaic efficiencies deviating from 100 % for oxygen evolution are obtained.[8] Electrolyte solutions with a high proton accepting ability, are

referred here as buffered systems (buffering around neutral *pH*), whereas electrolyte solutions with a poor proton accepting ability are in the following called unbuferring. in controlled potential experiments (1.3 V vs NHE) current densities of up to 1.5 mA/cm^2 in Pi electrolyte and 2.3 mA/cm^2 in borate base electrolyte (Bi) have been reported. For unbuffering electrolyte (potassium sulfate) the current density drops below 0.1 mA/cm^2.[8] The elemental composition of the catalyst showed a Co:P ratio of ~ 2:1 for films electrodeposited from Pi electrolyte solutions and a ration of Co:B of ~ 10:1 for the same deposition method using Bi as electrolyte. The anion composition is balanced by a monovalent cation independent of the Co to anion ratio. Therefore a common Co-oxide effective unit was proposed to be present in all films, with a unit size of < 5 nm.[8] More recent studies show that most likely the central structure unit in the catalytic film is a cluster of interconnected complete or incomplete Co^{3+} - oxo cubanes. Oxygen atoms from the phosphate group as bridging ligands of the Co atoms can be excluded, but a terminal ligation of phosphate atoms to the cluster is possible.[9] This ligation would lead to structural similarity of these cubanes to the structure of the Mn complex (oxygen evolving complex) in the photosystem II (PS II) in natural photosynthesis[10,11] Like the oxygen evolving complex in PS II the catalytic film shows self assembly upon electrodepostion and exhibits a repair mechanism: In Pi electrolyte, catalytic films under a potential bias (1.3 V vs NHE) show nearly no leaching of cobalt in contrast to films held under open circuit potential. Upon applying a potential bias again to the film cobalt is reabsorbed to the catalyst. Phosphate in general shows a higher exchange rate than cobalt but as well films held under potential bias release less phosphate than under open circuit potential. In unbuffered system such a repair mechanism could not be observed. Additionally films under open circuit potential leach less cobalt than under applied potential in case of unbuffering electrolytes. [7,12]

A possible working mechanism of the catalyst was proposed by *Kanan and coworkers*[7] (see Figure 4.1): Co^{2+} ions in the solution are oxidized on the electrode surface to Co^{3+} and form a deposit on the electrode together with the anion of the electrolyte (in the figure HPO_4^{2-} from phosphate electrolyte). In this deposit Co^{3+}- OH is further oxidized to Co^{4+} - oxo form, from which oxygen is released and cobalt is reduced back to a Co^{2+} form. Co^{2+} might leach into the electrolyte in order to be oxidized again immediately to start the catalytic cycle again.[7]

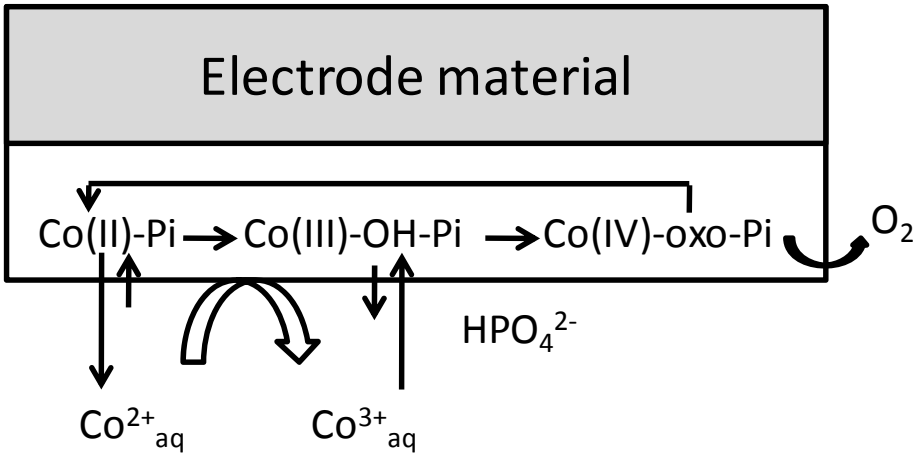

Figure 4.1: Possible working mechanism of the catalyst for water oxidation. Pi represents the anion of the used buffer. Scheme according to Ref [7]

In order to gain more knowledge about the working principle, the formation and the stability of the catalyst were studied with special attention towards possible applications in the given process of CO_2 recycling (see Chapter 1 and 2). Possible application for the water oxidizing catalyst would be in the water electrolyzer or in the LIOS two chamber electrolysis system. In the LIOS two chamber electrolysis system, a sodium sulfate solution is used, which will be acidified in the anode chamber. Therefore the stability of the catalyst is a crucial point. Mainly in situ spectroelectrochemical techniques were used in order to investigate the formation and the stability of the catalytic film.

4.2 Experimental

4.2.1 Cyclic Voltammetry

Cyclic Voltammetry (CV) is a very common technique in electrochemistry. In CV the potential is scanned linearly with a given scan rate (50 mV/s in all the experiments) between two values and then back to the initial value thus giving rise to a potential profile with a triangular shape. During the cycle the cell current is recorded as a function of the applied potential. The cell current is often dived by the active area in order to obtain the current density (j/mA*cm^{-2}) as a y axis value in the so called cyclic voltammogram.[13] For CV measurements an electrochemical measurement setup consisting of a potentiostat (Jaissle IMP 88 PC potentiostat/galvanostat) connected to a scan generator (ELCM-KIT 003 from IPS) and a computer, was used.

An electrochemical cell with an H shape was used in order to perform CV measurements. The cell contains 2 compartments that are separated by a frit and both are filled with electrolyte

solution. One compartment contains the working electrode (WE) and the reference electrode (RE) and in the other compartment a counter electrode (CE) is immersed in the electrolyte. As RE an Ag/AgCl (3M) from BAS (RE – 5B Ag/AgCl electrode) was used and all the potential values in cyclic voltammograms are referred to this electrode. A platinum plate was used as a counter electrode. For the working electrode either indium tin oxide coated glass (ITO, 15 ohm/sq from KINTEC) or Pt was chosen. The electrolyte solution contained 0.5 mM $Co(NO_3)_2.6H_2O$ (A.C.S. regagent from Sigma Aldrich) in 0.1 M neutral *pH* phosphate buffer unless stated otherwise. The buffer was prepared in the following way: KH_2PO_4 (purum, p.a. from Fluka Analytical) was dissolved in 18 MΩ water and the pH value was increased to 7 by addition of 2M KOH (prepared by dissolving a stoichometric amount of purum p.a. pellets from Fluka in 18 MΩ water) solution. Therefore the buffer contains KH_2PO_4 and K_2HPO_4. This type of buffer is usually called KPi in the present literature.[6,7,8,9,12]

4.2.2 Potentiostatic/galvanostatic experiments

The formation as well as the stability was monitored in either potentiostatic (constant applied potential) or galvanostatic (constant applied current) measurements. In case of potentiostatic experiments WE, RE and CE were mounted as described above in an H cell and a constant potential was applied. As WE, ITO or Pt was used. In glavanostatic experiments mostly two electrodes were used (WE and CE) unless stated otherwise. For galvanostatic measurements using 2 electrodes CE and RE were short cut on the Potentiostat/Galvanostat. The electrochemical measurement setup was the same as described above for CV measurement.

4.2.3 Quantification of gas production

The amount of gas produced using Pt as WE was measured using a Hoffman water electrolyzer apparatus. The electrolyte (5 mM $Co(NO_3)_2.6H_2O$ in 0.1 M KPi) was filled into the apparatus. A Pt plate (1 cm^2) was used as WE and another one (0.5 cm^2) was working as CE. The RE was immersed in the electrolyte in the reservoir. A constant current of 4 mA (2 mA/cm^2) was applied for 8 h. After every 30 min the amount of O_2 gas produced (in ml) was recorded. In order to make the reading of the ml gas produced easier the apparatus was filled with N_2 gas to a certain level. The read out ml was converted afterwards to mol by using the ideal gas law: At 25 °C one mol of ideal gas corresponds to 24.5 l.

4.2.4 In situ spectroelectrochemistry

Spectroelectrochemistry combines spectroscopic and electrochemical techniques meaning that spectroscopic investigations are done during an electrochemical process and are therefore called “in situ” techniques. Changes in the optical properties in the UV-Vis and in IR region were probed with two different techniques: in situ UV-Vis absorption and in situ FTIR Attenuated Total Reflection (FTIR-ATR).

4.2.4.1 In situ UV-Vis absorption

The spectroelectrochemical measurement cell is depicted in Figure 4. 2 contains WE and CE connected to a galvanostat. The cell is filled with electrolyte solution and mounted inside a two beam spectrophotometer (Varian 3G UV-Vis). The absorption spectrum is measured related to a reference cell that contains as well the electrolyte solution and WE. Due to this fact only absorption spectra of materials that change upon an electrochemical process will be obtained. As the electrolyte solution and the WE are assumed not to change their absorption behavior the absorption features of the film growing on WE will be measured. Care must be taken with the choice of WE: it needs to be transparent in the spectral region of interest. ITO fulfills this requirement as it has an optical transmittance (>90 %) from visible to near IR.[14] A coiled Pt wire is used as CE. During the time of electrolysis usually every 30 min an absorption spectrum was recorded.

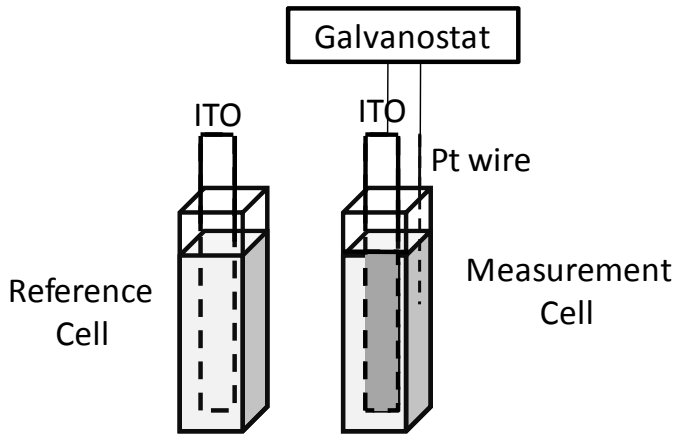

Figure 4. 2: Scheme of the spectroelectrochemical cell used for in situ UV-Vis absorption

4.2.4.2 In situ FTIR-ATR

In this technique a flow cell is used as electrochemical cell and placed inside a FTIR spectrometer (Bruker IFS66S). A schematic drawing is shown in Figure 4.3a and a picture of cell components in Figure 4.3b. The FTIR spectra were recorded by a MCT detector. Most of in situ techniques based on FTIR use reflection mode FTIR measurements. They can be divided into two groups: external and internal reflection. As in this work internal reflection was used, only this method will be described here.

In the internal FTIR reflection spectroscopy the IR radiation approaches the interface of electrode and electrolyte solution from the optical denser medium (eg the electrode or the optical crystal respectively). If the angel of incidence (θ) is larger than the critical angle (θ_c) total reflection inside the optical crystal (electrode) is obtained. θ_c is defined as:

$$\Theta_c = \sin^{-1}\left(\frac{n_1}{n_2}\right) \qquad \text{(eq. 4.1)}$$

where n_1 refers to the refractive index of the optical denser medium 1 and n_2 to the refractive index of the optical thinner medium 2.[15,16,17] The refractive index is defined as the ratio between the speed of light in vacuum and in a given material and is therefore a measure for how much the speed of light is reduced inside the material due to its interaction with the radiation.[18] Due to the superposition of incoming and reflected waves a standing wave pattern will be established. In the optical thinner medium an evanescent wave exists that has the same frequency as the incoming wave. Its electric field amplitude is exponentially decaying with the distance of the surface. The distance where the electric field amplitude reaches a value of 1/e of the value at the surface is called penetration depth d_p. The penetration depth is given by:

$$d_p = \frac{\lambda}{2\pi\sqrt{\sin^2\Theta - \left(\frac{n_2}{n_1}\right)}} \qquad \text{(eq. 4.2)}$$

where λ is the wavelength of the incoming light, θ the angle of incidence and n_1 and n_2 are the refractive indices of the two media.[15-17]

An IR absorbing substance near the surface of the optical thicker medium will interact with the evanescent wave and cause the resulting reflection to be attenuated. Thus this technique is called FTIR-ATR (attenuated total reflection).The reflection element used in this technique must have some important properties like conductivity, chemical and electrochemical stability, transparency in the IR region and a high refractive index. It is usually shaped in form

of a trapeze or a parallelogram with 45° entrance and exit surfaces. This geometry causes the IR beam to be reflected several times inside the crystal therefore an average spectrum of the whole crystal surface is obtained.[16,17]

Zinc selenide (ZnSe) was chosen as the material for the internal reflection element (10 x 10 x 1 mm or 10 x 10 x 2 mm) but it is a non conducting material. For this reason a thin layer of Pt (10.5 or 15 nm) was sputtered on top of one side in order for the crystal to be able to work as an electrode. A Cu wire was soldered by indium to the Pt layer for contacting with the electrochemical measurement system. A Pt plate was used as a counter electrode and both electrodes were connected to an electrochemical measurement setup (described above in 4.1) operating in galvanostatic mode. The FTIR-ATR cell (Figure 4.3b) was made out of Teflon and one side of the cell was the internal reflection ZnSe crystal. The cell was filled with electrolyte solution in such a way that during the whole measurement time a constant flow was obtained through the cell. A current density of ~ 0.3 mA/cm^2 was applied and over the time of 1 hour every 15 min a spectrum was recorded (aperture: 6 mm).

By this technique as mentioned above FTIR absorption features of substances on or near the electrode can be measured, thus the absorption characteristics of the electrolyte will as well be measured. The main interest is usually in the spectral information of a film on the working electrode. Therefore a reference spectrum is chosen and all subsequent obtained spectra are related to this reference spectrum. In herein presentenced studies the reference spectrum was chosen to be in case of FTIR-ATR spectra of water or the electrolyte the spectrum from the electrode (ZnSe crystal + Pt) or the spectrum of the electrolyte solution for FTIR-ATR spectra of the catalytic film. Due to the relation to a reference spectrum, spectra obtained by this technique are difference spectra. When plotted in units of absorption, new IR bands point upwards in the difference spectra, whereas IR bands pointing downwards are here related to species vanishing during the electrochemical process.

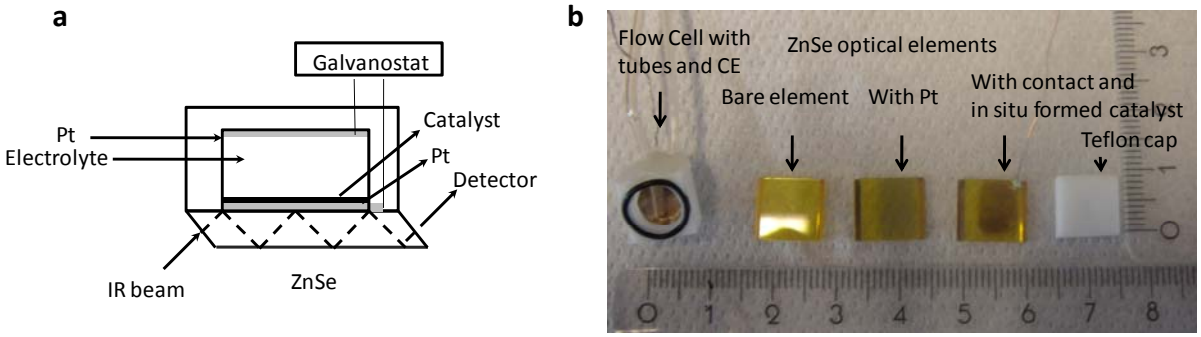

Figure 4.3a Scheme of the spectroelectrochemical cell for internal reflection spectroscopy **b** picture of the different cell components

4.2.5 FTIR spectroscopy

To study FTIR absorption of the catalytic material a film was formed on a Pt electrode in a galvanostatic experiment. A constant current density of 0.9 mA/cm^2 was applied for 4 h. The film was washed with 18 MΩ water and dried. Afterwards the film was scratched of the electrode and pressed together with KBr in a pellet. The pellet (dried over night at 80 °C) was mounted in a FTIR spectrophotometer (Bruker IFS66S) and the transmission properties were measured. The obtained spectrum was correlated to a blank spectrum of a pure KBr pellet.

4.2.6 Three chamber electrolysis with a catalyst coated anode

Due to the instability of the catalyst in acidic media (see Results and Discussion part below) an implantation of it in the two chamber electrolysis of Na_2SO_4 (puriss., p.a., from Fluka Analytical)solutions seemed not to be possible. Using a three chamber electrolysis process on the other hand allows the usage of Kpi as anolyte solution if a bipolar membrane (Typ BP-1E from Hescon) is used to separate anode and middle chamber. As already previously described a bipolar membrane does not allow the transport of ions through it: only neutral species like water can diffuse inside the membrane. At the interface of the cation and the anion selective membrane (these two membranes in close contact build up a bipolar membrane) water undergoes autoprotolysis into H^+ and OH^-. In the electric field these ions can migrate towards the electrodes if the bipolar membrane is mounted correctly inside the three chamber system (cation exchange membrane facing the cathode and anion selective membrane facing the anode respectively). This migration ensures electric conductivity over the bipolar membrane.[19,20,21] As three chamber electrolysis cell a Mirco Flow Cell (from ElectroCell) was used. The assembling of such a cell was already described in Chapter 3. A schematic drawing is shown in Figure 4.4. A bipolar membrane was used to separate the anode chamber from the middle chamber and the separation of middle and cathode chamber was done by a Nafion 324 membrane (from DuPont).The gap between cathode and anode was 9 mm (without counting the membrane thickness). The cathode was platinised Ti (Pt/Ti from ElectroCell) and as anode different metals (Pt/Ti, DSA) coated with the catalytic film were used. For pumping the electrolytes through the chambers a Medorex TU 200 peristaltic pump was used. The electrolyte solutions were recirculated through the chambers and the calibration of the pump was done by pumping the electrolytes through the thee chamber cell. For electrolysis the current source was an IPS IMP83 PC-10 Potentiostat/Galvanostat connected to a scan generator (ELCM-KIT 003 from IPS) and constant current density of 5 mA/cm^2 was applied

(active area 14.2 cm^2). The catalytic film was formed previous to the electrolysis (electrolyte solution: 0.5 mM $Co(NO_3)_2.6H_2O$ in 0.1 M KPi) in a beaker (one compartment electrochemical cell) using tape for masking the anodes active area. A Ni plate was used as CE and an Ag/AgCl (3 M) from BAS was used as RE. All potential values given in the description of the formation experiments are referred to this RE. After catalyst electrodepostion the film was rinsed with water, the tape was removed and the electrode was used as anode in the above described 3 chamber electrolysis. The anolyte solution was a 0.1 M KPi (*pH* = 7) and the initial electrolyte solution for middle and cathode chamber was a 1 M Na_2SO_4 solution. Due to the bipolar membrane function the solution in the middle chamber is acidified (diffusion of H^+ out of the membrane) and the catholyte solution alkalinity increases due to the electrode process. The counter ions for the OH^- produced at the cathode are Na^+ ions diffusing through the cation exchange membrane. The *pH* value (measured with a Profitrode connected to a 826 pH mobile readout unit, both from Methrom) in the anolyte solution is assumed to stay constant as (1) a buffer solution is used and (2) the generated H^+ at the anode will be compensated by the OH^- diffusing out of the bipolar membrane.

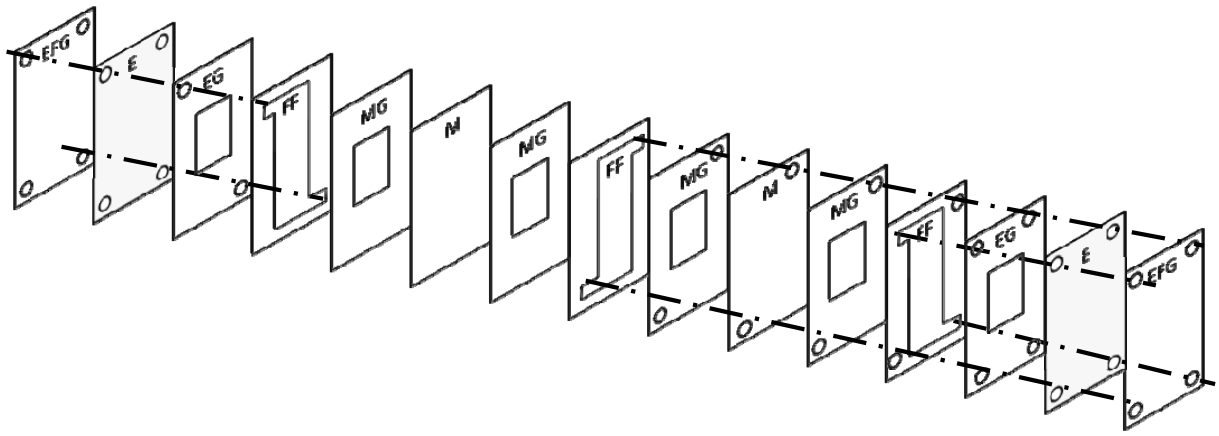

Figure 4.4 Schematic drawing of 3 chamber Micro Flow Cell from ElectroCell: EFG = end frame gasket, E = electrode, EG = electrode gasket, FF = flow frame with flow mesh, MG = membrane gasket, M = membrane

4.3 Results and Discussion

4.3.1 Catalyst Formation

4.3.1.1 Film Formation by CV

CV measurements were performed on ITO as well as on Pt as WE. The potential window was between 0 – 1.1 V for ITO and was expanded to a range of -0.5 – 1.1 V for Pt. The cyclic voltammograms with ITO as WE are depicted in Figure 4.5a-d. Figure 4.5a shows the first scan. It can be seen that at around 900 mV an oxidative wave arise that was assigned in the literature to $Co^{3+/2+}$ couple for cobalt ion with hydroxo ligands.[8] The oxidative wave is followed by a rising oxidative current and the catalyst is deposited (catalytic wave). In the back scan a reductive wave can be seen at 700 mV. Upon performing more consecutive scans (Figure 4.5b and Figure 4.5c) the oxidative as well as the reductive current is rising from scan to scan. This is usually assigned to the deposition of a electroactive material on an electrode., in good agreement with the given literature.[6-8,12] More consecutive CVs were performed (200 subsequent potential sweeps, Figure 4.5c) and clearly a deposition of a brownish-black film was observed. The blank CV (shown in Figure 4.5d) was performed in KPi without Co^{2+} ions and shows more or less a flat baseline.

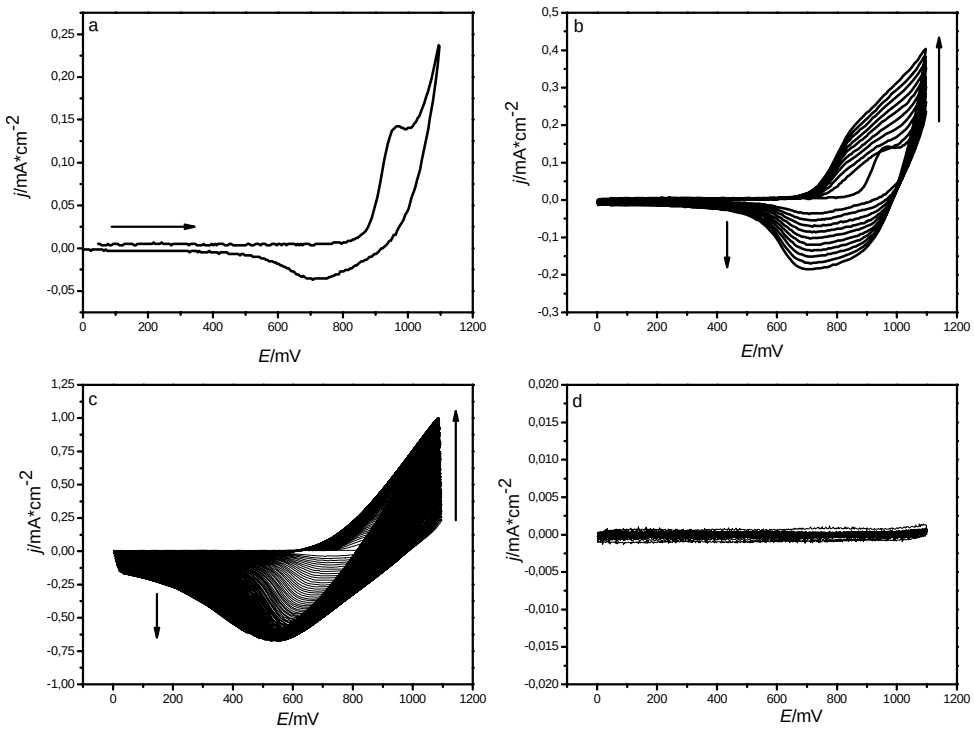

Figure 4.5 Cyclic voltammograms in 0.5 mM $Co(NO_3)_2.6H_2O$ in 0.1 M KPi with ITO as WE **a** first scan **b** 10 subsequent scans **c** 200 subsequent scans and **d** blank (no Co^{2+} ions present).

The same set of experiments was performed using Pt as WE (Figure 4.6a-d). Between +200 and +1100 mV more or less the same behavior as on ITO is observed: an oxidative wave followed by the onset of a strong catalytic wave and reductive wave in the backward scan (Figure 4.6a-c) and upon subsequent sweeping of the potential both currents rise (Figure 4.5b-c). In the region around 0 mV the CVs on ITO and PT as WE are different: A reductive wave arises which can be further resolved if the potential window is expanded to -500 mV (Figure 4.6b). This reductive wave can be explained by the reduction of protons for which Pt shows a rather low overpotential in comparison to ITO. On ITO the reduction of protons to hydrogen is impossible as ITO is not stable under higher negative potential (Figure 4.7). The blank electrolyte (Figure 4.6d) shows significantly higher current densities as on ITO but a factor of ~ 10 lower as in electrolytes with Co^{2+} ions, whereas the reduction wave assigned to protons shows similar current density. In general it can be concluded that the catalyst can be formed as well on Pt and shows catalytic activity even if Pt itself catalyses the oxidation of water.

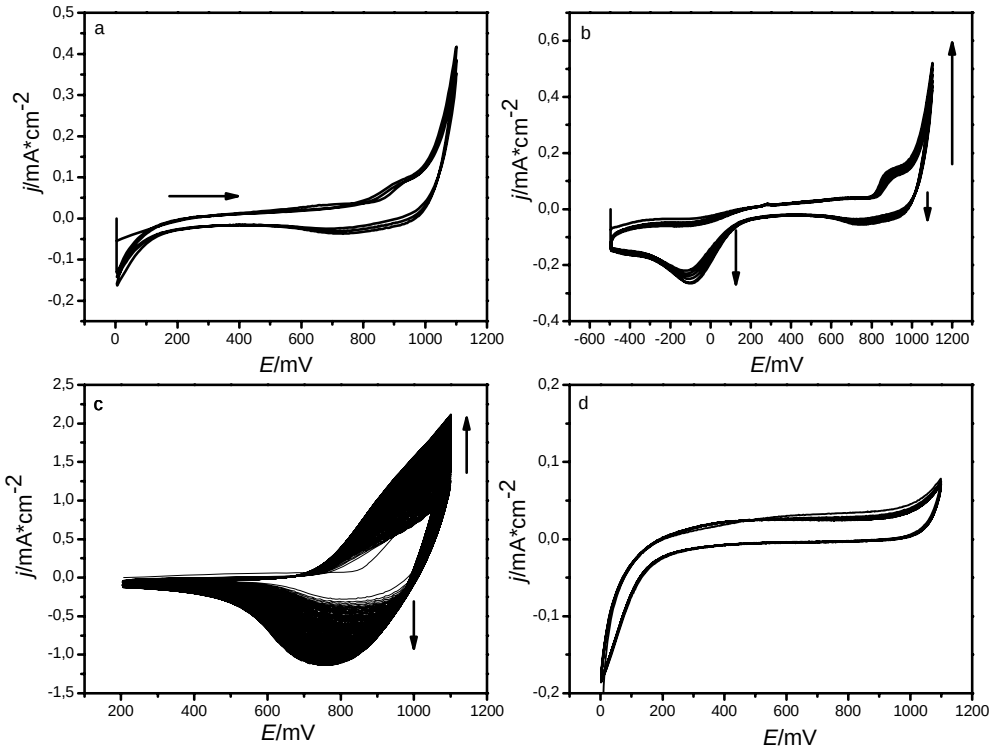

Figure 4.6 Cyclic voltammograms in 0.5 mM $Co(NO_3)_2.6H_2O$ in 0.1 M KPi with Pt as WE **a** first scans **b** 10 subsequent scans **c** 200 subsequent scans and **d** blank (no Co^{2+} ions present)

In Figure 4.7 the decomposition of ITO under negative potentials is shown: The CV in KPi electrolyte with 0.5 mM Co^{2+} shows the usual behavior under positive potentials (formation of the catalyst as see by a catalytic oxidative wave and a reductive wave in the backward scan) but at high negative potentials (~ -1 V) a reductive wave can be observed which is followed by a reoxidation wave if the potential is swept back to positive values. In the literature this reduction (in acidic solutions) is assigned to the dissolution of grain boundaries of ITO followed by a reduction of In^{3+} and Sn^{2+} during the reduction cycle and thus a formation of In-Sn particles. The oxidation current was explained to originate from metal ions layer formed on the surface from remnant metal ions.[22] Therefore no reduction of protons can be observed with ITO as WE as the overpotential for this is higher than the decomposition potential of ITO, meaning ITO is decomposed before protons can be reduced.

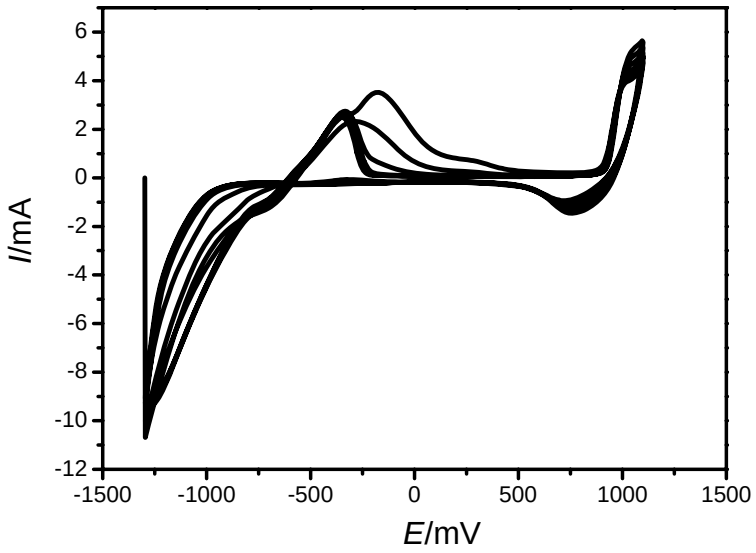

Figure 4.7 Cyclic voltammograms in 0.5 mM $Co(NO_3)_2.6H_2O$ in 0.1 M KPi with ITO as WE in the potential window from -1.3 – +1.1 V

4.3.1.2 Potentiostatic film formation

In addition to film forming by CV the catalyst can as well be formed by applying a constant potential (+1.1 V) over a certain time. The potentiostatic film formation was investigated on ITO and Pt electrodes as well. In Figure 4.8 the current density – potential profiles for both electrodes are depicted. Figure 4.8a shows the formation with ITO as WE and Figure 4.8b with Pt as WE. With this bulk electrolysis the current density trace is rising for both working electrodes with time. Using ITO as WE a current density of ~ 0.3 mA/cm^2 was reached after 8 h of constant electrolysis. This behavior is in good agreement with the present literature but the maximum reached *j* is a bit lower compared to the literature data. [6-8] Under the same experimental conditions bulk electrolysis with a Pt plate as WE resulted in a *j*~0.8 mA/cm^2 which is around factor 2 higher than with ITO as WE. In addition it can be seen that the current density reaches seems to reach a plateau if Pt is used as WE whereas on ITO even after 8 h *j* seems still to rise. A rather constant current density (over 2h) for the water oxidation catalyst was recently described in the literature using a borate buffer based electrolyte (with ITO as WE).[8] With finding the best combination of WE and electrolyte a rapid establishment of the catalyst and high current densities seem to be reachable, using Pt as WE might be one step towards this.

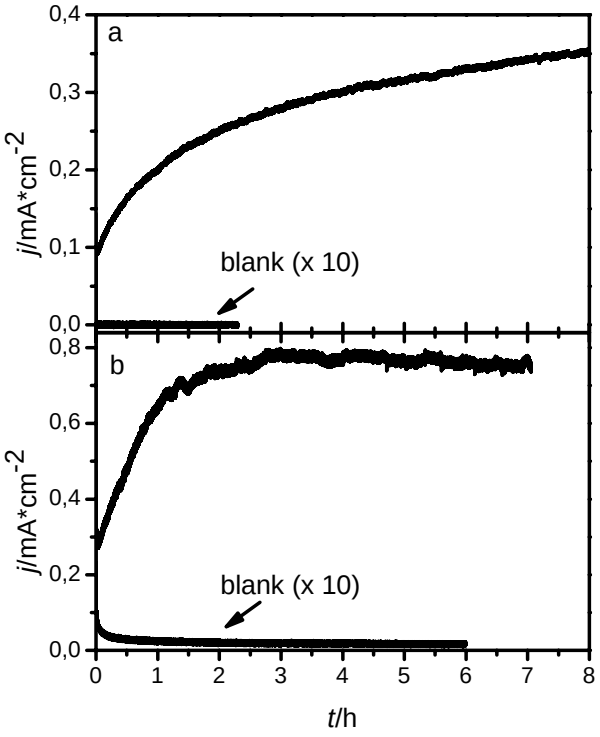

Figure 4.8 : Current density traces for bulk electrolysis in 0.1 M KPi with 0.5 mM Co^{2+} on **a** ITO **b** Pt as WE. Blank measurements were performed in 0.1 M KPi (no Co^{2+} ions present).

For comparison bulk electrolysis at +1.1 V was performed in the absence of Co^{2+} on both working electrode materials as can be seen as well in Figure 4.8 . Like in film formation with CV the current density is reasonable higher on Pt (Figure 4.8b) and on ITO (Figure 4.8b) which can be explained by the lower overpotential for water oxidation on Pt. The current density is decreasing with time on Pt electrodes upon bulk electrolysis in KPi without Co^{2+} ions whereas in KPi with 0.5 M Co^{2+} the current density is increasing to a certain value orders of magnitudes higher. Therefore it can be assumed that even if Pt itself shows some electrocatalytic effect for water oxidation the main contribution to the catalytic effect is the in situ formed water oxidizing catalyst.

4.3.1.3 O_2 evolution with catalyst formed on Pt

The oxygen evolution was monitored by using a Hoffman water electrolyzer. For the production of 1 mol O_2 4 mol e^- are needed. The amount of O_2 produced according to the theory can be calculated as follows: The number of electrons passed through can be calculated from the charge Q

$$Q = I \cdot t$$
$$N_{e^-} = \frac{Q}{e} \qquad \text{(eq. 4.3)}$$

As 4 e^- are needed the produced mol O_2 (n_{O2}) can be obtained by

$$n_{O_2} = \frac{\frac{N_{e^-}}{4}}{N_A} \qquad \text{(eq. 4.4)}$$

The comparison between the theoretical and the measured Faradaic efficiency is shown in Figure 4.9. It can be seen that the measured values do not differ significantly from a 100 % efficiency. The deviation from an ideal linear slope observed for the measured Faradaic efficiency is due to the experimental setup.

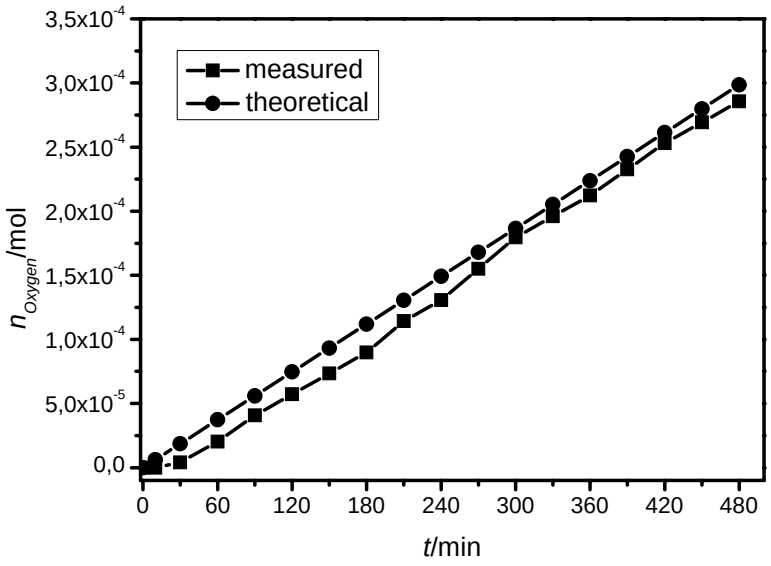

Figure 4.9 Faradaic efficiency using Pt as WE. Dots: Theoretical; Squares: Calculated form measured values.

The oxygen evolution for catalytic films electrodeposited on ITO using the same electrolyte soultuion was previously described in the literature.[6,7] The Faradaic efficiency is reported to be very close to 100 % (Figure 4.10).

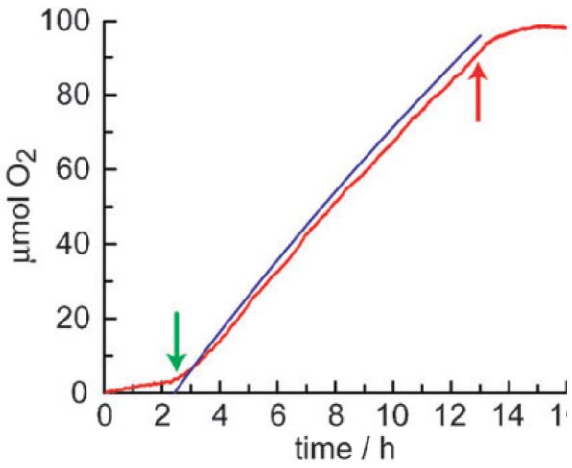

Figure 4.10 Red line: Production of oxygen (measured by a fluorescent detector). Blue line: Theoretical amount of produced oxygen (assumption: 100 % Faradaic efficiency). Reprinted from Ref [7].

4.3.2 Catalyst stability

The stability of the catalyst was investigated in two different types of electrolytes: buffered and unbuffered systems. As buffered system 0.1 M KPi was chosen and as unbuffering system a 0.5 M Na_2SO_4 was used as electrolyte solution.

4.3.2.1 Stability in KPi electrolyte solution

For testing the long term stability of the catalyst a catalytic film was electrodepostited on a Pt plate electrode in a galvanostatic mode (2.2 mA/cm^2 for 5 h) in a H cell filled with 0.5 mM $Co(NO_3)_2.6H_2O$ in 0.1 M KPi . The catalytic film was washed with water and dried over night. Then the Pt electrode with the catalyst was transferred to a H cell filled with 0.1 M KPi electrolyte and +1.1 V vs Ag/AgCl (3M) was applied over the time of 12 h. The current density trace of this experiment is plotted in Figure 4.11. In absence of Co^{2+} ions in the electrolyte the current density is not constant over the time of 12 hours. But even if *j* is decreasing with time it is still reasonable high after 12 h (0.75 mA/cm^2). The good stability in KPi is explained in the literature by the fact the cobalt does not leach out of the film under potential bias.[12]

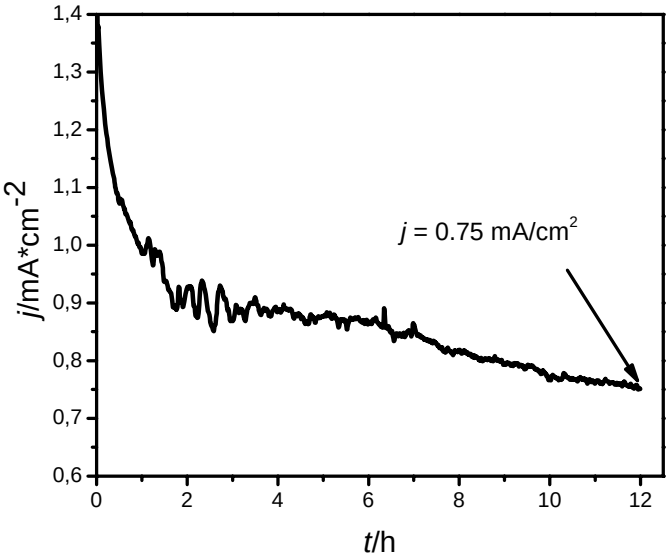

Figure 4.11 Current density trace for bulk electrolysis in 0.1 M KPi using a pre-electrodeposited catalyst on Pt.

4.3.2.2 Stability in sulfate electrolyte solutions

During stability testing in KPi a buildup of a *pH* difference between both compartments of the H cell is not expected due to the buffering ability of KPi. If the electrolyte solution is exchanged to 0.5 M Na_2SO_4 the situation is different as the electrolyte solution is a poor proton acceptor and therefore not buffering at neutral pH. Electrodepositing the catalyst from non buffering systems seems not to be practical as the concentration of Co^{2+} ions has to be ~ 100 times higher than in KPi. Furthermore it was reported that the Faradaic efficiencies for sulfate electrolyte could only be measured in a one compartment cell as the *pH* difference buildup is not that high.[8] Corrosion due to the attack of protons is the proposed reason for the low stability of the catalyst in non buffering systems.[8,12] One possible implementation of the catalyst would be a substitution of the DSA anode used in the two chamber electrolysis process for the regeneration of stripping acid and absorption solution. Thus the catalyst would be exposed to free protons and a study of the catalyst stability in this type of electrolyte solution is therefore necessary.

A catalytic film was formed on an ITO electrode by applying a current density of 1.3 mA/cm^2 over 5 h in a 0.5 mM $Co(NO_3)_2.6H_2O$ in 0.1 M KPi electrolyte solution (H cell). The film was washed carefully with water and dried over night. On the following day a 0.5 M Na_2SO_4 (pH = 6.4) solution was filled as electrolyte solution in the H cell. The preformed catalytic film on ITO was used as anode and a Pt plate was used as cathode. A constant current density of 1.2 mA/cm^2 was applied and every 15 min a pH measurement in both compartments was done by

dipping a *pH* electrode into the compartment. During the whole measurement time the electrolyte solutions in both compartments was stirred. The potential difference between the electrodes versus the measurement time is plotted in Figure 4.12b and the measured *pH* are shown in Figure 4.12a. The "spikes" in the potential trace (see inset of Figure 4.12) is due to the dipping in of the pH electrode. During the time of electrolysis in the anode chamber the *pH* value is decreasing with time due to production of protons upon water oxidation. At the same time the pH in the cathode compartment is increasing due to OH^- ions that are formed during the water splitting reaction on the cathode. At the end of the experiment the potential difference between the electrodes is rising till the maximum value of the galvanostat (10 V). This indicates in this case a drastic decrease in the anode activity, meaning that the potential difference between anode and cathode gets too high at the given current density.

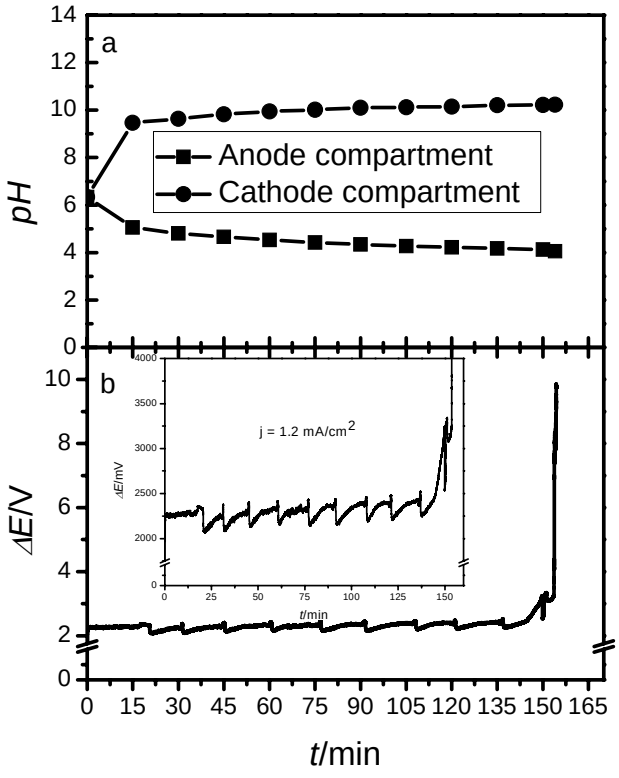

Figure 4.12 a *pH* of anode and cathode compartment during time of electrolysis **b** potential difference between anode and cathode versus time (j = 1.2 mA/cm^2, anode: ITO + catalyst, cathode: Pt) in 0.5 M Na_2SO_4. The inset shows a zoom in the potential trace.

4.3.3 In situ spectroelectrochemical studies on the catalytic film formation and stability

4.3.3.1 In situ UV-Vis spectroelectrochemistry

The catalytic film shows a brownish black color. First the formation of the film was monitored by in situ UV-Vis technique. As electrolyte solution 0.5 mM $Co(NO_3)_2.6H_2O$ in 0.1 M KPi was used in galvanostatic experiments. As all of the absorption features were measured relative to a reference all spectral features that arise upon formation of the catalyst on ITO are here assigned to the catalytic film itself. A constant current density of 0.45 mA/cm^2 was applied over the time of 11 h and 30 min. The potential difference between WE and CE during the time of galvanostatic electrolysis is shown in Figure 4.13.

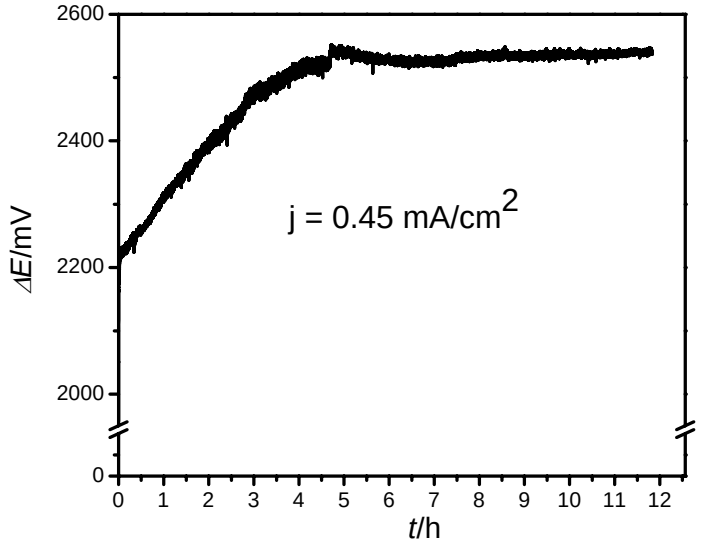

Figure 4.13 Potential difference profile during in situ UV-Vis spectroelectrochemical measurement: galvanostatic electrolysis in 0.1 M KPi with 0.5 mM $Co(NO_3)_2.6H_2O$ on ITO as WE

During the time of galvanostatic electrolysis every 30 min an absorption spectrum was measured. The spectra can be seen in Figure 4.14. After 30 min of electrolysis a distinct absorption feature that spreads out over the range of 300 – 900 nm can be observed. This feature grows upon prolonged electrolysis and can be explained by a growing catalytic film on ITO: As more material is electrodeposited the absorbance is increased. In the beginning of the electrolysis the difference between the two subsequent spectra is more pronounced and gets smaller with the time of electrolysis but is still increasing. The maximum of the

absorbance seems to be around 320 nm, which is around the absorption edge of ITO. Thus the absorbance might be spread out towards higher energies but this can not be resolved by using ITO. This experiment shows clearly that the formation of the catalyst can be followed by measuring in situ the absorption. The feature at 350 nm can be assigned to the expermimental setup: A filter wheel change in the absorption spectrometer becomes visible due to not perfect coverage of the sample chamber during in situ UV-Vis measurements.

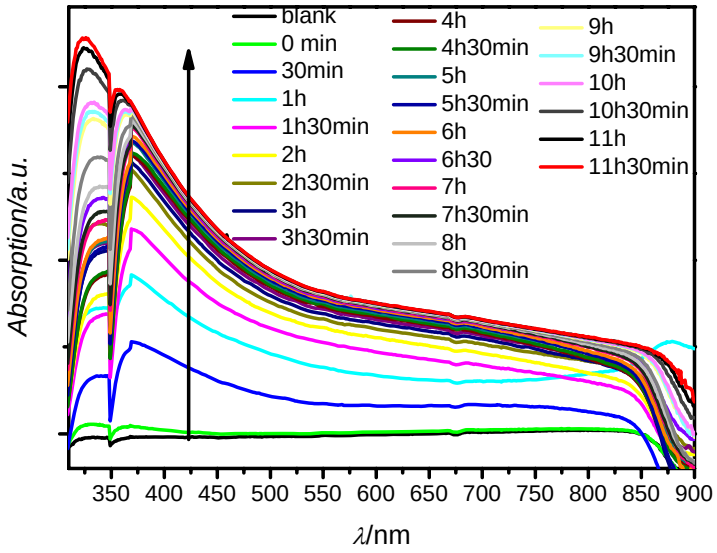

Figure 4.14 Absorption spectra upon galvanostatic catalyst formation on ITO

As the potentiostatic experiment (4.3.2.1) indicated a high stability in KPi in situ UV-Vis absorption spectroelectrochemistry was chosen in order to probe the stability. The catalytic film on ITO formed in the in situ UV-Vis formation experiment was carefully washed with water, dried over night and transferred the next day in 0.1 M KPi as electrolyte solution. Electrolysis was performed in a galvanostatic way by ensuring the same current density in the system as in the formation experiment (0.45 mA/cm^2). The time of electrolysis was 11 h 50 min. As can be seen from the inset of Figure 4.15 the absorption spectra do not change significant over the whole time of the experiment. The comparison of the absorption spectrum obtained after the formation experiment (blue line in Figure 4.15) with the spectrum after the stability experiment (orange line in Figure 4.15) shows that the absorption properties of the catalytic film are the same. The UV-Vis absorption of the catalytic film seems to remain unchanged upon electrolysis in 0.1 M KPi neither in terms of absorbance intensity nor in the spectral distribution which is in good agreement with the potentiostatic experiment.

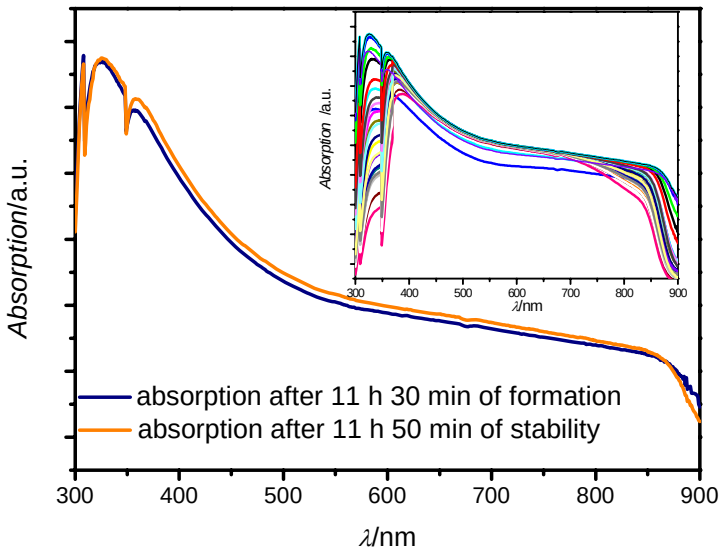

Figure 4.15 Absorption spectrum after 11 h 30 min of galvanostatic catalyst formation (0.5 mM $Co(NO_3)_2.6H_2O$ in 0.1 M KPi, blue line) and after 11 h50 min of galvanostatic catalyst stability (0.1 M KPi, orange line) on ITO. The inset shows all absorption spectra measured during the stability test.

In order to probe the instability in unbuffering systems in situ UV-Vis experiments were carried out because a significant anode activity decrease (see Figure 4.12) should be related to the catalyst as its poor stability in unbuffering systems was already described.[8,12] A catalytic film was formed on an ITO electrode applying 1.1 mA/cm^2 in 0.5 mM $Co(NO_3)_2.6H_2O$ in 0.1 M KPi electrolyte solution for 5 h. After washing with water and drying over night the catalyst coated ITO was used as anode for electrolysis of 0.5 M Na_2SO_4 in an optical cuvette (coiled Pt wire as cathode, j = 1.1 mA/cm^2) in a in situ UV-Vis spectroelectrochemical measurement setup. As this type of measurement is done in one compartment cell the buildup of a *pH* gradient in the electrolyte solution cannot be assumed. On the other hand due to the half reaction on the anode locally protons are produced. Contrary to a proton accepting electrolyte solution KPi, in the sodium sulfate solution they are not buffered away from the anode surface and can corrode the catalytic film. This shows as well the results for the first 3 h of electrolysis (see Figure 4.16). During this time the absorption features are decreasing from one spectrum to the other. After 3 h the electrolysis was stopped and the *pH* vaolue of the solution was measured by *pH* indicator paper. The electrolyte solution had a pH of ~ 5-6 (measured by *pH* indicator paper). In addition a greenish precipitate near the coiled Pt wire

was observed. A similar precipitate was mentioned in the literature to occur and was assigned to precipitated cobalt species.[23]

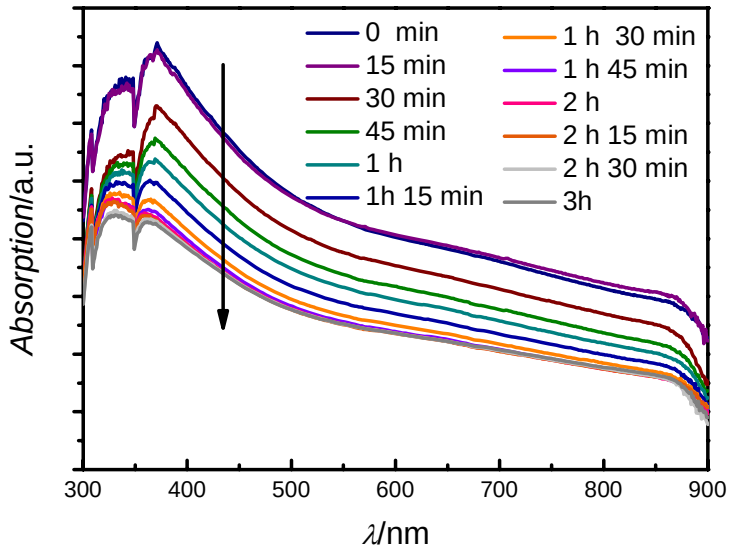

Figure 4.16 Absorption spectra upon galvanostatic stability test of the catalyst on ITO for 3 h of electrolysis in 0.5 M Na_2SO_4 (first stability test)

After this first stability measurement the electrolyte was replaced by fresh 0.5 M Na_2SO_4 and the same catalytic film on ITO was used again as anode. The same current density as before (1.1 mA/cm^2) was applied to the system. The measured spectra are shown in Figure 4.17. During the time of 1 h 30 min the absorption feature completely vanishes. Thus the catalytic film is dissolved in the solution. Therefore it can be concluded that the local attack of protons causes a corrosion that leads to a complete dissolution of the catalytic film.

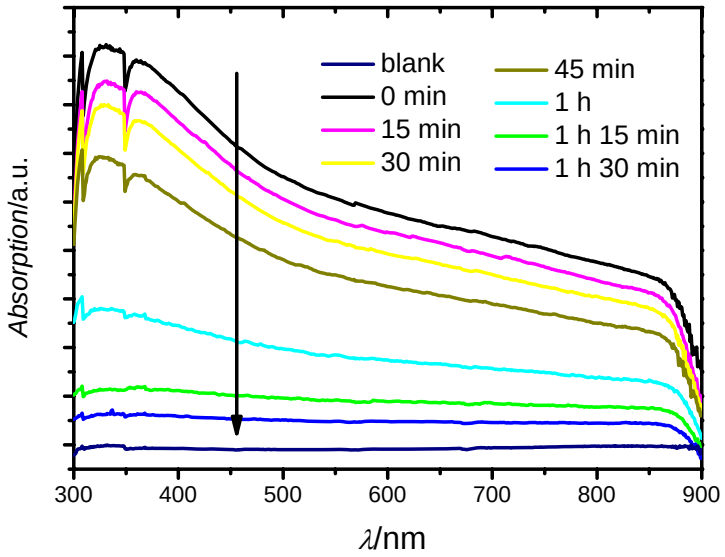

Figure 4.17 Absorption spectra upon galvanostatic stability test of the catalyst on ITO for 1 h 30 min of electrolysis in 0.5 M Na_2SO_4 (second stability test)

In Figure 4.18 the potential difference between anode and cathode is plotted for the last 1 h 30 min of electrolysis. A similar behavior as in the H cell can be seen: At the end of the experiment the potential difference between anode and cathode is rising towards the limit of the galvanostat (~ 4.3 V in this experiment due to a software limit). The results from the potential measurements together with the UV-Vis absorption behavior show that the anode activity decrease goes together with dissolution of the catalyst. This dissolution is as well clearly visible by eye.

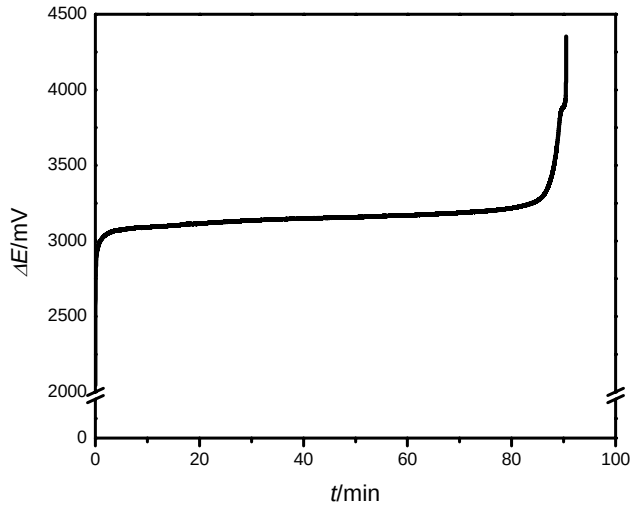

Figure 4.18 Potential difference between anode and cathode versus time (j = 1.1 mA/cm^2, anode: ITO + catalyst, cathode: Pt) in 0.5 M Na_2SO_4 (second stability test).

Figure 4.19 shows all measured absorption spectra (first and second stability test plotted together). The error bar indicates the electrolyte solution exchange. One can see that the intensity of the absorption features is constantly decreasing till it finally vanishes due to dissolution of the catalytic film.

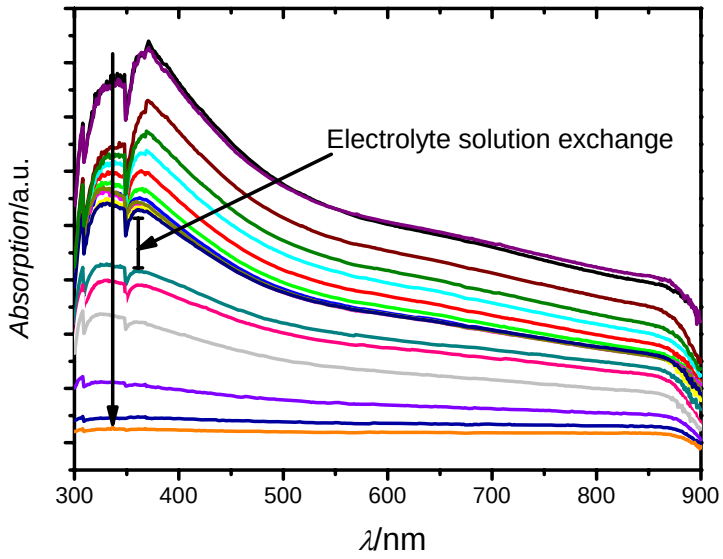

Figure 4.19 All in situ UV-Vis absorption of the catalyst on ITO spectra measured during galvanostatic electrolysis in 0.5 M Na_2SO_4 solution**.** The error bar indicates the electrolyte solution exchange.

4.3.3.2 In situ FTIR-ATR spectroelectrochemistry

With the in situ FTIR-ATR spectroelectrochemical technique FTIR difference spectra due to the formation of the catalytic film were measured. Before electrolysis FTIR-ATR difference spectra of the electrolyte and of water were recorded. The difference spectra related to the dry optical element are shown in Figure 4.20. Water shows IR bands at the following wavenumbers: a strong broad band between 3700 – 2700 cm^{-1}, a weak band with a maximum at 2100 cm^{-1}, a medium band at 1600 cm^{-1} (maximum) and a strong broad band in the spectral region of 1000 – 500 cm^{-1}. The first 3 bands can be found in FTIR spectra of H_2O.[24] The broad band between 3700 – 2700 cm^{-1} is usually assigned to the O-H stretching vibration, whereas the band at 1600 cm^{-1} is attributed to the wagging vibration of the water molecule. In the region between 1000 – 500 cm^{-1} vibration of coordinated water molecules can be found[25]. As these spectra were measured by FTIR-ATR technique this additional band could be due to coordination water on the crystal surface. The electrolyte solution shows the same IR bands as water except one additional band. This band is marked with a star in Figure 4.20 and has its maximum at 1075 cm^{-1}. From the literature it is known that phosphate solutions show a IR

band in this region[26]. Thus difference spectra of the electrolyte solution obtained by FTIR-ATR technique show vibrations of the phosphate group and mainly water vibrations in the IR region.

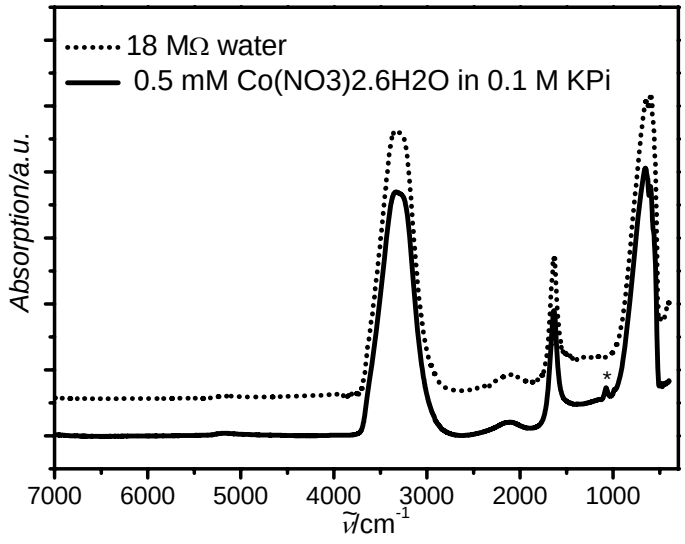

Figure 4.20 FTIR-ATR difference spectra of 18 MΩ water (dotted line) and 0.5 mM $Co(NO_3)_2.6H_2O$ in 0.1 M KPi(solid line). IR band of electrolyte not present in water is marked with a star.

During 1 h of galvanostatic electrolysis ($j \sim 0.3$ mA/cm^{-2}) in an ATR flow cell every 15 min a spectrum was recorded. All obtained spectra were related to a reference spectrum of the electrolyte solution and are depicted in Figure 4.21. The difference spectrum measured at the beginning of the electrolysis (0 min) shows more or less a flat line. After 15 min of electrolysis already new absorption features can be seen and upon prolonged time of bulk electrolysis these bands grow as more and more material is electrodeposited on the electrode. The IR bands appear between 3700 – 1700 cm^{-1}(strong, broad), at 1600 cm^{-1} (medium), 1020 cm^{-1} (strong), 880 cm^{-1} (shoulder) and 580 cm^{-1} (medium – strong). In order to see if changes in the IR bands can be observed between thicker dry catalytic films and upon catalytic film formation the following measurements were carried out. After electrolysis the catalytic film was grown a bit thicker (0.3 mA/cm^2 for 1 h) in a beaker, washed with 18 mΩ water, dried and mounted again in the ATR cell. The spectrum of the dry film was recorded (no electrolyte solution was circulated through the flow cell) and related to a ZnSe reference spectrum. A comparison of the difference spectra of the catalytic film after 60 min of electrolysis (under applied current, solid line) and of the dry film (no current applied, dotted line) is shown in Figure 4.22. In both difference spectra the same IR bands can be seen. In addition a catalytic

film electrodepostited on Pt was scratched off the electrode and pressed after drying together with KBr to a pellet. The FTIR transmission spectrum of this pellet was measured and related to a spectrum of a blank KBr pellet. The comparison of the difference spectrum of the dry film (dotted line) and the FTIR transmission spectrum is shown in

Figure 4.23. The spectral features on both spectra are overlapping and it can be assumed that the bands have the same origin. Thus IR bands in the difference spectra upon formation of the catalyst can be truly assigned to vibrations in the catalytic film and are not due to overcompensation of electrolyte solution vibrations.

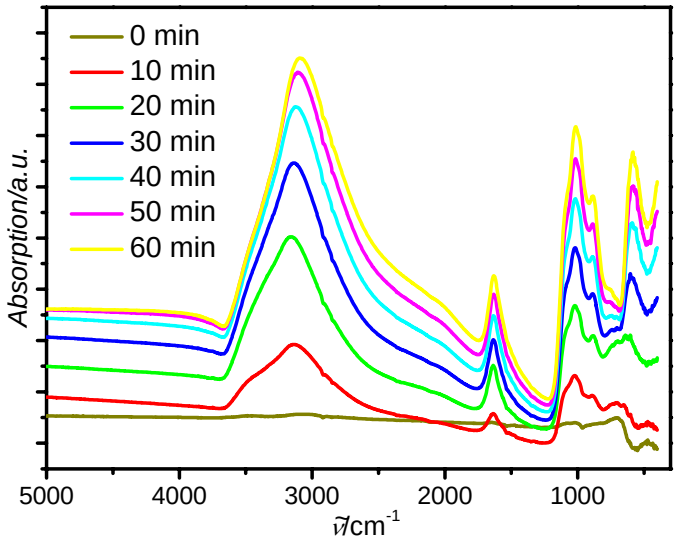

Figure 4.21 Difference spectra obtained by in situ FTIR-ATR during 1 h of electrolysis of 0.5 mM $Co(NO_3)_2.6H_2O$ in 0.1 M KPi

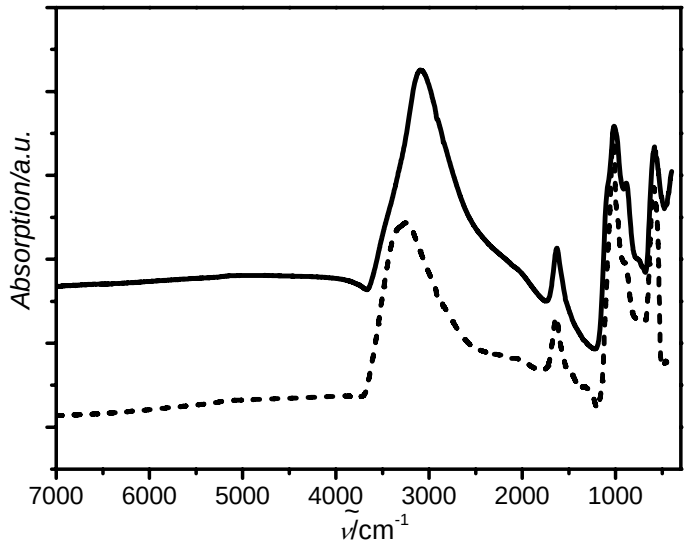

Figure 4.22 Difference spectrum (related to electrolyte reference spectrum) obtained by in situ FTIR-ATR after 1 h of electrolysis of 0.5 mM $Co(NO_3)_2.6H_2O$ in 0.1 M KPi (solid line) and difference spectrum of dry catalytic film (related to ZnSe reference spectrum, dashed line)

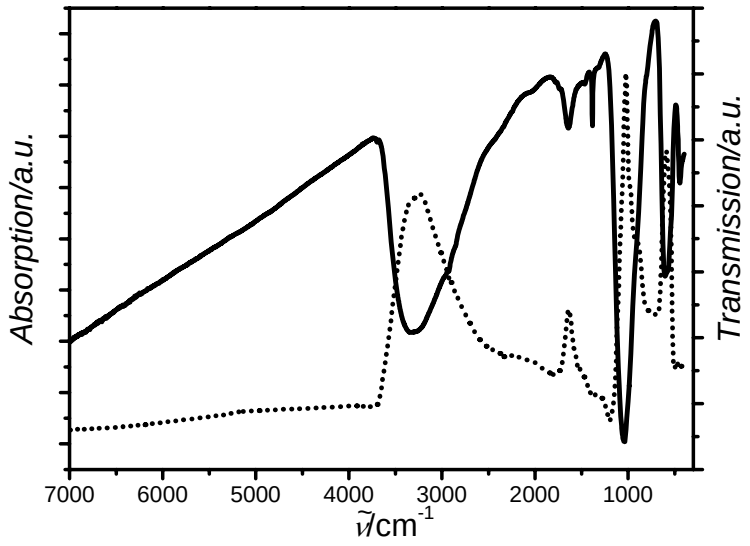

Figure 4.23 Difference spectrum of dry catalytic film (related to ZnSe reference spectrum, dotted line) and FTIR transmission spectrum of catalytic film in KBr (solid line)

Figure 4.24 shows the difference spectra of the electrolyte solution (grey line) and the catalytic film after 60 min of electrolysis (under applied current, orange line).The IR spectrum of the electrolyte solution was already discussed above. The broad IR band of the catalytic film in the spectral region between 3700 – 1700 cm^{-1} covers the same spectral region as the OH strechting vibration in the electrolyte solution but is broadened towards lower wavenumbers. It might come from OH vibrations of either water inside the catalyst or from the catalytic unit itself. The IR band at 1020 cm^{-1} with a shoulder at 880 cm^{-1} can originated from vibrations of two different IR active groups: a cobalt oxygen double bond (Co=O) or phosphor oxygen double bond (P=O) in the phosphate group. This vibration of the phosphate group is as well one possible explanation for the band at 580 cm^{-1} but a second group can be the reason for this band as well: O-H vibrations of a OH group bounded to cobalt (Co-OH)[25]. Therefore the IR bands in the lower wavenumber spectral region could be due to vibrations of the cobalt oxo core itself or the phosphate framework (or a superposition of viabrations due to both groups). The IR band at 580 cm^{-1} is very close to experimental limit of the setup (~500 cm^{-1}).

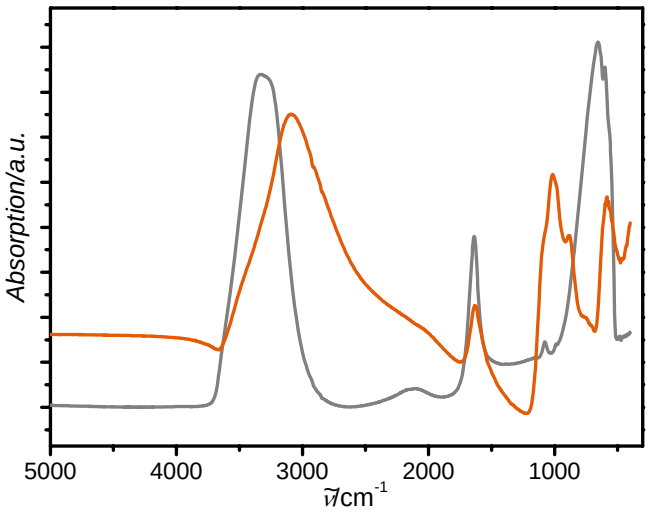

Figure 4.24 Difference spectrum (related to electrolyte reference spectrum) obtained by in situ FTIR-ATR after 1 h of electrolysis of 0.5 mM $Co(NO_3)_2.6H_2O$ in 0.1 M KPi (orange line) and difference spectrum of electrolyte (related to ZnSe reference spectrum, grey line)

The stability behavior in 0.5 M Na_2SO_4 was as well monitored by means of in situ FTIR-ATR. Before the experiment the FTIR-ATR spectra of the electrolyte solutions were measured and compared to water. The difference spectra (related to the ZnSe crystal with sputtered Pt) are shown in Figure 4.25. As can be seen the spectra of the 2 electrolytes show

nearly the same IR bands as 18 MΩ water. Additional IR bands not present in water, at 1075 cm^{-1} for the KPi solution and at 1120 cm^{-1} for the sulfate solution, are observed. An additional band at 1075 cm^{-1} for the KPi solution was already discussed before and related to vibrations of the phosphate group. In the sulfate electrolyte solution an IR band in nearly the same spectral region can be seen. It exhibits a maximum at around 1120 cm^{-1} and can be related to vibrations of the sulfate group. The IR active vibrations only visible in the electrolyte solutions are marked with a star in Figure 4.25.

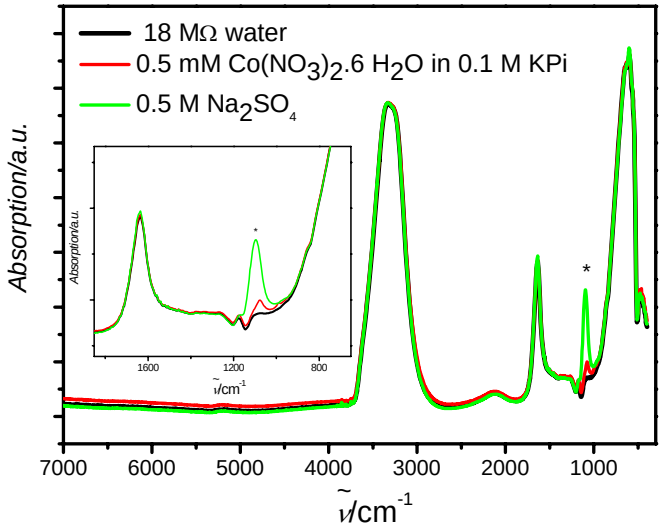

Figure 4.25 FTIR-ATR spectra of the 18 MΩ water (black line), 0.5 mM $Co(NO_3)_2.6H_2O$ in 0.1 M KPi (red line) and 0.5 M Na_2SO_4. The inset shows a zoom of the spectral region where IR bands of the electrolyte solutions appear (marked with a star).

Previous to the stability test a catalytic film was electrodeposited in the same way as described above in the formation study by in situ FTIR-ATR technique. After film formation water was circulated through the cell for 20 min to wash the catalytic film. Then the cell was filled with 0.5 M Na_2SO_4 and electrolysis was started again. A constant current density of ~ 0.3 mA/cm^2 was applied for 80 min and every 10 min a spectrum was collected. The difference spectra from this experiment are plotted in Figure 4.26. After 80 min the potential difference had again (like previously described 4.3.2.2 and 4.3.3.1) reached the maximum of the galvanostat. Thus one final spectrum without applied potential was measured (dark blue line in Figure 4.26). It can be seen from the spectra in Figure 4.26 upon prolonged electrolysis negative bands appear. IR bands that point downwards in difference spectra are here assigned to species vanishing during the electrochemical process. During the first 40 min of electrolysis the following negative spectral features can be observed: a strong band between

3700 – 2500 cm^{-1} with a maximum around 3300 cm^{-1}, a medium band around 1600 cm^{-1} and a strong band between 1130 – 550 cm^{-1} (the negative band at 2340 cm^{-1} can be assigned to incompensation of CO_2 in the atmosphere of the beam bath). After 40 min of electrolysis the IR bands in the difference spectra still grow in towards more negative values indicating that more and more species from the electrode surface are dissolving. In addition the strong band between 3700 – 2500 cm^{-1} is shifting and is broadened to the spectral region between 3700 – 1800 cm^{-1} with a maximum at around 3100 cm^{-1}. The position of the band at 1600 cm^{-1} remains unchanged. In the lower frequency region the IR band presents a different spectral shape.

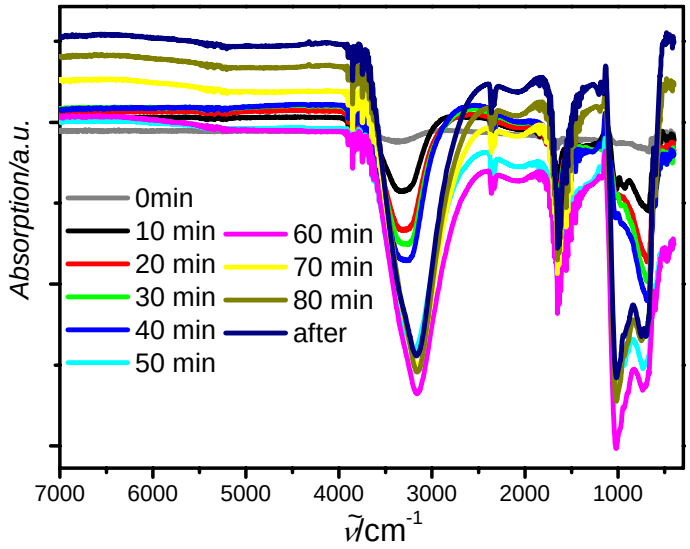

Figure 4.26 FTIR-ATR spectra during 1 h 20 min of electrolysis in 0.5 M Na_2SO_4 and after electrolysis (dark blue line).

A comparison of the difference spectra upon formation of the catalyst and the stability experiment in sulfate solution is shown in Figure 4.27. For the formation and stability experiments with the same ZnSe crystal under the same experimental conditions (j = 0.3 mA/cm^2) were carried out. In addition to the previous described shifting of the negative spectral features during electrolysis in sulfate solution, the IR bands not to show a full compensation of the IR bands obtained upon formation of the catalytic film. This suggests that due to electrolysis in sulfate solution IR active species are not vanishing in the same way as they were formed. A different active site in the catalyst formed from a sulfate electrolyte was already proposed in the literature.[8] The IR bands can be assigned again to either the active site (cobalt oxo core) or the framework of the catalyst.

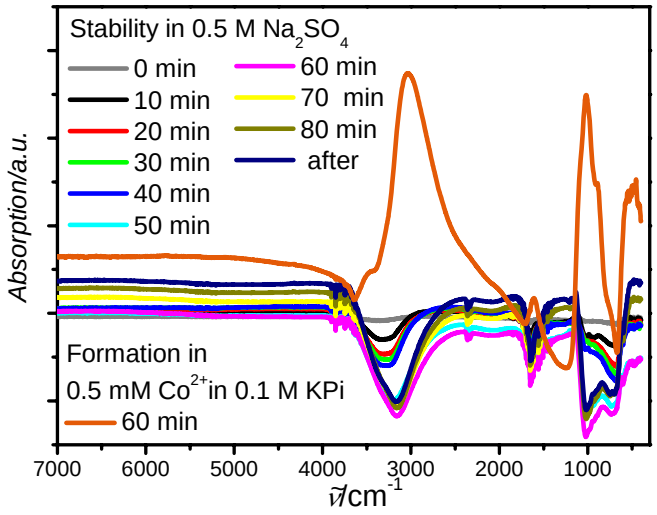

Figure 4.27 All ATR-FTIR difference spectra obtained during stability test in 0.5 M Na_2SO_4 compared to spectra obtained during formation in 0.5 mM $Co(NO_3)_2.6H_2O$ in 0.1 M KPi.

4.3.4 Combination of the water oxidation catalyst with a three chamber electrolysis using a sodium sulfate electrolyte solution

The above described results suggest that the catalyst instability in sulfate solutions leads to a complete dissolution of the film on the anode. For a possible implementation of this type of water oxidizing catalyst is has to be ensured that the catalyst is only operated in neutral *pH* buffered solutions. As this is not possible in a two chamber electrolysis of Na_2SO_4 solutions (see Chapter 3) a three chamber electrolysis was combined with the water oxidation catalyst. In this cell geometry a bipolar membrane can be used to separate anode and middle chamber. This bipolar membrane ensures a possible usage of KPi as anolyte and an acidification of the Na_2SO_4 solution in the middle chamber. During electrolysis the alkalinity of the catholyte solution is increased due to the electrode reaction. The charge neutrality of the catholyte solution is achieved by the migration of Na^+ from the middle chamber through the cation selective membrane (Nafion 324).

For this implementation the catalyst had to be electrodepostited on a larger electrode surface. A tape was used for masking a Pt/Ti electrode (WE). The active area after masking was around 26 cm^2. As counter electrode a Ni electrode was used. All three electrodes (WE, CE, RE) were immersed in a beaker filled with 500 ml 0.5 mM $Co(NO_3)_2.6H_2O$ in 0.1 M KPi as electrolyte solution (see Figure 4.28). In situ catalyst electrodepostion was performed by applying 1.1 V for 5 h 30 min. Figure 4.28b shows a picture of this process and by the dark color of the active area it can be seen, that the in situ formation of the catalyst is occurring.

The current density reaches around ~ 0.8 mA/cm^2 after around 5 h. The leveling off of the current density is observed later compared to small electrodes which might be explained by the larger electrode area. A total charge of 308 C passed through the system. It is know that electrochemically deposited films have different morphologies and therefore different performance dependent on the formation method. Galvanostatic deposited films on electrodes are sometimes reported to have enhanced performances compared to potentiostatic films.[27] For this reason a catalytic film was in addition prepared in a galvanostatic mode using the same electrochemical setup and the same electrolyte solution as described before. Again the active area (~ 24 cm^2) was masked by tape. 0.8 mA/cm^2 were applied for 5 h 30 min. During that time a total charge of 380 C passed through the system. The potential trace (Figure 4.30) shows after around 3 h 30 min a rather constant behavior (~ + 1.1 V vs Ag/AgCl(3M)). The spike in the trace is due to a movement of the RE.

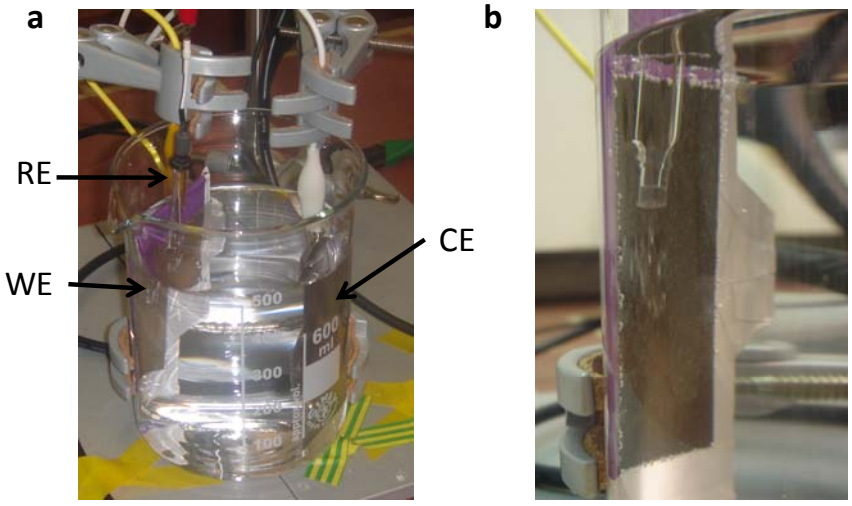

Figure 4.28a Picture of the electrochemical cell setup for large area electrodepostion of the water oxidation catalyst and **b** Picture of WE during in situ electrodepostion

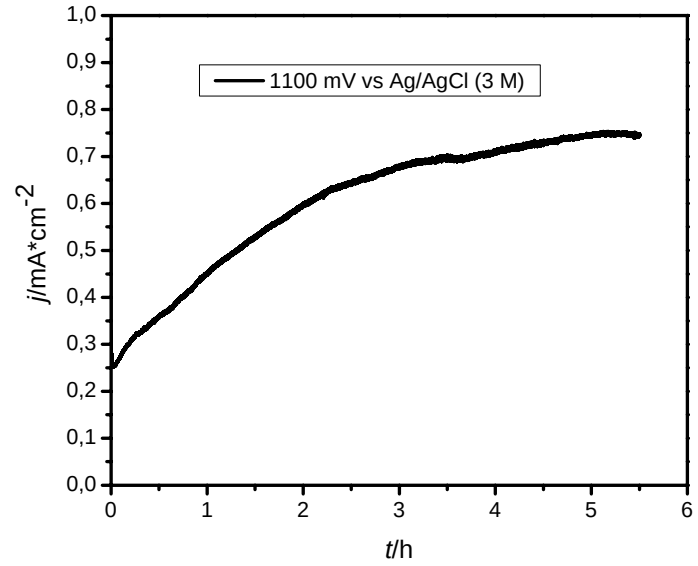

Figure 4. 29 Current density trace for potentiostatic electrolysis in 0.5 mM $Co(NO_3)_2.6H_2O$ in 0.1 M KPi using a large Pt/Ti electrode as WE.

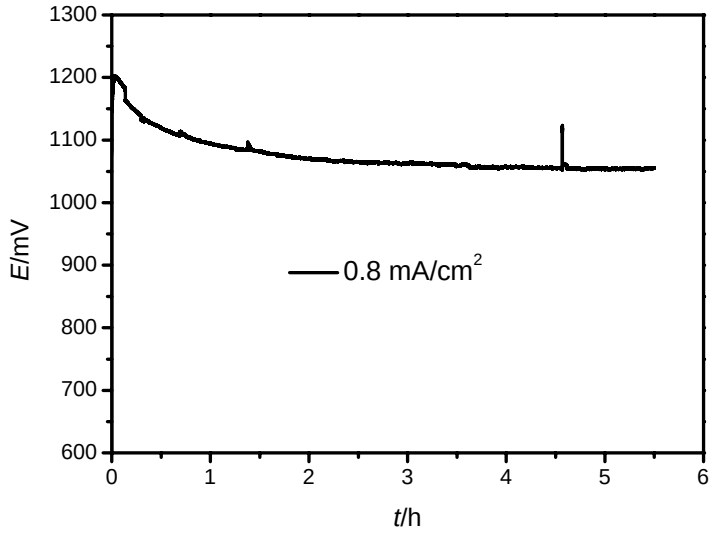

Figure 4.30 Potential trace for galvanostatic electrolysis in 0.5 mM $Co(NO_3)_2.6H_2O$ in 0.1 M KPi using a large Pt/Ti electrode as WE.

Both catalytic films were tested as anode in a three chamber process (9 mm gap) and compared to blank Pt/Ti and a DSA anode. For all experiments the electrolyte solutions were recirculated through the chambers during the time of electrolysis (1 h). The anolyte solution was 0.1 M KPi and the initial concentration of the electrolyte solutions in the middle and the cathode chamber was a 1 M Na_2SO_4. Electrolysis was performed in a galvanostatic mode (5

mA/cm^2) for 1 h. All electrolyte solutions were kept at room temperature. The flow rate was 100 ml/min for each electrolyte solution (Figure 4.31). The highest voltage after 1 h of electrolysis was observed of the bare Pt/Ti anode (~ 3.7 V). For this electrode the voltage is constantly rising during electrolysis time whereas for the other electrodes (catalyst on Pt/Ti or DSA) the potential difference trace shows a more constant profile. After 1 h of electrolysis a voltage of 3.5 V for the potentiostatic formed, and of 3.4 V for the galvanostatic formed catalyst, was found. The DSA anode shows a slightly lower voltage of 3.3 V. The spikes in the voltage trace for the DSA can be assigned to bad connection of the crocodile clamps to the electrodes. The *pH* values showed for all 4 different electrodes similar values after 1 h: The anolyte solution showed the assumed constant *pH* profile at *pH* = 7. The *pH* in the middle chamber was constantly decreasing to a value of 3.6 whereas the alkalinity in the catholyte solution was increasing to *pH* = 11.2 after 1 h. The *pH* values shows in the end the expected trend what proofs the working principle. The catalyst seems to improve the three chamber electrolysis process under the given experimental conditions compared to bare Pt/Ti electrodes. In addition the galvanostatic formed film seems to perform a bit better than the potentiostatic film. On the other hand the commercial available DSA anode seems to be still the best choice but the anode with the catalyst has not a much higher overpotential. DSA anodes are usually very expensive and the water oxidation catalyst could be an inexpensive alternative that does not show significantly higher overpotentials. After 1 h of electrolysis the catalytic film seems to be mechanically stable (Figure 4.32): The active area can be seen in the picture to be a bit darker than the surrounding catalytic film. As a Viton gasket was pressed on the non active area a bit of the catalyst was removed indicated by the lighter color.

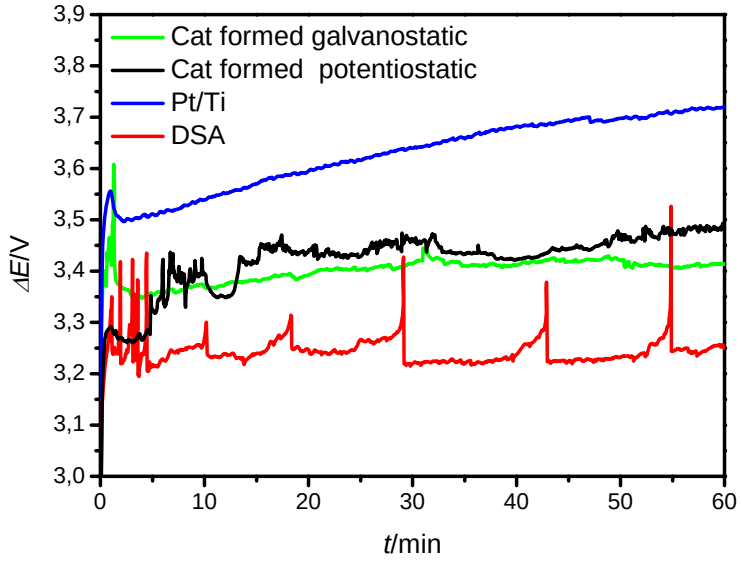

Figure 4.31 Potential difference traces for 3 chamber electrolysis at room temperature for 4 different anodes. Blue line: Pt/Ti, black line: potentiostatic formed catalyst on Pt/Ti, green line: galvanostatic formed catalyst on Pt/Ti, red line: DSA. Electrolyte solution flow: 100 ml/min, Current density: 5 mA/cm^2

Figure 4.32 Catalyst coated Pt/Ti electrode after 1 h of anode operation in a 3 chamber electrolysis.

The highest current density that could be applied in these experiments was around 5 – 10 mA/cm^2. Higher *j* values lead to dissolution of the catalytic film as shown in Figure 4.33a. The anode in this picture was used in a three chamber process with a current density of 50 mA/cm^2 and one can clearly see that on the active area no catalyst is present after electrolysis. In order to verify the dissolution at higher current densities a catalyst was electrodeposited on

Pt/Ti as previously described. Afterwards the film was rinsed in water and the electrolyte solution was exchanged to a 0.1 M KPi solution. In the same electrochemical setup (beaker with CE,WE and RE) electrolysis was initiated by applying 33 mA/cm^2 and immediately afterwards a dissolution of the catalyst was observed (Figure 4.33b).

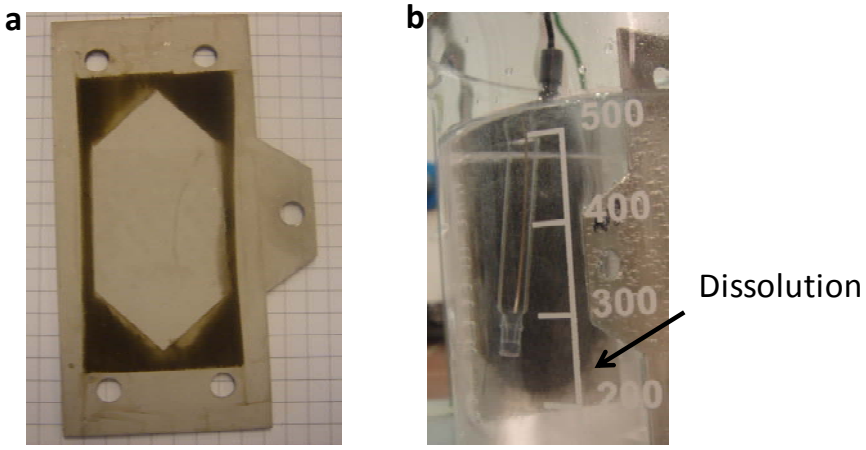

Figure 4.33a Catalytic film coated Pt/Ti electrode operated as anode with 50 mA/cm^2 b Dissolution of the catalytic film operating with 33 mA/cm^2

DSA anodes have usually a rather rough surface and still show the lowest overpotentials. Therefore a DSA anode was coated with the catalyst in order to see if the efficiency of the process gets enhanced. The catalyst was formed galvanostatically (0.8 mA/cm^2) on DSA as previously described in a beaker filled with electrolyte in which RE,CE and WE were immersed. After rinsing of the film with water it was used in a three chamber electrolysis under the same experimental conditions as described above. A comparison between bare a bare DSA anode and a catalyst coated one under the same experimental conditions is shown in Figure 4.34. Both electrodes seem to operate with rather similar efficiencies and the catalyst coated DSA shows again a slightly higher voltage as the bare DSA. In addition the catalyst was dissolved partly from the electrode during 1 h of electrolysis (Figure 4.35) where a difference between the color of the active area and covered but non active electrode surface can be seen.

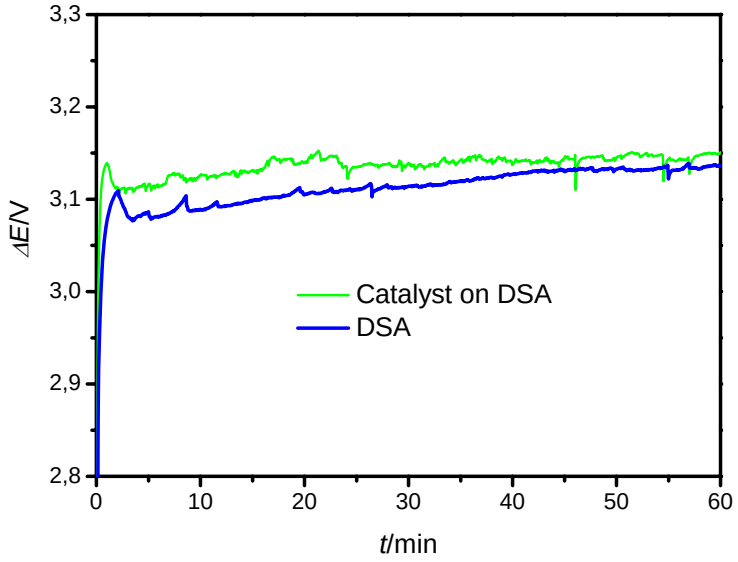

Figure 4.34 Comparison of 3 chamber electrolysis at room temperature with 2 different anodes. Green line: Catalyst on DSA, blue line: DSA. Electrolyte solution flow: 100 ml/min, Current density: 5 mA/cm^2

Figure 4.35 Catalytic film coated DSA electrode operated as anode with 5 mA/cm^2 for 1 h.

4.4 Summary

In situ formation of a water oxidation catalyst was achieved as described in the literature[6-9,12] on two different electrode materials: ITO and Pt. On Pt higher current densities can be reached by applying the same potential as on ITO indicating a better efficiency using Pt electrodes. The formation of the catalyst was monitored by means of in situ UV-VIS and in situ FTIR-ATR technique. Upon formation of the catalyst a UV-Vis absorption spectra in the Vis region and new bands in difference IR spectra can be observed. These IR bands can be either assigned to vibrations of Co-oxo core or of a phosphate frame work in which the active site of the catalyst is embedded. Another possibility is a superposition of both vibrations. The observed UV-Vis spectrum goes together with the observed black color of the catalyst. The stability of the catalyst was previously described in the literature to be very high in buffering (proton accepting) solutions whereas in electrolyte solutions that do not show this ability the stability was reported to be low due to corrosion caused by proton attack.[8] Stability measurements were as well performed with the above mentioned in situ spectroelectrochemical techniques. 12 h of electrolysis in KPi electrolyte solution did not change the UV-Vis absorption significantly. On the other hand catalytic films electrodeposited from KPi and transferred to non proton accepting solutions (Na_2SO_4 solution) dissolve after a certain time as shown by in situ UV-Vis absorption. In addition IR bands pointing downwards were observed by in situ FTIR-ATR. Downwards pointing bands are here assigned to species vanishing during an electrochemical process. The downward pointing bands do not represent a complete mirror image of IR bands observed in the difference spectra upon formation of the catalyst. This indicates that upon dissolution IR active species do not vanish in the same way as they were formed. A different active site for catalyst electrodeposited from sulfate electrolyte solutions was already proposed in the literature.[8] All these results show that the catalytic film cannot be operated as anode in acidic media and thus an implementation in a two chamber electrolysis process of Na_2SO_4 solutions seems to be impossible. On the other hand using a three chamber geometry with a bipolar membrane separating anode and middle chamber is feasible. Results show that electrodeposition of the catalyst on larger electrodes suitable for usage in a Micro Flow Cell is possible. Three chamber electrolysis using a catalyst coated Pt/Ti shows lower voltages compared to bare Pt/Ti and *pH* values confirm the working principle of the electrolysis. During more than 1 h of electrolysis the catalyst seems to be rather stable if 5 mA/cm^2 are applied. Higher current densities cause a dissolution of the catalyst. Compared with bare DSA anodes the catalyst coated DSA electrodes show slightly higher voltages. As the values are

not significantly higher for a large area application the catalyst might be more beneficial as it is electrodeposited from inexpensive electrolytes and while DSA electrodes are usually expensive. The working principle by combining the catalyst with a three chamber process was proven. However, further studies to address the long time stability and adhesion properties of the catalyst on various electrodes are still needed.

4.5 References

[1] C.A. Grimes, O.K. Varghese, S. Ranjan In *Light, Water, Hydrogen The Solar Generation of Hydrogen by Photoelectrolysis,* Springer Science+Business Media, LLC,2008,Chapter 2
[2] P. Vanysek, *Electrochemical Series* In D.R. Lide (Ed) *CRC Handbook of Chemistry and Physics,* electronic version 0.9, CRC Press LLC, 2002
[3] T.A.Betley, Q. Wu, T. Van Voorhis, D.G. Nocera, *Inorg. Chem.*,**47**,2008, 1849-1861
[4] D.G. Nocera, *ChemSusChem,***2**,2009,387-390
[5] M.Yagi, E. Tomita, S. Sakita, T. Kuwabara, K. Nagai, *J. Phys. Chim*,**4**,2005,21489-21491
[6] M.W. Kanan, D.G. Nocera, *Science*,**321**,2008,1072-1075
[7] M.W. Kanan, Y. Surendranath, D.G. Nocera, *Chem. Soc .Rev.*,**38**, 2009,109-114
[88 Y]. Surendranath, M. Dinca, D.G. Nocera, J. Am. Chem. Soc., **131**, 2009,2615-2620
[9] R.Risch, V. Khare, I. Zaharieva, L. Gerencser, P. Chernev, H. Dau, *J. Am. Chem. Soc.*, **131**, 2009,6939-6937
[10] K. N. Ferreira, T. M. Iverson, K. Maghlaoui, J. Barber, S. Iwata, *Science*, **303**,2004,1831-1838
[11] Dau, H.; Grundmeier, A.; Loja, P.; Haumann, *M. Philos. Trans. R. Soc.London, Ser. B*, **363**,2008, 1237-44.
[12] D.A. Luttermann, Y. Surendranath, D. Nocera, *J. Am. Chem. Soc*., **131**,2009,3838-3839
[13] A.J. Bard, L.R. Faulkner, *Electrochemical Methods*, John Wiley & Sons, 2001
[14] S. D'Elia, N. Scaramuzza, F. Ciuchi, C. Versace, G. Strangi, R. Bartolino, *Appl. Surf. Sci.,***225**,2009,7203 - 7211
[15] H. Neugebauer, *Macromol. Symp.*,**94**,1995, 69-73
[16] C. Kvarnström, A. Ivaska, H. Neugebauer In *Advanced Molecules and Polymers, Volume 2, Processing and Spectroscopy*, Ed: H.S. Nalwa, 2001, Chapter 6
[17] B. Meana Esteban, *Doctoral Thesis: Aromatic Fused Ring Systems: Synthesis and Characterizatioby Electrochemical and Spectroelectrochemical Methods,* Åbo Akademi University, 2006
[18] P.W.Atkins, *Physikalische Chemie*, Wiley -VCH, 1988
[19] K.N. Mani, *J. Membr. Science*., **58,** 1991,117 - 138
[20] S. Koter, A. Warszawski, *Pol. J. Environ. Stud.*, **9 (1)**, 2000, 45 - 56
[21] F.G. Wilhem, *PhD. Thesis: Bipolar Membrane Electrodialysis,* Universtiy of Twente, Twente University Press, 2001
[22] K. C. Li, C.A. Huang,G. C. Tu, W. S. Wang, *Mat. Res. Soc. Symp. Proc*., **747**, 2003, V1.2.1-V1.2.7
[23] Supporting Information of Ref [8]
[24] *The Aldrich Library of FT-IR Spectra,* Sigma Aldrich Co, 1997
[25] G. Socrates, *Infrared and Raman Characteristic Group Frequencies, Tables and Charts, Third Edition*, John Wiley & Sons Ldt., 2001
[26] H. Neugebauer, A. Neckel, N.S. Sariciftci, H. Kuzmany, *Synthetic Met.,***29**, 1989, E185-E192
[27] M.A. Abdel Rahim, H.B. Hassan, *Thin Solid Films*, **517**, 2009, 3362-3369

Chapter 5

Overview over different CO_2 reduction stragtegies

Possible CO_2 reduction methods were presented in Chapter 1 (1.2.3). An overview over possible CO_2 reduction pathways is shown here in Figure 5.1. Direct reduction is here interpreted as a method were no additional energy carrier as reducing agent is used. This methods are electrochemical and photochemical reduction of CO_2. By using either hydrogen gas of NADH as reducing agent CO_2 can be reduced as well, these are the here so called indirect reduction pathways.

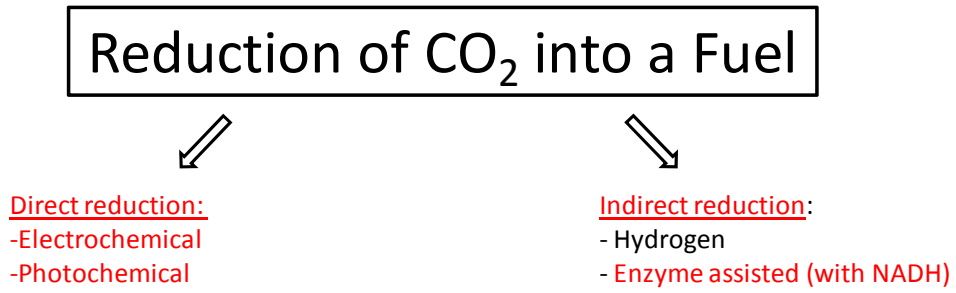

Figure 5.1 Possible pathways for the reduction of CO_2 into a fuel

The indirect reduction pathways using hydrogen gas are previously described (1.2.3.1 – 1.2.3.4). Thus the main focus in this chapter is on the other reduction pathways: direct electrochemical and photochemical reduction and the indirect enzyme assisted reduction with NADH. Note that only an overview over some selected literature reports in each topic is given.

5.1 Electrochemical CO_2 reduction

For the reduction of carbon dioxide to fuels or fuel precursors like syngas (CO and H_2) proton coupled multi electron steps are necessary. In general they are more favored as thermodynamically more stable molecules are formed.[1] Electrochemical CO_2 reduction on cathods yields in different compounds like carbon monoxide,methane, alcohols (eg. methanol), formic acid, etc. Generally the most common reaction are:[1,2]

$$CO_2 + 2H^+ + 2e^- \rightarrow CO + H_2O \quad \varepsilon^0 = -0.53 \text{ V} \tag{5.1}$$

$$CO_2 + 2H^+ + 2e^- \rightarrow HCOOH \quad \varepsilon^0 = -0.61 \text{ V} \tag{5.2}$$

$$CO_2 + 6H^+ + 6e^- \rightarrow CH_3OH + H_2O \quad \varepsilon^0 = -0.38 \text{ V} \tag{5.3}$$

$$CO_2 + 8H^+ + 8e^- \rightarrow CH_4 + 2H_2O \quad \varepsilon^0 = -0.24 \text{ V} \tag{5.4}$$

The ε^0 values are given at $pH = 7$ in aqueous solutions vs. NHE, 25 °C, 1 atmosphere for gases and 1 M for the other solutions. The theoretical required voltage for CO_2 reduction to methanol (-1.20 V) or methane (-1.06 V) is lower than for water splitting (-1.23 V) (all calculated from ΔG^0)[3]. The reduction should thus be thermodynamically favored but large overpotentials (kinetic barriers) hinder the reactions thus electrocatalyst are needed. Due to the close proximity of the cathodic reduction potentials of carbon dioxide to the reduction potential of protons (ε^0 = 0 V) the reduction of carbon dioxide is usually accomplished by hydrogen evolution. In addition product mixtures are often obtained. Therefore it is necessary to find electrodes and conditions to prepare a majority of a single product.[2] The research in the field of direct electrochemical reduction of CO_2 can be categorized according to catalytic systems used. Two groups can be found:

- Heterogeneous catalysts using solid electrodes: Here cathodes of bulk or particulate metals are used that show particular product properties.
- Catalytic systems based on transition-metal complexes.

Solid electrodes have the advantage of reliability over a long term and good mechanical, thermal and chemical stability whereas catalytic systems based on transition metal complexes are highly selective and show low operating potentials but lack of stability. The solubility of carbon dioxide in water is rather limited (33 mM at 25 °C at 1 atm CO_2) whereas in non aqueous systems, especially in aprotic ones, the solubility is higher.[4] Therefore the catalytic systems can further be divided in aqueous and non aqueous supporting electrolytes. Another approach is to use supercritical CO_2 as electrolyte with additives to improve the conductivity.[5]

5.1.1 Solid electrodes

Jitaru and coworkers[11] propose to classify electrochemical carbon dioxide reduction on the nature of the cathode (*sp* or *d* group metal electrodes) and of the solvent used for the supporting electrolyte (aqueous or non aqueous solutions). A large number of papers in recent years deal with the electrochemical reduction with main topics like the electrocatalytic activity for the CO_2 reduction.[6,7,8,9,] The reduction processes are usually sensitive to the cathode material as well as to the combination with the electrolyte solution.

5.1.1.1 Aqueous supporting electrolytes

Metal electrodes can be used for the electroreduction of CO_2 an can be divided into groups depending on the main product formed (but usually other reduction products can be found as well):

- Hydrocarbons and alcohols using Cu electrodes: Using copper cathodes a variety of hydrocarbons can be obtained (liquid and gaseous). The reduction is sensitive to the surface structure of copper, *pH*, CO_2 concentration and temperature. [10]
- Carbon monoxide using electrodes from Ag, Au, Zn[11],
- Formic acid using In, Sn, Hg and Pb as electrode material[12]

Carbonate solutions are often used as electrolyte solutions. As mentioned above due to the low solubility of CO_2 current densities are usually limited. Operation under pressure, the usage of gas diffusion electrodes[13] or metal coated ion exchange membranes [14] is proposed in the literature. A very interesting work was reported by *Delacourt and coworkers*[15]: They used an electrolysis cell design close to that of PEM fuel cells in order to simultaneously reduce CO_2 and H_2O to syngas at room temperature. A standard PEM fuel cell device configuration was shown to be unfavorable for CO_2 reduction (only H_2 evolution). The insertion of a *pH* buffer layer (aqueous $KHCO_3$) enhanced the cathode selectivity for CO_2 reduction to CO. As cathode material Ag and as anode material a Pt/Ir alloy was used (both supported on the membrane). The energy efficiency of the overall cell was dependent on the current density: At low current densities (5-20 mA/cm^2) it is almost constant (~ 0.45) and decreases quickly as the current density is further increased.

5.1.1.2 Non aqueous supporting electrolytes

The main reason not to use aqueous electrolytes is to increase the solubility. Ni and Pt electrodes in TEAP/PrC(tetra-ethyl ammonium perchlorate/ propylene carbonate) supporting electrolyte solution form mainly CO and HCOOH whereas on Pd or Fe electrodes with

similar experimental conditions the formation of CO and oxalic acid was observed.[2] The main products on electrocatlytic electrodes were found to be

- Oxalic acid on Pb[16], Tl, Hg[2]
- CO and carbonate ions on Cu, Ag, Au, In, Zn, Sn only CO on Ni, Pd, Pt[2]
- CO and oxalic acid Al, Ga, and Group 8 elements (except Ni, Pd, Pt) [2]

Especially methanol seems to be a very interesting electrolyte for various metal electrodes such as Ag[17], Au[18], Pb[19], Ti[20] (main products CO and formic acid) using a KOH – methanol electrolyte solution and Cu[21] using a CsOH – methanol electrolyte solution (main products are methane, ethylene, ethane, CO and formic acid).

5.1.1.3 Conducting polymer electrodes

Studies on the usage of conducting polymer electrodes like polyaniline (PANI) and polypyrrole (PPy) have been performed recently. The main advantage of these materials is their simple preparation methods. PANI based electrodes were used by *Aydin and coworkers*[22] in a $MeOH/LiClO_4/H^+/H_2O$ electrolyte solution. They report a negative potential of -0.4 V vs. SCE and the main products were formaldehyde (current efficiency: 26.5 %), formic acid (current efficiency: 13.1 %) and acetic acid (current efficiency: 57 %). Electrochemical impedance spectroscopy on such a system was performed by *Köleli and coworkers* [23] to find the transfer coefficient and the optimum electrolysis potential (between -0.35 and -0.4 V). *Aydin and coworkers* [24] used further PPy as cathode in a $MeOH/LiClO_4/H^+/H_2O$ electrolyte solution. At 20 bar the products were formaldehyde (current efficiency: 1.8 %), formic acid (current efficiency: 40.5 %) and acetic acid (current efficiency: 62.2 %)

5.1.2 Catalytic systems based on transition metal complexes

Usually transition metal complexes are thought to be operated as homogenous catalyst however they can be used in a heterogeneous mode in which the catalytic material is deposited on an electrode surface[4] or inclusion into a polymer like Nafion.[25] Transition metal catalysts show mostly a high selectivity and activity but their main drawback is the stability. Their characteristic factors like thermodynamic and kinetic properties can be tuned by the metals centers via appropriate ligand systems. An overview over the literature reports in this topic is provided by *Saveat.*[25] *Benson and coworkers*[1] propose in their review article to divide the homogenous catalyst into 3 major groups:

- Catalysts with macrocycles
- Catalysts with bipyridine ligands

- Catalysts with phosphine ligands

5.1.2.1 Metal complexes with macrocyclic ligands

Co and Ni phathalocanines were among the first materials investigated. No clear analysis on current efficiencies and products was performed. Later Co and Ni azomacrcocylic compounds were employed and they show the formation of CO or a mixture of CO and H_2 with high current efficiencies (up to 98 %) but low turnover frequencies. Ni^{II}(cyclam) complexes were as well investigated and show good stability and Faradaic efficiency in the production of CO. They were sensitive to the *pH* and required the usage of Hg electrodes. [1]

5.1.2.2 Metal complexes with bipyridine ligands

Mainly Re, Ru, Rh, Ir and Os complexes with bipyridine ligands were reported. $Re(bipy)(CO)_3Cl$ was shown to be selective for CO in a DMF-H_2O based electrolyte solution. $Ru(bipy)(CO)_2^{2+}$ and $Ru(bipy)(CO)_2Cl^+$ were found to electrocatalytically reduce carbon dioxide to CO, H_2 and $HCOO^-$. *Cis*-[$(Rh(bpy)_2Cl]$ and *cis*-[$(Rh(bpy)_2OTf]$ predominantly reduce CO_2 to formate. $[Os(bpy)(CO)H]^+$ and $[Ru(bpy)(CO)H]^+$ showed under anhydrous condition the reduction to CO and upon addition of water formate (25%) was formed. [1]

5.1.2.3 Metal complexes with phosphine ligands

The first reported transition metal electrocatalyst with phosphine ligands were based on Rh. With a current efficiency of around 42 % the formate anion was formed for short time electrolysis but the current efficiency decreased with prolonged electrolysis time.[1] The use of Pd based complexes with polydentate phoshine ligands have been widely studied by the DuBois group.[26] $[Pd(triphosphine)(solvent)]^{2+}$ complexes are active catalysts for the reduction of CO_2 to CO. [26] Trinuclear Ni clusters with bis(diphenylphosphino)methane[27] or with bis(diphenylphosphino)amino ligands[28] were shown to electrocatalyze the CO_2 reduction.

5.1.3 Summary

A large amount literature is available on the direct reduction of CO_2 to various compounds. Only a view selected references are given in the description above. In general the direct electrochemical reduction is very interesting due to lower thermodynamically required voltages for some products compared to the electrochemical water splitting. On the other hand in practice high overpotentials are given and electrocatalysts are needed. Among metals

electrode materials Cu seems to be very attractive for pratical applications as a various valuable hydrocarbons are formed. Using non aqueous electrolytes mainly CO is formed for various electrode materials. Transition metal based complexes usually show higher product selectivity but their low stability is still an issue. The electrochemical reduction is still at a development stage even though intensive research is carried out and technical applications will need several more years.

5.2 Photochemical CO_2 reduction

The usage of light to reduce CO_2 into a fuel would be a very elegant way mimicking photosynthesis. Plants are using photosynthesis in which the energy of light in transformed into chemical energy. Artificial systems should therefore be able to use light for the reduction of CO_2. Photocatalysts based on semiconducting materials are used to drive the reduction of carbon dioxide into a fuel under the presence of light radiation. Under radiation with energy equal or larger as the bandgap energy of the semiconductor, an electron-hole pair is generated. After charge separation the electron is used for the reduction process. The rate of the photocatalytic reaction is based on the light absorption, the transport of the photogenerated charges on the catalyst surface, e^- and h^+ reaction on the surface, recombination and mass transfer of the reactants on the catalyst surface. A good photocatayst catalyst should show high photon conversion efficiency in addition to a high specific surface area[29] and should be

- photoactive
- able to utilize VIS and/or near UV light
- biologically inert
- chemically inert
- photostable
- inexpensive
- non toxic.[30]

In addition the redox potential of the photogenerated hole must be sufficiently positive in order to allow the hole to act as an acceptor and the redox potential of the photogenerated electron must be negative enough for the electron to act as donor, respectively. A commercial and economical availability is beneficial.[31] The reaction mechanism in the photoreduction of CO_2 involves mainly two species, a hydrogen atom, $H^{\cdot}$ and a carbon dioxide anion radical $^{\cdot}CO_2^-$:

$$H^+ + e^- \rightarrow H^{\bullet} \qquad (5.5)$$

$$CO_2 + e^- \rightarrow {}^{\bullet}CO_2^- \quad (5.6)$$

Multielectron reaction like 5.1 – 5.4 compete with these reactions (5.5 – 5.6).[32] The usage of large bandgap semiconductors is promising because they provide sufficient negative and positive redox potentials. The disadvantage is that therefore a high energy light input is required. Some researches replaced water by other reductans as the solubility of CO_2 in water is low and the CO_2 photoreduction process is competing with H_2 and H_2O_2 formation. But water remains still the primary hole scavenger used. Higher temperatures can help to increase the reaction rate by raising the collision frequency and the diffusion rate. Increasing the pressure is a method to increase the CO_2 concentration in aqueous media as mentioned before. Another approach to overcome the low solubility in water is to use CO_2 in gas-solid systems. Zeolithes and silicate frameworks offer nanoscaled pore reaction fields. Photocatalysts prepared within the zeolithe cavity and framework have very special local structures and show high selectivity in photoreduction.

The first reported CO_2 reduction in aqueous solution was reported in 1979 and the products were found to be formaldehyde, formic acid, methanol and traces of methane by using various semiconductors like WO_3, TiO_2, ZnO, CdS, GaP, SiC.[32] A chronological compilation of CO_2 photocatalysis literature can be found in the review of *Usubharatana and coworkers*[31]. Some of the mentioned photocatalysts will be described in the following part.

5.2.1 Titanium dioxide TiO_2

Titianium dioxide is one of the most widely used photocatalytic semiconducting materials and has a bandgap of 3 eV[33]. *Anpo and coworkers*[34] found that UV radiation of different active TiO_2 catalysts under the presence of CO_2 and H_2O led to the formation of CH_4, CH_3OH and CO as the main products. The yields were strongly depending on the catalyst kind (*e.g.* finely powdered or single crystalline), the reaction temperature and the ratio of CO_2 and H_2O. Highly efficient and selective photocatalytic reduction of CO_2 with H_2O to CH_3OH was observed by using Ti- containing zeolithe catalysts with highly dispers Ti oxides in their frameworks as active species.[35,36] The photocatalytic properties of TiO_2 nanoparticles were investigated by *Koci and coworkers*[29] . They found that with smaller particle size higher yields of methanol and methane over the TiO_2 nanoparticles under illumination can be obtained. The optimum particles size was reported to be around 14 nm. *Wu and coworkers*[37] designed an optical fiber photoreactor and applied it to the photoreduction of CO_2 with H_2O using TiO_2, Cu/TiO_2, $AgTiO_2$, $Cu\text{-}Fe/TiO_2\text{-}SiO_2$ and dye sensitized Cu-Fe/P25 (P25 is a commercial TiO_2 powder from Degussa) coated optical fibers. The reduction by

photocatalysts over various supported TiO_2 materials like Pt, Au etc was previously reported in the literature.[31]

5.2.2 Zinc sulfide ZnS and Cadmium sulfide CdS

The bandgap of bulk ZnS is 3.6 eV and bulk CdS has a bandgap of 2.4 eV.[33] Both of them show low electrochemical stability. However, the use of sacrificial electron donors that have high activities for donating electrons to irradiated photocatalysts allows their use. These sacrificial electron donors pick up the photogenerated holes and therefore prevent the the photodissolution of the catalytic material. Such sacrificial electron donors are for example trimethylamine and triethanolamine.[38] *Yoneyama*[38] summarizes results obtained by using quantized nanoparticles form ZnS and CdS with sacrificial electron donors. The main reduction products were found to be formic acid or CO. It was concluded that the use of sacrificial electron donors is not recommended for CO_2 reduction as water should act as h ole scavenger.

5.2.3 Zirkonium oxide ZrO_2

The bandgap of ZrO_2 is 5 eV.[33] *Kohno and coworkers*[39,40,41] reported that CO_2 is reduced to CO by either H_2 or CH_4 under irradiation of ZrO_2 at room temperature to CO. The CO_2 adsorbed on the surface produces a CO_2^- radical anion upon irradiation and hydrogen reacts with this. The reaction mechanism using CH_4 is similar except that a carbonaceous residue is formed by the reaction of CO_2 and CH_4. The photoreduction of CO_2 to CO seems to proceed regardless of the reductant as long as a surface formate is formed.

5.2.4 Magnesium Oxide MgO

Magnesium oxide is an insulator. But upon irradiation in the reduction process of CO_2 the CO_2^- radical can be stabilized. *Kohno and coworkers*[42] used similar to the above described photoreduction using ZrO_2 as catalyst, H_2 as reductant. The reaction proceeds via a surface formate ion as intermediate. This surface ion does not decompose to yield CO but acts actually as a reductant to convert another CO_2 molecule into CO upon irradiation. Therefore the reaction seem to consist of two independent photoreactions. Later *Teramura and coworkers*[43] compared the photoycatalytic reduction of CO_2 to CO in the presence of H_2 or CH_4 as a reluctant over MgO. They found that CO_2 is adsorbed on MgO and activated to a CO_2^- radical anion under irradiation. The radical anion is further reduced to a surface bidentate formate in the dark. The photoactive species was identified to be this surface

bidentate formate which was found to be very stable on MgO and further reduces CO_2 to CO in the gas phase.

5.2.5 Zinc oxide ZnO and Nickel oxide NiO

The selective photoreduction of CO_2 into methanol using a 355 nm laser irradiation has been studied by *Yahaya and corworkers*[44] using TiO_2, NiO (bandgap: 3.7 eV[45]) and ZnO (bandgap: 3.37 eV[46]) as photocatalyst. They used an aqueous media and the before mentioned semiconductors as powders. A maximum yield for photoconversion over one hour of laser irradiation with NiO and the minimum yield for TiO_2 were observed. The hydrogen production yield over TiO_2 was the highest while the overall production of hydrogen was reduced for all three catalysts in the presence of CO_2. $NiO/InTaO_4$ showed selective photoreduction of CO_2 into methanol.[37] ZnO on activated carbon was used by *Gokon and coworkers*[47] at high temperatures as a photocatalyst for the gasification with CO_2 (Boudouard reaction). An improved gasification (around 2 fold) was observed under irradiation with a concentrated Xe beam.

5.2.6 $K_2Ti_6O_{13}$ based photocatalysts

$K_2Ti_6O_{13}$ as photocatalyst was combined with either Fe based catalyst or a Cu/ZnO catalyst, respectively by *Guan and coworkers*.[48,49] They used aqueous systems and concentrated sunlight for irradiation. The $K_2Ti_6O_{13}$ photocatalyst was found to produce H_2 from water decomposition which later serves as reducing agent for CO_2 hydrogenation over the second catalyst of the hybrid system. Using a Fe based catalyst resulted in the formation of organic compounds such as CH_4, HCOOH, HCHO, CH_3OH and C_2H_5OH. The implantation of Cu/ZnO in a composite catalyst structure leads to the reduction of CO_2 into CH_3OH. However the methanol yield was quite low.

5.2.7 Metal organic complexes

The systems can be divided into several groups

- $Ru(bpy)_3^{2+}$ acts as both photsensitizer and catalyst
- $Ru(bpy)_3^{2+}$ acts as photosensitizer and another metal complex as catalyst
- $ReX(CO)_3(bipy)$ or similar as a photosensitizer
- Metallophorphyrins act as both photosensitizers and catalysts
- Organic photosenesitziers and transition-metal complexes.[3]

Due to their photochemical properties Rhenium bipyridine complexes have received a lot of attention. Rhenium(I)bipyridine tricarbonyl complexes are widely used. Mostly CO and sometimes formate as reduction product is formed.[3,31]

5.2.8 Summary

The use of photocataylsis for the reduction of CO_2 is an innovative technology. A summary over some semiconducting materials used for CO_2 and their bandgap is given in Table 5.1.

Table 5.1 Overview over selected semiconductors investigated for photochemical CO_2 reduction and their bandgap.

Material	*bandgap*/eV
TiO_2	3
ZnS	3.6
CdS	2.4
ZrO_2	5
ZnO	3.4
NiO	3.7

Potential photocatalytic reactor systems for both UV or solar radiation have been already proposed in the literature,[31,32] but this is still a topic of basic research. A deeper understanding of the parameters that influence the photocataylsis is needed and is essential for developing such a technology in practical use. Literature reports still deal with low yields and a low selectivties. Three general methods for improving the efficiency are proposed[31]:

- The usage of semiconductors with an appropriate band gap. A proper structure can improve selectivity and yield and increase therefore the reaction rate. Thus the preparation of the catalytic system is one of the most important steps.
- The development of reductants. Water is the most common used reductant but has a low solubility for CO_2 and the reaction is in competition with the H_2 and H_2O_2 formation. Carrying out the reaction in the gas phase represents an alternative as well as the usage of hydrogen or organic solvents as reductants.
- The optimization of the reaction conditions. This includes temperature, pressure, light intensity and operating wavelength. This can lead to high reaction activity and an improvement of selectivity and yields.

The achievement of a high selective photocatalyst that shows a good yield will be important for the future in this research field. Still this technology will need several years to become commercially available in large scale.

5.3 Enzyme assisted CO_2 reduction

The main idea is to use enzymes that can catalyze the reduction of CO_2 to e.g. methanol. In nature the electron donor is nicotinamide adenine dinucleotide (NADH). NADH is oxidized in this process to NAD^+. Biotechnological reactors can operated at mild conditions like ambient temperature and pressure and at neutral *pH*. The selectivity is usually very high. For a process application NAD^+ should be regenerated to NADH as it is a very expensive cofactor. One gram of the reduced dipotassium salt cost around 470 €.[50] A scheme of a biochemical reduction process is shown in Figure 5.2. The NADH recycling can be done over catalysts either electrochemically or photochemcially.

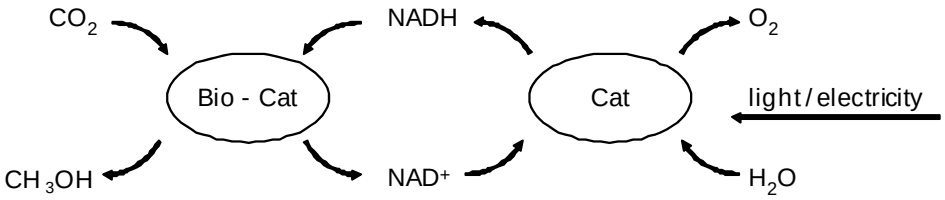

Figure 5.2 Schematic drawing of the biochemical CO_2 reduction process. Reprinted with friendly permission from Ref [51]

Thus the main steps for biocatalytic CO_2 reduction can be divided into the following problems

- Enzyme assisted CO_2 reduction
- NADH regeneration
    - Photocatalytically
    - Electrocatalytically

5.3.1 Enzymes for CO_2 reduction and their immobilization

For developing biocatalytical systems for performing CO_2 reduction, immobilization of the enzymes is necessary. In 1999 *Obert and coworkers*[52] reported a consecutive reduction approach of carbon dioxide to methanol with tree dehydrogenases. Initially CO_2 is reduced to formate catalyzed by formate dehydrogenase, followed by the reduction of formate to formaldehyde by formaldehyde dehydrogenase. Finally formaldehyde is reduced to methanol

by methanol dehydrogenase. NADH was used as terminal electron donor for each dehydrogenase catalyzed reduction. Thus for the conversion of one mol CO_2 into one mol methanol three moles of NADH are required. They found that by encapsulation of the enzymes into a porous silica sol – gel matrix the methanol production yield is increased compared to solution media. With a methanol/NADH ratio of 0.02 the yield was increased from 7.8 % in solution to 91.2 % with the encapsulated enzymes. However, the overall production yield of the reaction in solution was very low (μmoles). The low water solubility and reactivity of silica precursors for sol-gel processes necessitate cosolvents and catalysts. Modified sol – gel techniques have thus been developed.[53] Researchers have use alginate-silica hybrid gels[53,54], polymeric particles (polystyrene)[55], titania particles[56] etc. Usually rather high yields of methanol production are reported but very little data about the absolutely achieved amounts of methanol is given. Available data report some μmoles of methanol. Biocatalytical processes in industry are usually applied to the production of fine chemicals especially if enatioselectivity and regioselelectivity is needed.[57] A biochemical method always competes with standard chemical catalytic synthesis methods. A thermodynamic analysis by *Xu and coworkers*[53] at 25 °C, *pH = 7* and 100 kPa for the conventional chemical catalysis

$$CO_{2\ (g)} + 3\ H_{2\ (g)} \rightleftharpoons CH_3OH_{\ (g)} + H_2O_{\ (g)} \qquad (5.7)$$

gives $\Delta G_r^{\ 0}$ of 3.79 kJ/mol whereas for the biocatalytical reaction

$$3NADH + 3H^+ + CO_{2\ (g)} \rightleftharpoons CH_3OH_{\ (l)} + 3\ NAD^+ + H_2O_{\ (l)} \qquad (5.8)$$

$\Delta G_r^{\ 0}$ is – 67.84 kJ/mol. The equilibrium constant was found to 0.217 for the conventional chemical and 9.6 x 10^6 for the biocatalytical conversion.

5.3.2 NADH regeneration

Nicotinamide adenine dinucleotide is an expensive cofactor which is consumed by the dehydrogenases for the reduction of CO_2 to methanol. In order to save costs it should be regenerated by catalytic reduction. The energy for the reduction can be provided by electricity or by sunlight. Another approach is the use of substrate driven enzyme catalyzed reactions.[55] The main disadvantage of using another enzyme for NADH regeneration is that a second enzymatic system is needed. With this system another substrate has to be transformed into a product in order to regenerate NADH. This product should be then transferred back into the substrate again in order to have a continuous cycle but this again costs energy. In the best case the reaction medium consist of two substances after reaction competition but more often a mixture of four substances can be found that have to be separated afterwards.[58] In addition this system has to deal with moderate enzyme stability and inflexibility with respect to

different coenzyms.[61] Thus direct regeneration using electrochemical or photochemical methods seem to be much more advantageous and shall be discussed in the following. If electricity is used for regeneration it should be taken into account that the same amount of energy for water splitting using commercially available water electrolyzeres could be used in order to produce H_2 for a hydrogenation reaction of CO_2 (like described in Chapter 1). From thermodynamics ΔG^0 for

$$NAD^+ + H^+ + 2e^- \rightleftharpoons NADH \tag{5.9}$$

is approximately 62 kJ/mol and ε^0 is -0.32 V (pH = 7, 25 °C, $a(NAD^+)$ = 1).[51] By electrolysis in aqueous solutions the other half reaction will be water oxidation

$$H_2O \rightleftharpoons 2\,H^+ + \frac{1}{2}\,O_2 + 2\,e^- \tag{5.10}$$

with $\varepsilon^0$is 0.816 V at pH = 7 and 25 °C. Thus for NADH electrolysis ΔE^0 is -1.136 V which is slightly lower than water electrolysis (ΔE^0 = -1.23 V). For the biochemical pathway to be interesting the NAD^+ reduction should be done photochemically or by electrolysis that reaches the same technical standard as commercially available water electrolyzers. [51]

5.3.2.1 Electrochemical NADH regeneration

As mentioned above in ideal case -321 mV are needed for reaction 5.9. *Damian and coworkers*[59] studied the NAD^+ reduction on gold. They found that the reduction is irreversible and to initiate the reduction an overpotential of around -200 mV is needed. For the reaction to occur at an appreciable rate a cathodic overpotential of larger than -500 mV is necessary. Depending on the applied reduction potential different molar ration between enyzmatically active NADH and inactive NAD_2 was obtained. NAD_2 is an inactive dimer formed by radical coupling. The ratio was decreased by increasing overpotentials which was assigned to a higher dimerization rate due to an increased surface concentration of formed radicals. Previous literature reports have used mercury and various carbon materials as cathodes. Due to the formation of side products in direct electrochemical regeneration, catalyst, so called mediators, are used, as indicated in Figure 5.3. The mediator takes up 2 electrons from the cathode and reduces NAD^+ via hydride transfer. The mediator should meet several criteria for application:

- The mediator must transfer two electrons of one hydrid ion in one step and must not transfer the electrons back to the substrate.
- The electrochemical activation energy must not be less negative than the potential for direct reduction (which is found to be around -0.9 V vs SCE including overpotentials)

- Only the enzymatically active form of NADH must be formed.[60]

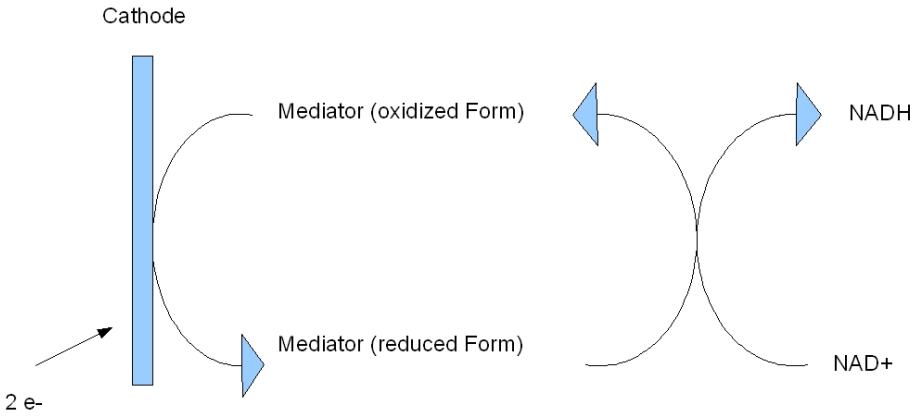

Figure 5.3 Scheme of NADH regeneration using mediators. Reprinted with friendly permission from Ref [51]

One of the first substances that was found to meet these criteria was a bipyridyl rhodium complex. Later these types of complexes was improved by using the petamethycyclopentienyl (Cp^*) as a ligand. High regioselectivity was obtained.[60] *Hollmann and coworkers*[61,62] for example showed that $[Cp^*Rh(bpy)(H_2O)]^{2+}$ is a versatile tool for electrochemical NADH regeneration. It is active over a broad *pH* and temperature range and very stable. Various enzymatic synthesis reaction with electrochemical NADH regeneration using Cp*Rh(bpy)L systems are listed in reference 60. *Song and coworkers*[63] used Pt nanoparticles to enhance the electron transfer between NAD^+ and $[Cp^*Rh(bpy)Cl]^+$. The nanoparticels worked as homogenous catalyst and as secondary mediator to improve the turnover kinetics of $[Cp^*Rh(bpy)Cl]^+$. As the difficulty is to find electrochemically redox catalysts that fulfill the above mentioned criteria, several attempts have been made to regenerate the cofactor indirectly by coupling with a second enzymatic reaction. But with this the advantage associated with electroenyzmatic synthesis of having no need for a second regeneration enzyme is lost. Several examples can be found and are listed in reference 60.

5.3.2.2 Photochemical NADH regeneration

In nature $NADP^+$ is reduced to NADPH by ferredoxin and $NADP^+$ reductase in photosystem I under irradiation. Contrary to the electrochemical regeneration of NADH not as much research was performed on photochemical regeneration methods. A few studies on photochemical cofactor regenerations using enyme mediators are reported like *Sagawa and coworkers*[64] who used a multilayer TiO_2 film excited with a 500 W Xenon lamp. The film

showed photocatlytic activity for the reduction of methylviologen that can be used as efficient mediating electron carrier and lipoamide dehyrdogenase as enzyme for the NADH regeneration. The main drawback is the use of a enzyme mediator that suffers from low specific activity and yield, substrate inhibition and high costs. [65] *Kunkley and Vogler*[66,67,68] worked on the photochemical reduction of MNA^+ which represents the redox active site of NAD^+. They used ion pairs and outer-sphere charge transfer excitation. In 2005 *Jiang and coworkers*[65] used carbon containing TiO_2 as photocatalyst in conjunction with a rhodium complex and electron donors. Upon irradiation (8 W lamp, with $\lambda > 400$ nm) electron hole pairs are created. The electrons are transferred to $[Cp^*Rh(bpy)(H_2O)]^{2+}$ producing Cp*Rh(bpy) and subsequently with one proton the hydridorhodium complex ($[Cp^*Rh(bpy)H]^+$):

$$[Cp^*Rh(bpy)(H_2O)]^{2+} + 2e^- \rightarrow Cp^*Rh(bpy) + H_2O \quad (5.11)$$

$$Cp^*Rh(bpy) + H^+ \rightarrow [Cp^*Rh(bpy)(H)]^+ \quad (5.12)$$

$[Cp^*Rh(bpy)H]^+$ shows high activity for the transformation of NAD^+ to NADH.

$$[Cp^*Rh(bpy)(H)]^+ + NAD^+ + H_2O \rightarrow [Cp^*Rh(bpy)(H_2O)]^{2+} + NADH \quad (5.13)$$

The holes regain electrons in the oxidation of the electron donors. Electron donors like H_2O, ascorbic acid, sodium formate, EDTA and mercaptoethanol were tested. It was found that in the photoregeneration of NADH the conversion is low if H_2O is used as electron donor but still promising. At a temperature of 37 °C, *pH* = 6, $c(NAD^+)$ = 0.2 mM and $c([Cp^*Rh(bpy)(H_2O)]^{2+})$ = 0.3 – 0.5 mM a maximum conversion of ~ 64 % was achieved. With mercaptoethanol a conversion of ~ 94 % in the presence of H_2 was obtained.

Park and coworkers[69] used a visible light photocatalyst $W_2Fe_4Ta_2O_{12}$ ($\lambda > 420$ nm) and $[Cp^*Rh(bpy)(H_2O)]^{2+}$ as mediator. The reactions can be summarized like previously described for carbon containing TiO_2 photocatalyst. In the final step NADH was consumed by a enzymatic reaction. The photoregeneration was tested in phosphate buffer (*pH* = 7) at room temperature with H_2O or EDTA as electron donors. With EDTA a two to threefold increase in the NADH yield was observed compared to H_2O. NADH photoregeneration with EDTA led to 65% conversion after 24 h. The bioreactor was completed by the enzymatic conversion of α-ketoglutarate to L-gluatamate (glutamate dehydrogenase). With TiO_2 as photocatalyst no conversion was observed while $TiO_{2-x}N_x$ as photocatalyst gave only 4 %. With $W_2Fe_4Ta_2O_{12}$ a 15 % conversion of α-ketoglutarate to L-gluatamate was observed.

Recently *Lee and coworkers*[70] showed that eosin Y which is known to work as dye in dye-sensitized solar cells[71] can act as well as photosenzitiers. $[Cp^*Rh(bpy)(H_2O)]^{2+}$ was used as mediator for NAD^+ recycling with triethanolamine as sacrificial electron donor. In the dark

state no reduction of NAD^+ was observed. Upon 30 min visible light irradiation a maximum yield of 71 % was observed. Enzymatic synthesis of L-gluatamate from α-ketoglutarate by glutamate dehydrogenase was performed. Without light no L-gluatamate formation could be observed as well as in case of a system without the mediator or the eosin Y dye. With all components present and after 80 min of reaction yields of ~ 90 % are reported. The turnover frequency was shown to be significantly higher compared to other photocatalysts. This high turnover frequency (and rate) was assigned to a reversible bond formation between eosin Y and the mediator (photosensitizer – electron relay dyad) enabling an efficient transfer of electrons for NADH regeneration. Inspired by that work the same group screened ten other xanthenes dyes for visible light driven, non enzymatic NADH regeneration coupled with the α-ketoglutarate to L-gluatamate reaction by glutamate dehydrogenase.[72] The highest turnover frequency of a photosenszitizer was found by using phloxine B and with similar levels eosin Y, erythrosine B and rose bengal. General the photo- and electrochemical properties of these type of dyes are effected by their halogen substitution, which seems to be a important criteria for an efficient light induced electron transfer from the donor (dye) to the mediator.

5.3.3 Summary

The CO_2 reduction to fuels with NADH and enzymes is very attractive way (from thermodynamics) and a very active field of research. Enzyme assisted CO_2 reduction to methanol was shown to be possible by several groups with immobilization of the enzymes. Even though high yields are published the overall production is usually in the µmol range mainly due to the high price of the enzymes. But biocatalytical processes are already industrially applied. A crucial point in this field is the regeneration of NADH which is used for the reduction process assisted by enzymes. High costs of NADH require an efficient regeneration without the use of other enzymes. Possible methods are the electrochemical and the photochemical way. In the electrochemical NADH regeneration still high overpotentials are reported in the literature. Cathodic reduction usually leads to the formation of enzymatically active NADH and inactive NAD_2. Due to the formation of side products mediators are widely used and discussed. Rh based bipyridine complexes seem to be versatile tools. Despite all the research efforts of improving the performance of the mediators, the productivity is still rather low in addition to a too low concentration of practical synthesis. Research effort has to be as well dedicated to the electrochemical cell design. Thus it will still take some time before it can be applied on an industrial scale. The photochemical NADH regeneration goes into the direction of mimicking the photosystem I in photosynthesis. The

most promising results were obtained by using mediator based systems. Several photocatalysts are reported in the literature while as mediator usually $[Cp^*Rh(bpy)(H_2O)]^{2+}$ is used. Especially the work of *Lee et al*[70,72] seems to be very promising in terms of turnover frequencies. They used xanthene based dyes as photocatalysts. In addition they used a whole photosynthetic concept and were not focusing only on the regeneration part. For regeneration of a 1 mM NAD^+ at maximum ~ 0.7 mM NADH were regenerated. The total photoenyzmatic system based on eosin Y as a dye showed a conversion of ~ 90 % after 80 min. These results are very promising but still in developing stage.

In general the enzyme assisted CO_2 reduction pathway with a suitable NADH regeneration could be very interesting for a CO_2 recycling process in several years of active research in this field.

5.4 References

[1] E.E. Benson, C.P. Kubiak, A.J. Sathrum, J.M. Smieja, *Chem. Soc. Rev.,***38**, 2009, 89-99 and the references therein

[2] M. Jitaru, *Journal of the University of Chemical Technology and Metallurgy,* **42 (4)**, 2007, 333-344

[3] H. Arakawa, M. Aresta, J.N. Armor, M.A. Barteau, E.J. Beckman, A.T. Bell, J.E. Bercaw, C. Creutz, E. Dinjus, D.A. Dixon, K. Domen, D.L. DuBois, J. Eckert, E. Fujita, D.H. Gibson, W. Goddard, D.W. Goodman, J. Keller, G.J. Kubas, H.H. King, J.E. Lyons, L.E. Manzer, T.J. Marks, K. Morokuma, K.M. Nicholas, R. Periana, L. Que, J. Rostrup-Nielson, W.M.H. Sachtler, L.D. Schmidt, A. Sen, G.A. Somorjai, R.C. Stair, B.R. Stults, W. Tumas, *Chem.Rev.,***101**, 2001, 953-996

[4] C.M. Sanchez-Sanchez, V. Montiel, D.A. Tryk, A. Aldaz, A. Fujishima, *Pure Appl. Chem.*, **73 (12)**, 2001, 1917-1927

[5] A. Bandi, M. Specht, T. Weimer, K. Schaber, *Energy Convers. Mtgm.,***36 (6-9)**, 1995, 899-902

[6] R. Schrebler, P. Cury, F. Herrera, H. Gomez, R. Cordova, *J. Electroanal. Chem.*,**516 (1-2)**, 2001, 23-30

[7] Y. Hori, H. Konishi, T. Futamura, A. Murata, O. Koga, H. Sakurai, K. Oguma, *Electrochim. Acta*, **50**, 2005, 5534-5369

[8] P. Dube, G.M. Brisard, *J. Electroanal. Chem.*, **582**, 2005, 230-240

[9] H. Yano, T. Tanaka, M. Nakayma, K. Ogura, *J. Electroanal. Chem.*,**565 (2)**, 2004, 287-293

[10] M. Gattrell, N. Gupta, A. Co, *J. Electroanal. Chem.*, **594**, 2006, -19

[11] M. Jitaru, D.A. Lowy, M. Toma, B.C. Toma, L. Oniciu, *J. Appl. Electrochem.*, *27*, 1997, 875-889

[12] H. Noda, S. Ikeda, Y. Oda, K. Imai, ;. Maeda, K. Ito, *Bull. Chem. Soc. Jpn.,***63**, 1990, 2459-2462

[13] N. Furuya, T. Yamazaki, M. Shibata, *J. Electroanal. Chem.*, **431**, 1997, 39-41

[14] Y. Hori, H. Ito, K. Okano, K. Nagasu, S. Sato, *Electrochim. Acta.,***48**, 2003, 2651-2657

[15] C. Delacourt, P.R. Ridgway, J.B. Kerr, J. Newman, *J. Electrochem. Soc.*, **155 (1)**, 2008, B42-B48

[16] S. Kaneco, N.H. Hiei, Y. Xing, H. Katasuma, H. Onishi, T. Suzuki, K. Otha, *Electrochim. Acta.,***48 (1)**, 2002, 573-578

[17] S. Kaneco, K. Iiba, K. Ohta, T. Mizuno, A. Saji, *Electrochim. Acta.,***44**, 1998, 573-578

[18] S. Kaneco, K. Iiba, K. Ohta, T. Mizuno, A. Saji, *J. Electroanal. Chem.,* **441**, 1998, 215-220

[19] S. Kaneco, R. Iwao, K. Iiba, K. Otha, T. Mizuno, *Energy,* **23**, 1998, 1107-1112

[20] T. Minzuno, M. Kawamoto, S. Kaneco, K. Otha, *Electrochim. Acta.,***43 (8)**, 1998, 899-907

[21] S. Kaneco, K. Iiba, K.H. Hiei, K. Ohta, T. Mizuno, T. Suzuki, *Electrochim. Acta.,***44**, 1999, 573-578

[22] R. Aydin, F. Köleli, *J. Electroanal. Chem.*, **535**, 2002, 107-112

[23] F. Köleli, T. Röpke, C.H. Hamann, , *Electrochim. Acta.,***48**, 2003, 1595-1601

[24] R. Aydin, F. Köleli, *Synth. Met.*, **144**, 2004, 75-80

[25] J.M. Saveant, *Chem. Rev.,***108**, 2008, 2348-2378

[26] M.R. DuBois, D.L. DuBois, *Accounts Chem. Res.,* published online

[27] D.A. Morgenstern, G.F. Ferrence, J. Washington, J.I. Hendereson, L. Rosenheim, J.D. Heise, P.E. Fanwick, C.P. Kubiak, *J. Am. Chem. Soc.,* **118**, 1996, 2198-2207

[28] E. Simon-Manso, P. Gantzel, C.P. Kubiak, *Polyhedron*, **22**, 2003, 1641-1644

[29] K. Koci, L. Obalova, L. Matejova, D. Plcah, Z. Lacny, J. Jirovsky, O. Solcova, *Appl. Catal. B-Envir.*, **89**, 2009, 494-502

[30] D. S. Bhatakhande, V.G. Pagarkar, A.A.C.M. Beenackers, *J. Chem. Technol. Biotechnol.,***77**, 2001, 102-116
[31] P. Usubharatana. D. McMartin, A. Veawab, P. Tontiwachwuthikul, *Ind. Eng. Chem. Res.*, **45**, 2006, 2558-2568
[32] G. Centi, S. Perathoner, *Catal. Today*, **148**, 2009, 191-205
[33] R.M. Navarro Yerga, M.C. Alvarez Galvan, F. del Valle, J. A. V. de la Mano, J.L.G. Fierro, *Chem. Sus. Chem.*, 2, 2009, 471-485
[34] M. Anpo, H. Yamashit, Y. Ichihashi, S. Ehara, *J. Electroanal. Chem*., **396**, 1995, 21-26
[35] M. Kitano, M. Matsuoka, M. Ueshima, M. Anpo, *Appl. Catal. A-Gen.*, **325**, 2007, 1-14
[36] H. Yamashita, Y. Fujii, Y. Ichihashi, S.G. Zhang, K. Ikeue, D.R. Park, K. Koyano, T. Tasumi, M. Anpo, *Catal. Today,***45**, 1998, 221-227
[37] J.C.S. Wu, *Catal. Surv. Asia*, **13**, 2009, 30-40
[38] H. Yoneyama, *Catal. Today*, **39**, 1997, 169-175
[39] Y. Kohno, T. Tanaka, T. Funabiki, S. Yoshida, *Chem. Commun.,* 1997, 841-82
[40] Y. Kohno, T. Tanaka, T. Funabiki, S. Yoshida, *Phys. Chem. Chem. Phys.*, **2**, 2000,2635-2639
[41] Y. Kohno, T. Tanaka, T. Funabiki, S. Yoshida, *Phys. Chem. Chem. Phys.*, **2**, 2000, 5302-5307
[42] Y. Kohno, T. Tanaka, T. Funabiki, S. Yoshida, *Phys. Chem. Chem. Phys.*, **3**, 2001,1108-1113
[43] K. Teramura, T. Tanaka, H. Ishikawa, Y. Kohno, T. Funabiki, *J. Phys. Chem. B,* **108**, 2004, 346-354
[44] A.H. Yahaya, M. A. Gondal, A. Hameed, *Chem. Phys. Lett.*, **400**, 2004, 206-212
[45] J.M. Choi, S. Im, *Appl. Surf. Sci.*, **244**, 2005, 435-438
[46] O. Lupan, T. Pauporte, L. Chow, B. Viana, F. Pelle, L.K. Ono, B. Roldan Cuenya, H. Heinrich, *Appl. Surf. Sci.*, **256**, 2010, 1895-1907
[47] N. Gokon, N. Hasegawa, H. Kaneko, H. Aoki, Y. Tamaura, M. Kitamura, *Sol. Energy Mater. Sol. Cells.*, **80**, 2003, 335-341
[48] G. Guan, T. Kida, A. Yoshida, *Appl. Catal. B-Envir.*, **41**, 2003, 387-396
[49] G. Guan, T. Kida, T. Harada, M. Isayama,A. Yoshida, *Appl. Catal. A-Gen.*, **249**, 2003, 11-18
[50] Sigma Aldrich, β-nicotinamide adenine dinucleotide, reduced dipotassium salt., http://www.sigmaaldrich.com/austria.html (December 2009)
[51] M. Egginger, G. Waldstein, A. Fuchsbauer, E. Portenkirchner, M. Kruijen, B. Meana Esteban, E. Avci, P. Thamyongkit, D. Egbe, K. Oppelt, P. Trefflinger, S. N. Sariciftci *,Solar Fuel Project overview*, LIOS, 2009
[52] R. Obert, B.C. Dave, *J. Am. Chem. Soc.*, **121**, 1999, 12192-12193
[53] S. Xu, Y. Lu, J. Li, Z. Jiang, H. Wu, *Ind. Eng. Chem. Res.*, **45**, 2006, 4567-4573
[54] Y. Lu, Z. Jiang, S. Xu, H. Wu, *Catal. Today*, **115**, 2006,263-268
[55] B. El-Zahab, D. Donnelly, P. Wang, *Biotechnol. Bioeng.*, **99(3)**, 2008, 508-514
[56] Q. Sun, Y. Jiang, L. Zhang, S. Sun, J. Li, *Ind. Eng. Chem. Res.*, **48**, 2009, 4210-4215
[57] R.N. Patel, *Coord. Chem. Rev.*, **252**, 2008, 659-701
[58] M. Andersson, H. Holmberg, P. Adlercreutz, *Biotechnol. Bioeng.*,**57(1)**, 1998, 78-86
[59] A. Damian, S. Omanovic, *J. Mol. Catal. A- Chemical*, **253**, 2006, 222-233
[60] C. Kohlmann, W. Märkle, S. Lütz, *J. Mol. Catal. B-Enzym.*, **51**, 2008, 57-72
[61] H. Hollmann, B. Witholt, A. Schmid, *J. Mol. Catal. B-Enzym.*, **19-20**, 2003, 167-176
[62] H. Hollmann, A. Schmid, E. Streckhan, *Angew. Chem.,* **113**, 2001, 190-193
[63] H.K. Song, S.H. Lee, K. Won, J.H. Park, J.K. Kim, H. Lee, S.J. Moon, D.K. Kim, C.B. Park, *Angew. Chem. Int. Ed.*, **47**, 2008, 1749-1752

[64] T. Sagawa, R. Sueyoshi, M. Kawaguci, M. Kudo, H. Ihara, K. Ohkubo, *Chem. Comm.*, 2004, 814-815
[65] Z. Jiang, C. Lü, H. Wu, *Ind. Eng. Chem. Res.*, **44**, 2005, 4165-4170
[66] H. Kunkely, A. Vogler, *Inorg. Chim. Acta*, **300-302**, 2000, 1090-1093
[67] H. Kunkely, A. Vogler, *Inorg. Chem. Comm.*, **3**, 2000, 624-626
[68] A. Vogler, H. Kunkely, *Coordin. Chem. Rev.*, **3**, 2002, 147-152
[69] C.B. Park, S.H. Lee, E. Subramanian, B.B. Kale, S.M. Lee, J.O. Baeg, *Chem. Comm.*, 2008, 5423-5425
[70] S.H. Lee, D.H. Nam, J.H. Kim, J.O. Baeg, C.B. Park, *Chem. Bio. Chem.*, **10**, 2009, 1621-1624
[71] S.S. Kim, J.H. Yum, Y.E. Sung, *Sol. Energy Mater. Sol. Cells*, **79**, 2003, 495-505
[72] S.H. Lee, D.H. Nam, J.H. Kim, J.O. Baeg, C.B. Park, *Adv. Synth. Catal.*, **351**, 2009, 2589-2494

Chapter 6
Summary and Conclusion

Several different pathways for converting CO_2 from air into possible fuels by using electric energy from renewable sources are present in the literature. They have all in common, that CO_2 is captured from air, released afterwards and converted into a fuel by different reduction processes. For a small to mid scale installation the technically most feasible pathway includes a capturing by an absorption process using NaOH or KOH solution (forming a carbonate solution), a subsequent desorption of CO_2 by acidification of the carbonate solution and final reduction of CO_2 with hydrogen gas. The acid generation, with simultaneous absorption base generation, based on electrochemical water splitting can be done by electrodialysis or electrolysis processes. A prototype from Solar Fuel GmbH demonstrated the practical feasibility for converting CO_2 from air into a fuel first time end of November 2009. The main energy consuming parts are the electrodialysis stack (for acid generation) and the alkaline water electrolyzer for hydrogen generation.

One possibility for an efficiency increase could be the usage of an electrolysis instead of the electrodialysis process for acid generation. The improvement potential is based on the fact, that an electrolydialysis stack, contrary to an electrolysis cell, does not produce significant amounts of hydrogen (needed for fuel synthesis). An electrolysis process with an outside acidification was studied in detail. A two chamber electrolysis cell was operated with Na_2SO_4 as electrolyte and the influence of several parameters were tested. The best operated system was based on Pt cathodes and DSA anodes, which both have very small overpotentials for the given electrode reaction. Higher flow rates, elevated temperatures and small gap between the electrodes increase the performance. In a first estimation the energy demand of the best

operating two chamber electrolysis system was found to be lower than using an electrodialysis. For a better comparison both systems, two chamber electrolysis and electrodialysis, have to be compared in future under similar operating conditions in future. A further operating possibility for electrolysis processes was discussed: By operation of the cell under pressure (with carbonate as electrolyte), CO_2 stays in physical solution. In a similar way the electrodialysis stack is operated in the prototype. No additional overpoentials due to the produced CO_2 bubbles inside the electrolysis cell can be expected.

From the two half reactions in electrochemical water splitting, the oxidation process is considered to be more complex, thus catalytic materials are needed. The working principle and stability of the cobalt based water oxidation catalyst is currently addressed in the literature. The formation and stability of the catalytic film was monitorized by in situ UV-Vis and in situ FTIR-ATR spectroelectrochemistry. The results show that implementation of the catalyst as anode in a two chamber electrolysis process of sodium sulfate solutions is not feasible due to the instability in acidic media. Preliminary studies in a three chamber geometry were performed where the anode chamber was separated from the middle chamber by a bipolar membrane. Due to the properties of bipolar membranes the electrolyte in the anode chamber can be a buffering solution as required for catalyst stability. By using sodium sulfate as electrolyte in the middle and cathode chamber the generation of a stripping acid and the regeneration of the CO_2 absorption base is possible. Compared to bare Pt/Ti as anode the catalyst coated anode showed lower operating voltages at 5 mA/cm^2. On the other hand commercially available dimension stable anodes (DSA) still perform better and further studies for a long time stability and the adhesion properties of the catalyst on various electrodes are needed for large scale implementation.

A literature overview on reduction pathways of CO_2 to a fuel (excluding hydrogenation) was presented in the previous chapter of this thesis. This methods include here so called direct reduction methods (electrochemical and photochemical) and one indirect method, the enzyme assisted CO_2 reduction. All these methods are energetically very interesting, but still deal with several problems related mostly to the used catalyst. The technical most mature way for final CO_2 reduction is still the hydrogenation. State of the art water electrolyzers produce hydrogen with acceptable efficiencies, but new technologies like SOE electrolyzers show high potentials for further improvement. Other reduction methods are energetically very interesting, but are still a topic of basic research and need for sure several more years to become available for larger scale applications.

Appendix A
Water electrolyzers

Electrochemical water splitting[1,2] for hydrogen generation has a long history: In the year 1800 electrolytical water splitting was observed by Nicholson and Carlisle. Hundred years later 400 industrial water electrolyzers were in operation.[3] Electrochemical water splitting can be divided into 2 half reactions (ε^0 are the standard electrode potentials for the half reactions[4]):

$$\begin{array}{ll} \text{Oxidation: } O_2 + 4\,H^+ + 4\,e^- \rightleftharpoons 2\,H_2O & \varepsilon^0 = 1.229\ \text{V} \\ \text{Reduction: } 4\,H^+ + 4\,e^- \rightleftharpoons 2\,H_2 & \varepsilon^0 = 0\ \text{V} \\ \hline 2\,H_2O \rightarrow 2\,H_2 + O_2 & \Delta E^0 = -1.229\ \text{V} \end{array} \qquad \text{(A.1)}$$

The standard Gibb's free energy ΔG^0 is given by

$$\Delta G^0 = -nF\Delta E^0 \qquad \text{(eq. A.1)}$$

Where n is the number of electrons and F the Faraday constant. Thus the Gibb's free energy is positive (ΔG^0 = 237.2 kJ/mol) for the water splitting reaction and non spontaneous. For the reaction to take place this change in the Gibb's free energy has to be supplied to the system in equivalent of electrical energy. This is done in electrolytic cells upon applying a potential difference between the two electrodes that are immersed in an electrolyte. To drive the reaction, ΔG has to be supplied to the system in form of electrical energy (by applying the potential difference to the electrodes). The minimum voltage difference ΔE_{rev} to drive this reaction can be calculated as follows

$$\Delta E_{rev} = -\frac{\Delta G}{nF}. \qquad \text{(eq. A.2)}$$

Thus ΔE_{rev} is the reversible work and called therefore as well thermodynamic reversible potential and is equal to -1.229 V at standard conditions. At these conditions, the reaction is endothermic ($\Delta H > 0$). In general the relation between ΔG, ΔH and ΔS is

$$\Delta G = \Delta H - T\Delta S . \qquad \text{(eq. A.3)}$$

For the water splitting reaction ΔH is larger than ΔG as $\Delta S > 0$ due to an entropy increase during the reaction. Therefore heat energy can either be absorbed from the system in order to allow the entropy to increase (this would lead to a cooling of the system as long as thermal energy is available) or be supplied from outside the system. Electrolyzers are usually operated in an isothermal mode (constant temperature) and hence the heat energy (= $T\Delta S$) will be absorbed from the system. If the operating voltage is higher than ΔE_{rev}, heat will be generated inside the system due to losses in the cell and a part of the energy is used for providing the heat energy. Thus the energy corresponding to ΔH is often considered as the energy that has to be supplied to the system in terms of electrical energy. The voltage that corresponds to this is referred to as thermoneutral voltage and can be calculated by

$$\Delta H = -nF\Delta E_{th} . \qquad \text{(eq. A.4)}$$

It has a value of 1.481 V. At this voltage, the electrolyzer generates enough heat to "compensate" $T\Delta S$. If the electrolyzer is operated at $\Delta E > \Delta E_{th}$ the system becomes exothermic and heat must be removed from the system in order to guarantee isothermal conditions. However, energy losses that can be associated to reaction kinetics and charge transport through electrical leads and the electrolyte solution, force an electrolyzer to operate in this voltage regime. The operating voltage ΔE_{op} is the sum of all overpotentials (coming from the electrodes, the reaction kinetics and the resistive losses in the cell) and ΔE_{th}. The efficiency of water electrolyzeres is defined as the ratio of the energy content of hydrogen to the electrical energy supplied. In terms of voltage it can be expressed as

$$\eta = \frac{\Delta E_{th}}{\Delta E_{op}} . \qquad \text{(eq. A.5)}$$

For water splitting, pure water is seldom used due to poor ionic conductivity leading to enormous ohmic overpotentials. By addition of acids or bases the conductivity is significantly enhanced as they offer high ionic (H^+ or OH^-) concentrations and mobilities. Alkaline electrolytes are usually preferred to the acidic ones as corrosion can be easier controlled and the used materials are cheaper. Based on the type of the used electrolytes electrolyzeres are in general classified in 3 types: alkaline, proton exchange membrane (PEM) and solid oxide electrolyzers (SOE).

Alkaline electrolyzers

As indicated by the name, electrolytes with a high *pH*, usually aqueous sodium or potassium hydroxide, are used. The technology can be considered as the oldest and most developed method and is therefore widely spread. Alkaline electrolyzers consist of a cell frame, an anode and a cathode compartment with the respective electrodes and a sparator between these compartments (Figure A.1). The cell frame is usually made from stainless steel. The electrolyte needs to have a high ion conductivity, should not chemically decompose under operation and should be capable of withstanding *pH* changes during the process (mainly due to changes in the H^+ concentration at the electrodes). Aqueous electrolyte solutions show higher conductivity at elevated temperatures therefore these types of electrolyzers are operated between 70 – 90 °C. The electrolyte solution is circulated through the cells and the concentration is maintained by addition of high purity water as water is consumed by the hydrogen production. To divide the compartments and to prevent mixing of gases separators like porous diaphragm are used. They have to allow the passage of the electrolyte solution while preventing gas passing them. The placement of the electrodes close to the separator reduces the voltage drop and minimizes heat losses. The separator materials must be corrosion resistant and structurally stable. Common used materials are asbestos, polymer materials on polysulfonate basis and oxide ceramic materials (e.g. barium titanate). To decrease the overpotentials, electrocatalytic materials are used as electrodes in various types of geometries. Group 8, 9 and 10 elements from the periodic table of elements as well as their alloys are conventionally used. Widely used anode materials are Ni, Co and stainless steel as they show low overpotentials in NaOH and KOH solutions. The cathode is usually made from Ni or Ni coated stainless steel. A lot of research is done in order to enhance the electrocatalytic properties of the electrodes. Alkaline electrolyzers usually consist of several cells in stack. Conventional cells operate at 1.8 – 2.2 V with current densities below 0.4 A/cm^2 whereas advanced cells show lower voltages (1.6 V) and higher current densities (2 A/cm^2). The efficiencies are in the range of 60 – 80 %, but with modern type of electrolyzers (zero gap) the efficiency can be up to 90 %.[1,2] Most of the commercial electrolyzers can be traced back to 2 pioneer systems: the atmospheric electrolyzer by BAMAG and the pressurized system from Lurgi.[5]

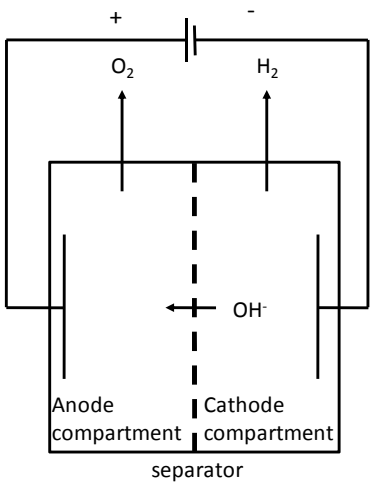

Figure A.1 Schematic drawing of an alkaline electrolyzer

PEM electrolyzers

The development of PEM electrolyzeres (Figure A.2) is closely related to PEM fuel cells ("inverse PEM fuel cell"). The main unit of such an electrolyzer type is an electrode-membrane-electrode structure. It consist of the PEM (usually a Nafion membrane) coated on both side with a catalyst acting as electrodes. A module consists of several such structures connected in series. The PEM acts as electrolyte and separator and is impermeable to water and product gases. It conducts the protons from the anode to the cathode compartment. Nobel metals such as Pt, Ir, Rh, Ru or their oxides (and alloys) are used as electrode materials. The electrode-membrane-electrode structure is pressed from both sides by porous, gas permeable plates that provide support to the structure and guarantee a homogenous current distribution across the whole membrane surface. These plates ensure exit pathways for the produced gases and usually Pt or carbon are used at the anode side and nowadays carbon is the material of choice on the cathode side. This gives a porous cell structure and adjacent cells are separated by bipolar plates (usually made of graphite) that allow the current to pass from one cell to the other. High purity water is circulated through the cell. In comparison to alkaline electrolyzers, PEM electrolyzers are more efficient (a standard device operates at 80 – 90 %) and produce very high purity hydrogen. In addition, no risk of corrosive or chemical leakage is given as the electrolyte is solid. Cells are operated at 80 – 150 °C and pressures around 30 bar. Current densities up to 2 A/cm^2 can be reached and voltages are in the range of 1.4 – 2 V. The main disadvantages are the high costs due to the PEM and noble metal electrodes and the requirement of very high purity water. Small PEM electrolysis units are becoming commercially available now.[1,2]

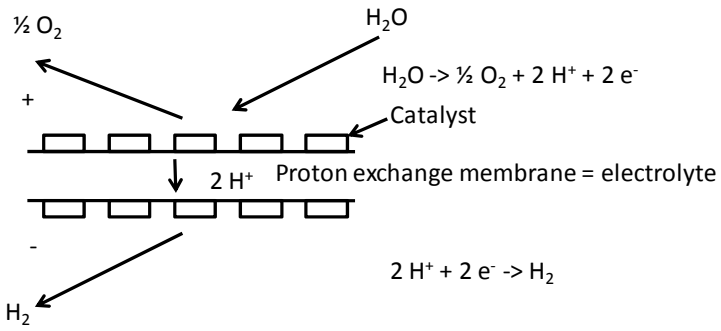

Figure A.2 Working principle of a PEM electrolyzer

Solid oxide electrolyzers (SOE)

SOE are operated at high temperatures (~ 1000 °C), which is advantageous for the thermodynamic and kinetic parameters of water splitting. ΔH and ΔG values are lower for gaseous water (by the enthalpy of evaporation). For splitting of water in the vapor phase, the values are as follows: ΔH^0 = 241.8 kJ/mol, ΔG^0 = 228.6 kJ/mol.[6] Therefore ΔE_{rev} is -1.184 V and ΔE_{th} is found to be -1.253 V. The difference between these two voltages is 0.069 V, which is lower than the same difference for splitting of liquid water (0.252 V). The reason is that in the case of liquid water, more energy has to be supplied to the system in order to overcome the enthalpy of evaporation. But still there is the energy (resulting from the TΔS term) that has to be applied in addition, as the reaction is still endothermic and ΔS > 0. Higher temperatures lower ΔE_{rev} (at 1100 K ΔE_{rev} is -0.969 V) and as well the overpotentials. For this reason, electrical requirements are lower for electrolysis in the vapor phase but higher heat energy is required. The lower electrical energy requirements allow this electroylzer type to operate at reduced voltages (0.95 – 1.33 V) compared to other eletrolyzers. SOE electrolyzers use solid ceramic electrolytes like yttria stabilized zirconia which are good O^{2-} conductors at high temperatures (1000 °C). The operating temperature is chosen depending on the conductivity of the electrolyte. In Figure A.3, the working mechanism of a SOE electrolyzer cell is depicted: A feed gas (steam mixed with hydrogen) passes through the cathode compartment. The electrolyte itself is impermeable to the product gases and water vapor and only O^{2-} can migrate through. At the porous anode, O_2 is generated. Common cathode materials are Ni-ZrO_2. As anode conducting perovskites like $LaNiO_3$, $LaMnO_3$ and $LaCoO_3$ are used. The SOE technology is still in the development stage. The efficiency can essentially be 100 % and compared to other electrolyzers the power consumption is less (~ 10 % compared to alkaline electrolyzers). [1,2]

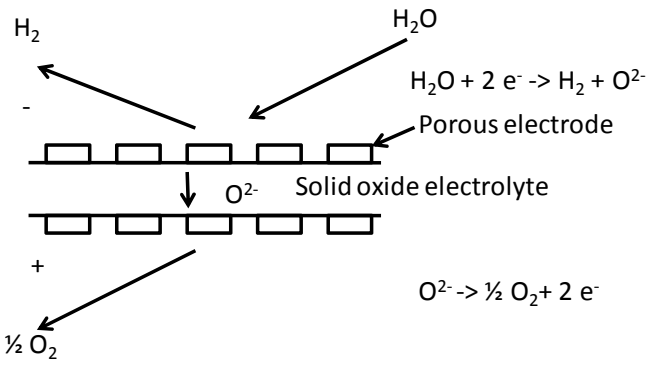

Figure A.3 Working principle of SOE

References

[1] C.A. Grimes, O.K. Varghese, S. Ranjan *Hydrogen generation by water splitting* In *Light, Water, Hydrogen The Solar Generation of Hydrogen by Photoelectrolysis,* Springer Science+Business Media, LLC,2008,Chapter 2

[2] P.A. Lessing, *Materials for Water Electrolysis Cells* in R.H. Jones, G.J. Thomas (Eds) *Materials for the Hydrogen Economy*, CRC Press, Taylor & Francis Group, LLC, 2008, Chapter 2

[3] W. Kreuter, H. Hofmann, *Int. J. Hydrogen Energy,* **23 (8)**, 1998, 661-666

[4] P. Vanysek, *Electrochemical Serie,* in D.R. Lide (Ed) *CRC Handbook of Chemistry and Physics,* electronic version 0.9, CRC Press LLC, 2002

[5] U. Zuberbühler, A. Bandi, M. Specht, *Screening of Methods of CO_2 Capture with Subsequent Fuel Synthesis in Remote Areas,* ZSW, 2009

[6] L.V. Gurvich, V.S. Iorish, V.S. Yungman, O.V. Dorofeeva, *Thermodynamic Properties as a Function of Temperature,* in D.R. Lide (Ed) *CRC Handbook of Chemistry and Physics,* electronic version 0.9, CRC Press LLC, 2002